GSI-2015-2
REPORT
April 2015

News and Reports from

High Energy Density generated by Heavy IOn and Laser Beams

HEDgeHOB Collaboration at FAIR - Report 2013/2014

Title picture: Towards HEDP and WDM experiments at FAIR – The FAIR construction site east of the existing GSI facility in February 2014, seen from the SIS-18 hill

(Photograph by Karin Weyrich)

News and Reports from

High Energy Density generated by Heavy IOn and Laser Beams

2013 - 2014

April 2015

Editor: K. Weyrich

Co-editor: D.H.H. Hoffmann

Editorial

Dear Colleagues,

Finally we are back again, even if it took some time. With this issue of the report on *High Energy Density Physics* we want to continue a tradition of more than 3 decades.

The construction of FAIR at the site of GSI is now clearly visible as can be seen from our title page. GSI with its scientific and technical personnel has to bear the main burden of the construction work. This caused a complete revision of the internal GSI organization and for a number of years GSI will have to place its main efforts onto the FAIR construction process. Research activities will continue, though on a reduced scale. With this new version of our report we want to give an overview on the activities of the HEDgeHOB collaboration worldwide. However, this report is open to all institutes and individual researchers, who feel attached to the field of High Energy Density Physics. Our aim is that all HEDgeHOB member institutes contribute to this report with at least one contribution. We also want to document the scientific progress in our field.

In the last year 2014 the *20th Symposium on Heavy Ion Fusion* took place at the Institute of Modern Physics in Lanzhou. This symposium is a traditional meeting place for scientists of our field and in this report we present a summary of this event. Ion driven high energy density physics is taken up at a number of new facilities that are emerging worldwide, among them are the NURA facility at Astana, Kazakhstan and the NICA facility in Dubna. Moreover a High Intensity Accelerator Facility (HIAF) is in the planning stage in China, and a new facility in South Korea. The NDCX II facility in Berkeley will start during this year to be a user facility. More details on this can be found in this report.

Also our colleagues from Laser Plasma Interaction and Laser Driven Fusion were able to report considerable progress. Most remarkable is the experimental progress towards ignition at the NIF facility in Livermore. So we especially acknowledge that Eduard Dewald (LLNL), who early in his scientific career did research at GSI-Darmstadt, contributed with a paper on 'Progress towards Indirect Drive ICF Ignition at NIF' to this report.

Since this is a new start, we encourage all contributors and interested scientists to advise us to improve this report und participate in future editions.

With kind regards,

Karin Weyrich, GSI (editor) and Dieter HH Hoffmann, TUD (co-editor)

January 2015

Contents

4 Theory for HEDP/WDM in Plasma-, Laser- and Atomic Physics

Conference Summary

HIF 2014, Lanzhou, China

The 20th Symposium on Heavy Ion Fusion was held at the Institute of Modern Physics in Lanzhou, China. This series of conferences started 1976 in Berkeley and was held since then at intervals of about 2 years. In this millennium the conference was held in places like Moscow, Russia (2002), Princeton, USA (2004), Saint-Malo, France (2006), Tokyo, Japan (2008), Darmstadt, Germany (2010), Berkeley, USA (2012) and now this year (2014) in Lanzhou, China. Even though the conference series now has a long tradition, a large number of young researchers were present, which supports the impression that this conference is dealing with a topical issue, which is of broad interest to the scientific community and beyond. Since Fusion Energy has a long term perspective as an abundant and environmentally acceptable energy source this topic will surely continue to attract bright young scientists for many years to come.

A total of about 150 participants from 9 different countries and about 40 institutes presented their ongoing research, and thus assured that the meeting was lively and scientifically very rewarding. This conference may well be compared to the large conference on Inertial Fusion-Science and Applications. While that conference is held bi-annually in France, Japan and USA, this symposium is organized in USA, Asia and Europe. Due to this schedule, the conference advisory committee decided to organize the next meeting in Astana, Kazakhstan. Since some part of Kazakhstan extends westward well beyond the Ural mountain line, the European committee members agreed to the suggestion to have the upcoming HIF 2016 conference in Astana, Kazakhstan, and Nazarbajev University as well as Nazarbajev research institution will be hosts to the conference.
Inertial fusion is viewed by many scientists as laser fusion. However, when ignition has been demonstrated in the laboratory under controlled and reproducible conditions, an efficient driver is necessary, and here the accelerator option is still open, since accelerators already today have an efficiency above 20% to convert electric power into kinetic energy of heavy ions, which is then efficiently deposited deep in the volume of the fusion target. Evaluating the latest scientific progress at the National Ignition Facility (NIF, Livermore USA) which achieved results that points to significant alpha particle heating of the fuel, we certainly are on the eve of seeing a fusion target ignited on a laboratory scale at NIF. The progress at NIF therefore was a major topic at the conference, and it was well demonstrated that there is a clear research path to determine what is missing to finally ignite a fusion target This research effort at NIF will be corroborated by all laser facilities with an inertial fusion program, and the participants noticed the upcoming laser facilities in China, as well as the current research programs in Beijing, Shanghai and Mianyang as well as laser plasma interaction research at smaller facilities. Great interest was directed towards new hohlraum shapes and irradiation schemes aiming at ideal irradiation symmetry.

The concept of particle acceleration with high power lasers is a very strong topic of High Energy density Physics. Novel schemes have been presented, and here for the first time we learnt about the role of Carbon-nanotubes irradiated with a strong laser pulse. Once Warm Dense Matter (WDM) is produced, the problem of diagnostic arises. In this respect the formation and subsequent spectroscopy of hollow ions is a scheme that promises progress in WDM diagnostic and will certainly gain more interest in future. Apart from spectroscopic investigation it was pointed out that understanding the equation of state of WDM is important for laboratory inertial fusion science.

It is encouraging to note that many heavy ion accelerator laboratories engage in beam plasma interaction, and high energy density physics related to heavy ion driven fusion issues. In Korea and Kazakhstan new facilities are planned and next year the NDCX II facility will start as a user facility. An important, as well as impressive example is the host laboratory of HIF 2014, the Institute of Modern

Physics at Lanzhou. Only a few years ago this laboratory took up this research topic following the example of its partner institute GSI in Darmstadt, Germany. Today we see a very active young group of scientists engaged in research on heavy ion energy loss in ionized matter, developing advanced diagnostic methods with intense high energy proton and electron beams. Moreover plans of the Institute of Modern Physics for a project on a High Intensity Accelerator Facility (HIAF) were presented and issues of this high intensity accelerator were discussed in some detail. The community welcomed this plan enthusiastically and impatiently awaits the start signal for this project. It will provide outstanding research prospects and will complement the options that are envisioned at the Facility for Antiproton and Ion (FAIR) accelerators in Darmstadt. Several aspects of the high intensity facility FAIR were presented, these ranged from accelerator issues to High Energy Density Physics. While HIAF is waiting for approval, civil construction started at FAIR. A new diagnostic tool, proton radiography, which was first introduced at Los Alamos laboratory, was discussed and first experimental results from different accelerator laboratories were presented. The community is convinced that this method will provide new insight into the properties of High Energy Density matter and moreover will allow to investigate material properties under extreme conditions of pressure and temperature. It was also demonstrated that very high energy electrons when they are available, will be a very useful diagnostic tool. At HIAF a high energy electron accelerator will be available with a diagnostic beam line directed towards the HED- experimental area. Energy loss of ions in ionized matter is a key topic of ion-beam plasma interaction. For ideal plasma there now exist some experimental data points for a wide range of heavy ions as well as a wide range of energies and here the data do agree reasonably well with standard stopping theories. However for strongly coupled plasmas practically no data exist. A question was raised if the stopping in degenerate matter, which is expected to be much less than in ordinary cold matter, increases the demands on drivers for inertial fusion. This problem will be studied in the future. Something was however missing. No new scenarios on Heavy Ion Driven Fusion were presented. The last study, HIDIF dates back into the 90s of last century. On the other hand a lot of technological progress in accelerator technology was presented. Therefore as soon as ignition on the laboratory scale is demonstrated, probably at NIF, the search for an efficient driver will start and here ion accelerators have an advantage.

The physics of ion driven fusion constitutes a rich field of interesting research topics with progress in all areas. Therefore we thank all participants for coming to Lanzhou and we are looking forward to meet again in Astana, Kazakhstan in 2016.

Yongtao Zhao, Dieter HH Hoffmann, Xinwen Ma and Guoqing Xiao

1 New Facilities for HEDP/WDM Research

High Energy Density Research at the future project HIAF in China

Y. Zhao, R. Cheng, Y. Wang, X. Zhou, Y. Lei, Y. Sun, G. Xu, J. Ren, Z. Zhang and G. Xiao
IMP, Lanzhou, China, email: zhaoyt@impcas.ac.cn

After successful construction of the CSR (Cooling Storage Ring) in Lanzhou, a large scale scientific research platform, named the High Intensity heavy-ion Accelerator Facility (HIAF), was proposed with regard to new trends and developments in nuclear physics and the associated high energy heavy ion research fields. The proposed platform will be one of the 16 approved projects for basic sciences and technologies as the 12th five-year-plan in China; it will be a laboratory open to the outside world, similar to CSR which was built as the 9th five-year-plan in China [1]. The HIAF complex, as shown in Fig. 5, includes a SECR (Superconductive Electronic Cyclontron Resonance) ion source, an ion linear accelerator (i-Linac), a Booster Ring (BRing), a Spectrometer Ring (SRing), a Compression Ring (CRing) and about 8 experimental terminals.

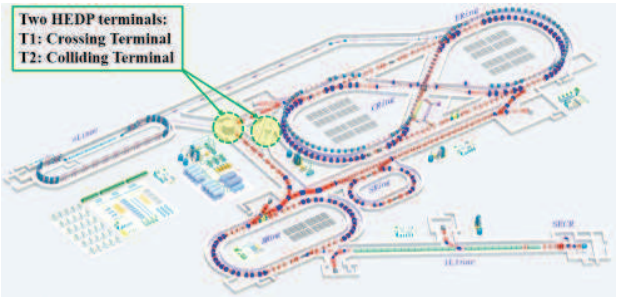

Figure 1: Layout of the HIAF complex and the two terminals for HEDP research

Since both BRing and CRing can produce high-energy and high-intensity ion beams, two terminals for HEDP (High energy density physics) research were proposed at HIAF, one for crossing (T1) and the other for colliding (T2) of the beams from BRing and CRing at the target area. Due to the budget limitation and technique challenges, only T1 is included in the first stage of the HIAF project, and more details are shown in Figure 2. The high energy density matter will be generated by the beam from CRing and be diagnosed by the proton radiographic beam from BRing. Besides, high energy electron radiography [2] was also proposed to act as a potential diagnostic tool in the HEDP experiments at HIAF. Main topics of HEDP at HIAF will include for example, the properties of WDM and the related hydrodynamic instabilities, planetary sciences, beam-plasma interaction, fast flyers driven by intense ion beam, target physics associated with ICF and the related accelerator physics and technologies.

In comparison to FAIR, the power of the final beam for driving an HED sample at HIAF will be improved due to the design in particular in the following aspects: 1: higher energy of the injection beam from the i-Linac, ensuring a higher space charge limit; 2: the larger acceptance of the booster ring; 3: the powerful electron cooler in CRing, ensuring a better focusing and better compression.

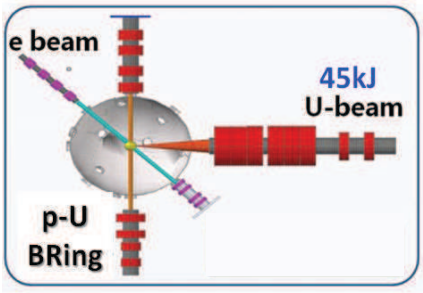

Figure2: Crossing Terminal @ HIAF

The key parameters related to HEDP research at HIAF and other advanced heavy ion drivers are listed in Table 1, where E_0, N, E_{total}, S_f, t and $E\rho$ is the particle energy, the beam intensity (unit, ppp), the total beam energy per pulse, FWHM of the beam spot, the pulse duration and energy density in a lead target (J/m^3), respectively.

Table 1. Key parameters related to HEDP research at HIAF and other heavy ion drivers (for uranium beam).

	SIS-18	FAIR(Ph-I)	HIAF (Ph-I)[a]
$\mathbf{E_0}$	0.4GeV/u	1 GeV/u	1.1 GeV/u
N	4×10^9	4×10^{11}	1×10^{12}
$\mathbf{E_{total}}$	0.06 kJ	15 kJ	41 kJ
$\mathbf{S_f}$	~1 mm	~1 mm	1 - 0.5 mm
t	130 ns	50 ns	130 - 30 ns
$\mathbf{E_\rho}$	2×10^{10}	2.4×10^{12}	$6\text{-}24\times10^{12}$

[a] The upper limit may rely on the budgets of HIAF.

References

[1] Y. Zhao, et al, High energy density physics research at IMP, Lanzhou, China. High Power Laser Science and Engineering, 2, (2014) e39 doi:10.1017/hpl.2014.44.

[2] Zhao Y. T. et al. 2013 *A high resolution spatial-temporal imaging diagnostic for high energy density physics experiments* to be submitted.

Heavy-Ion Collisions and Dense Matter Physics at the NICA facility

Grigory V. Trubnikov
Joint Institute of Nuclear Research, Dubna

The Nuclotron-based Ion Collider fAcility (NICA) in Dubna will provid an infrastructure for forefront research in a globally competitive field of particle physics: the exploration of extreme states of matter including phase transitions between them; and investigation of nucleon spin structure and polarization phenomena.

Of particular interest is the hadron-to-quark matter transition with its main aspects: chiral symmetry restoration, deconfinement and color superconductivity (Fig.1). To perform precision studies with a discovery potential in this field, dedicated heavy-ion collision experiments with fine steps scanning on the energy and system size, with acceptance coverage close to four-pi geometry, and providing high performance in particle identification and energy resolution, are required. Four places in the world can compete in this research: BES RHIC (Brookhaven), SPS CERN (Geneva), FAIR (Darmstadt) and NICA JINR (Dubna). The NICA collider (Fig.2) will be the 3rd generation heavy-ion machine which provides ion beam collisions of average luminosity up to 10^{27}cm^{-2}s^{-1} at the energies of $\sqrt{s_{NN}}$ ~ (4 – 11) GeV. The NICA collider will operate with the Multi-Purpose Detector (MPD) allowing to accumulate high statistics data starting in 2019. The experiment Baryonic Matter at Nuclotron (BM@N) is planned to start data taking already in 2015 in the ion beams up to 5.8 GeV/u for A/Z = 2, extracted from the Nuclotron (superconducting synchrotron operating at JINR since 1993).

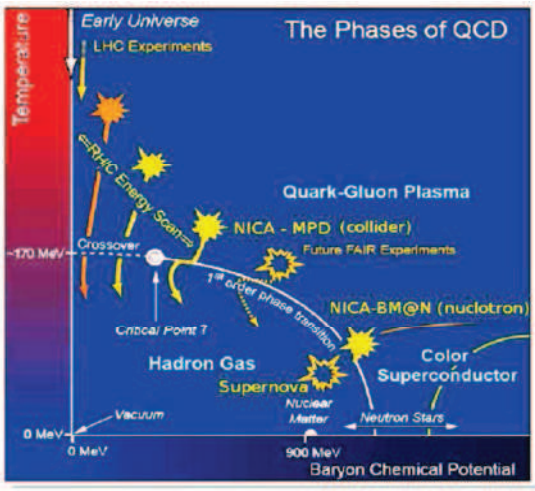

Fig. 1: NICA domain for the exploration of the QCD phase structure

For the discovery of signatures of a first order phase transition in the QCD phase diagram as well as a critical endpoint the relevant cms energy range must be rather low, $\sqrt{s_{NN}}$<15 GeV. Collider experiments are advantageous for such beam energy scan due to their almost homogeneous coverage of the phase space. This poses a challenge for the development of high-luminosity collider experiments at these energies.

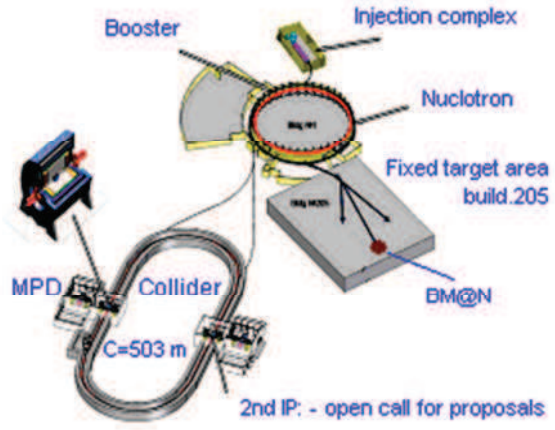

Fig. 2: Layout of the NICA facility with its main components

Both, the BM@N and the MPD experiments, are operated with the ion beams (from protons and deuterons up to the gold) at the indicated energy range. The Nuclotron has been recently modernized in order to provide better beam quality and higher intensities for the envisaged experimental programs. Parameters of the Nuclotron facility are given at http://nucloweb.jinr.ru/index.htm. Further details are given in the MPD conceptual design report (http://nica.jinr.ru/) and in the NICA White Paper (http://theor.jinr.ru/twiki-cgi/view/NICA/WebHome).

The NICA collider will also provide polarized proton and deuteron collisions up to $\sqrt{s}$ = 26 GeV and 12.5 GeV/u, respectively, with the average luminosity of 10^{31} cm^{-2} s^{-1}. It is foreseen at the second stage of the project realization. The Spin Physics Detector (SPD) experiments, proposed at the second interaction point of the NICA collider, will have a number of advantages for DY measurements related to nucleon structure studies. Such possibilities permit for the first time to perform comprehensive studies of all leading twist PDFs of nucleons in a single experiment with minimum systematic errors.

NICA is the flagship project in high energy physics at JINR Dubna. Its realization is funded by the JINR member countries and associated members as well. In addition, the NICA project is included in the list of "Mega-Science" projects of the Russian Federation, which are proposed for funding from the dedicated

budget. All this provides main confidence of the NICA project realization.

For many decades JINR participates in all major particle physics experiments with intellectual and financial contributions (CERN, FNAL, BNL, DESY, GSI, FZJ, INFN, IN2P3, GANIL, PSI, and others). Besides the professional experience, the JINR has created a variety of educational programs for training the young generation of scientists. Particularly strong are the ties with the FAIR program and its development from which synergy effects arise. This potential forms the intellectual basis for the NICA project with its experiments BM@N and MPD.

The experiments at NICA are prepared by the international collaborations. JINR as an international and intergovernmental institution provides an excellent basis for their activity. Besides this, strong international research alliances are already formed for support of the NICA construction. The NICA project realization attracted international interest indicated in the list of official protocols of bilateral cooperation. The proposed physics at NICA is collected in the NICA White Paper, which comprises contributions from 140 scientists of 70 institutions in 24 countries at present:

(http://theor.jinr.ru/twiki-cgi/view/NICA/WebHome)**.**

The NICA complex will provide unmatched possibility to carry out experiments for studying hot and dense nuclear matter under extreme conditions, which are not available at other accelerator centers around the world in the energy region optimal for this task. The relevance and high significance of the scientific program agenda of the NICA project is proved by the investigations under implementation at the RHIC collider (USA) and also by the research program at the accelerator complex FAIR, which is under construction at Darmstadt (Germany). The FAIR accelerator complex is complementary to NICA with respect to the range of energies and the beginning of operation, but it uses the different method – extracted ion beams on the fixed targets. In opinion of the international scientific community and in accordance with the established practice, the competiveness of independent projects is the guarantee of reliability of the obtained results.

The infrastructure of the project within the Laboratory's territory includes the distributed system of collective use of the accelerator complex, experimental facilities, taking and processing large amount of experimental data, the supply system of the complex. The infrastructure involves provision for necessary conditions for efficient collective work of scientists and specialists, representatives of dozens of states from research institutes from around the world, which are involved in the scientific and innovation programs implementation.

The presence of an international research center with the advanced complex of unique modern facilities aimed at fundamental and applied research in Russia will encourage the formation of a new focus of interests for the talented youth from around the world.

Megaprojects such as experiments at the Large Hadron Collider and the collider NICA require development of a distributed data-processing network (so called GRID). It enables scientists to work with experimental data at all stages of experiments not only at the place of an experiment performance but at all collaborating institutes and research centers provided that they are integrated into the GRID system. Such a system is under active development at JINR.

As a result of the NICA project implementation a unique, unparalleled complex will be created comprising linear accelerators, several superconducting accelerator rings and experimental setups, which are based on advanced technologies.

Thus, the NICA complex construction and the implementation of its research program will allow Russia and the JINR member states to participate on equal terms in the development and implementation of the world's joint program on research with heavy ion and high energy polarized particle beams and will provide favorable conditions for the complex's natural integration into the world's research infrastructure.

Nazarbayev University Research Accelerator (NURA): A New Linac for WDM, HEDP and HIF Investigations

A. Tikhonov[1], A. Urazbayev[1], M. Kaikanov[1], J.W. Kwan[1], E. Henestroza[1], and W. Waldron[2]
[1]Nazarbayev University, Kabanbay batye ave. 53, 010000 Astana, Kazakhstan; [2]LBNL, Berkeley, CA 94720, U.S.A.

Introduction

Nazarbayev University in Astana, Kazakhstan is planning to build a new accelerator facility for studying WDM/HEDP physics as part of their inertial fusion energy research program. This new accelerator, named as Nazarbayev University Research Accelerator (NURA), is conceived to be an induction linac with architecture similar to the NDCX-2 (Neutralized Drift Compression eXperimet) at LBNL [1]. In some ways different than NDCX-2, the initial NURA conceptual design will use helium ions instead of lithium ions, and optimized with electrostatic quadrupole focussing instead of pulsed solenoids. This paper provides a brief description of the beam line and updated design considerations. More details can be found in Reference [2].

The Beam Parameters

Our goal is to adequately heat a mm-size spot on a micrometer-thick solid target to a final temperature of 1 eV using a sub-nanosecond ion beam pulse [3]. The amount of heat required is 50 mJ.

Recent experience at NDCX-2 found that the current density and durability of a lithium alumino-silicate ion source were unsatisfactory. Since the Bragg Peaks for He+ and Li+ ions in gold are correspondingly at 1.25 MeV and 3 MeV, a helium beam machine will require less kinetic energy but more ion charge on target. Heating of the foil material is uniform if the ion beam pulse is relatively short compared to the hydrodynamic expansion time of ~ 1 ns. For a 1.2 MeV helium ion, ~700 keV is deposited uniformly in a 1 μm foil, and the ion will exit with a remnant energy of 500 keV which can be utilized for diagnostics. In general, there can be a range of target temperatures and densities achieved depending on target composition and focal spot intensity profile.

In comparison to the original NDCX-2 parameters (40 nC of Li+ at 3 MeV), NURA will produce 70 nC of He+ at 1.2 MeV. For design purpose, we assume a transverse normalized emittance of ~ 1 π mm·mr from the ion source and may increase up to 2x as the beam is transported through the linac. For longitudinal emittance, the initial beam pulse length is a few hundred ns at the ion source and will be compressed during acceleration and neutralized drift compression to less than 1 ns at the target [4]. The beam current at the ion source would be 250 mA with a pulse length of 280 ns.

The Linac Design

NURA can adopt an ESQ injector similar to the one for the earlier ELISE project [5] which had demonstrated 0.46 A of K+ ion beam current at 1.8 MeV using a 10-cm diameter hot plate ion source (later increased to 0.8 A when using a 17-cm diameter source).

The induction cells used in NDCX-2 were refurbished from the previous ATA machine by replacing the original dc solenoid with pulsed solenoid, but keeping the ferrite core unaltered. The maximum bore diameter is 22.2 cm, which will be used as the ground pipe diameter for designing NURA's ESQ modules. The standard rule of R/a = 1.146 is used where R is the quadrupole electrode radius and a is the aperture radius. At this ratio, the dodecapole component of the focusing electric field is zero. The result is an aperture radius of 4.0 cm. The half-lattice period is 27.9 cm based on the ATA cell housing length, thus the length of the quadrupole rods can be 15 cm to provide an ESQ occupancy ratio of 54%.

As the helium beam is accelerated from 0.5 MeV, 0.25 A, 0.050 μC/m (at the injector exit) to 1.2 MeV, 1.25 A, 0.15 μC/m (at the end of accelerator), the corresponding quadrupole voltages will increase almost linearly from +/- 30 kV to +/- 63 kV. Therefore, the quadrupole rods should have a clearance spacing to ground potential of up to 2 cm to prevent electrical breakdown. There is a 6 cm axial spacing to allow for electrical connections in each module. The field from the accelerating gap is partially shielded from the quadrupole field by limiting the aperture size at the ground plates.

There will be 12 induction cells in the linac. The first 5 pulsers will deliver voltage ramps (0-->Vmax) where Vmax=110, 112, 114, 116, and 118 kV. The next 4 pulsers will deliver flat-top constant voltages of V= 60, 60, 60, and 50 kV. Then the 3 remaining pulsers will deliver reverse ramps (Vmax-->0) where Vmax=110, 120 and 140 kV. This accelerating schedule will accelerate the ion beam from 0.5 MeV (injector output) to 1.25 MeV while compressing it from 280 ns to 56 ns before reaching the Final Focus Section.

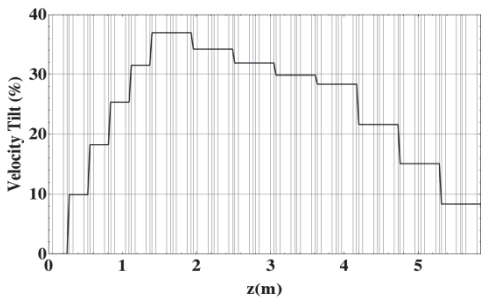

Figure 1: Velocity tilt profile for the NURA accelerator. The vertical thin lines show the locations of the gaps (narrow spaces) and quadrupoles (wider spaces).

The "velocity tilt", defined as ΔV/V, with the beam bunch tail going faster than the head, peaks at 37% for beam compression and then reduces to 8% when exiting the linac going into the neutralized drift compression section. The velocity tilt history is shown in figure 1. Figure 2 shows the beam pulse length being compressed from 280 ns to 56 ns, thus a corresponding 5 times increase in beam current from 0.25A to 1.25A.

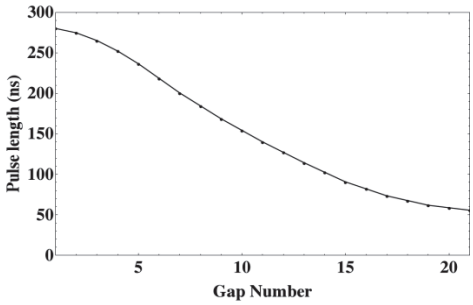

Figure 2: Compression of beam pulse length in the linac.

The preliminary physics design presented here does not include detailed accelerating waveforms, therefore we estimate the longitudinal dynamics based on the experience from NDCX-2 physics design. With a velocity tilt of 8% at the end of the accelerator, i.e., when entering the Neutralized Drift Compression section, it will take 700 ns for the beam to compress from 56 ns to 0.5 ns. At 1.2 MeV, a helium ion will travel a distance of 5.32 m in 700 ns and the corresponding beam bunch length when entering the neutralized section is 43 cm. Adding another 20 cm for the length of the final focus solenoid, therefore a total length of 6 m of Neutralized Drift Compression section is required.

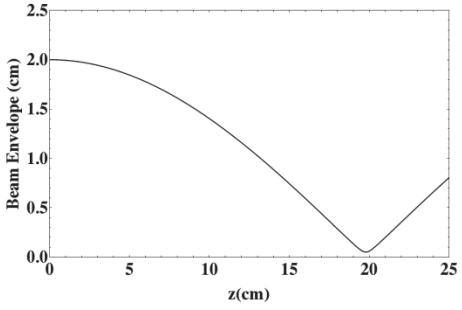

Figure 3: Using a 5-T solenoid for final focusing to a spot radius of 0.5 mm.

It can be calculated that a 20 cm long, 5 Tesla solenoid can be used to do the final focusing of a neutralized, 1.2 MeV helium beam of ~2 cm radius, with a normalized emittance of ~2 π-mm·mr (80 π-mm·mr unnormalized) down to a final spot radius of 0.5 mm. In this case, the aperture radius of the solenoid should be about 3 to 4 cm to avoid non-linear fields. The beam envelope is shown in figure 3

Alternate Concepts

Since the point design as described above did not use the maximum available volt-seconds for acceleration, or use the maximum quadrupole voltages (near breakdown limits), there is room to modify the design to match other target materials and other ion beam species in order to achieve desirable WDM conditions. The base design can also be modified to consider other types of injectors or focusing elements.

At present, we are also considering accelerator architecture based on the single-gap pulsed-power designs of the earlier Light-ion Fusion Project [6]. This option can reach high power areal densities to heat up thicker targets to WDM conditions in a compact configuration and possibly at a modest cost.

Summary

A research facility at Nazarbayev University, Kazakhstan, called "NURA", is currently being designed for studying WDM/ HEDP. The machine is similar to NDCX-2 at LBNL by using an induction linac, but with the differences of using helium ions and ESQ beam transport. It will be designed to allow the flexibility of adding laser heating beam in combination with the ion beam.

The linac consists of a 1.25 m long 500 kV injector, a 6 m long 1.2 MV induction linac, and a 6 m long neutralized drift compression section. The preliminary design shows the potential that 70 nC of He+ ions can be accelerated to 1.2 MeV and compressed to a 0.5 mm spot radius and 0.5 ns pulse length for heating a 1 μm gold foil to above 1 eV. It is hoped that with more optimization (e.g., running WARP-3D simulations to acquire a more dynamic acceleration schedule customized for the short beam pulse), the performance can be further improved.

References

[1] Waldron, W.L., & Kwan, J.W. Status of the neutralized drift compression experiment (NDCX-II), Proc. 2011 Par-ticle Accelerator Conference, New York, NY, March 2011, pp.1939–1941.

[2] K. Baigarin, et al., Planning of a New Research Facility for HEDLP Studies in Kazakhstan, Proc. 20th international symposium on Heavy-ion Inertial Fusion, HIF-2014, Lanzhou, China, August 11, 2014

[3] Barnard, J.J. et. al. NDCX-II target experiments and simulations, Nuclear Instruments and Methods in Physics Research A, v.733, p. 45-50, (2014)

[4] A. Friedman, et al. Beam dynamics of the Neutralized Drift Compression Experiment-II, a novel pulse-compressing ion accelerator, Phys. Plasmas, 17, DOI: 10.1063/1.3292634. (2010)

[5] Bieniosek, et. al., 2-MV ESQ Injector for Heavy Ion Fusion, Physical Review Special Topics (PRST) Accelerators and Beams, 010101, (2005)

[6] H. Bluhm et al, "Experiments on KFK'S Light Ion Accelerator KALIF", Proc. of the 5th IEEE Pulsed Power Conference, Arlington (1985), p.114/I17

Progress Towards Indirect Drive ICF Ignition on the National Ignition Facility*

The ICF Program Collaboration[1-11]

[1] *Lawrence Livermore National Laboratory, Livermore, CA, USA*
[2] *Laboratory of Laser Energetics, University of Rochester, Rochester, NY, USA*
[3] *General Atomics Corporation, La Jolla, CA, USA*
[4] *Los Alamos National Laboratory, Los Alamos, NM, USA*
[5] *Sandia National Laboratories, Albuquerque, NM, USA*
[6] *Massachusetts Institute of Technology, Cambridge, Massachusetts, USA*
[7] *Atomic Weapons Establishment, Aldermaston, Reading, Berkshire, UK*
[8] *Commissariat à l'énergie atomique et aux énergies alternatives (CEA), France*
[9] *National Security Technologies, LLC (NSTec), Livermore, CA, USA*
[10] *University of California, Berkeley, Berkeley, CA, USA*
[11] *Duke University, Durham, NC, USA*

A primary goal of the Inertial Confinement Fusion (ICF) Program on the National Ignition Facility (NIF) is to implode a low-Z capsule filled with 0.2 mg of deuterium-tritium (DT) fuel with > ~370 km/s velocity via laser indirect drive ICF and demonstrate fusion ignition and propagating thermonuclear burn with net fusion energy gain (fusion energy/laser energy >1). This requires assembling the DT fuel at implosion stagnation into a dense ~1000 g/cc shell with an areal density of ~1.5 g/cm^2 surrounding a lower density hot spot with ~10 keV temperature and ~ 0.3 g/cm^2 areal density.

On the NIF, prior to performing high yield DT implosions, a suite of precision experiments using DT capsule surrogates are assessing crucial parameters for ignition such as imploding capsule shape, shock timing, implosion velocity and the ablator-fuel mix. The 2009-2012 National Ignition Campaign (NIC) focused on developing and improving these experiments and on assessing the performance of high convergence (>40) low fuel adiabat implosions of plastic (CH), DT-filled capsules driven by a 4-shock laser pulse (Fig. 1) [1].

These experiments, despite reaching 80-90% of required parameter values for ignition, have shown typically only ~ 1-10% of the predicted DT yield. The low yield was attributed to ablation front instabilities, causing fuel-ablator mix and asymmetry reducing the hot spot pressure. Recent experiments have employed a different "High Foot", higher adiabat, 3-shock laser pulse to drive the same target. These implosions with relaxed convergence (~ 35) have shown low mix and have resulted in performance similar to calculations with record neutron yields that in some cases have exceeded the kinetic energy coupled to the DT fuel [2]. They have also demonstrated a significant contribution of α-particle self-heating to the yield - a crucial stepping stone in our quest towards fusion ignition [2] (Fig. 1).

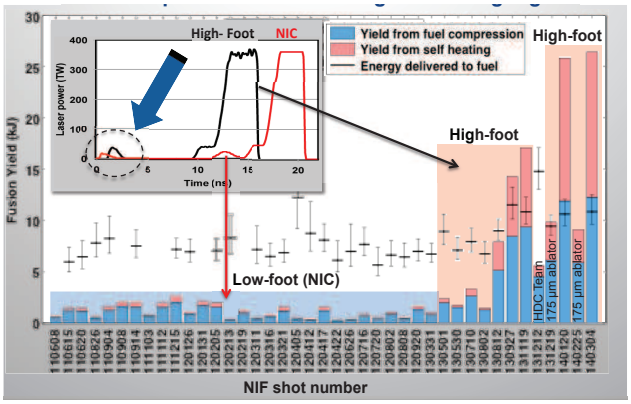

Figure 1. Neutron yield and energy delivered to fuel of NIC and HiFoot DT implosions [1], [2].

Further increases in capsule performance will require higher convergence and higher velocity implosions with improved symmetry while maintaining low mix. Focused physics experiments are underway to better understand key target physics to chart a path forward. Some of these paths consider laser pulse adiabat shaping, diamond (HDC) and beryllium ablators as well as hohlraums with alternate geometries. This talk highlights a summary of past and future ICF studies on the NIF.

*This work was performed under the auspices of the U.S. Department of Energy by LLNL under Contract DE-AC52-07NA27344.

References

[1] M.J. Edwards et al, *Phys. Plasmas* **20**, 070501 (2013).
[2] O. Hurricane et al, *Nature* **506**, 343 (2014).

Contact E-mail: dewald3@llnl.gov

The Kumgang Laser : a High-Power, High-Repetition Rate Beam Combination Laser*

Hong Jin Kong[1,#], Heekyung Ahn[1], Seongwoo Cha[1], Hwihyeong Lee[1], Jungsuk Oh[1], Sangwoo Park[1], Soungwoong Choi[2], Bong Ju Lee[2], and Jom Sool Kim[3]

[1]KAIST, Daejeon, Republic of Korea; [2]Handong Global University, Pohang, Republic of Korea; [3]Laser Spectronix, Seoul, Republic of Korea.

In this report we introduce the Kumgang laser and its current status. It is a 4 kW beam combination laser combining four 1 kW beams using self-phase controlled stimulated Brillouin scattering phase conjugate mirrors (SC-SBS-PCM). If the Kumgang laser functions successfully, it will be the most important step towards a Dream laser, a hypothetical laser with unlimited power and a high repetition rate

Beam Combination Laser

Beam combination can contribute to the development of high-power, high-repetition-rate lasers. There are two main lines of research in beam combination, namely beam combination of fiber lasers and beam combination of bulk lasers. Bulk lasers have higher output power and a relatively small number of lasers are needed to achieve high power and a high repetition rate. But the high-power bulk lasers tend to have lower beam quality than the fiber lasers. To coherently combine bulk lasers, one should flatten the wavefront of the combining beams via active control or passive control. Double-pass amplification with the stimulated Brillouin scattering phase conjugate mirror (SBS-PCM) as the back reflector is a simple passive method to control the wavefront of the combining beam. But the phase of the reflected beam from the SBS-PCM is inherently random.

H. J. Kong, the main author of this paper, proposed the simplest technique for controlling the phase of an SBS-PCM[1]. A beam combination laser using this 'self-phase controlled' SBS-PCM (SC-SBS-PCM) is indefinitely scalable because the combining beams are not optically interconnected.

Kumgang Laser

A project for a 4 kW beam combination laser system using SC-SBS-PCMs began in 2012 and the laser is called 'Kumgang', meaning diamond (or very important) in Korean[2,3]. Four sub-beams, each with an energy of 0.1 J/10 ns pulse width and a repetition rate of 10 kHz, are coherently combined to produce an output beam with an energy of 0.4 J. It is a master oscillator power amplifier (MOPA) system and all of its pre and main amplifiers are diode-pumped Nd:YAG amplifiers. The project will be completed by the end of 2015 and its first application will be a patterned 2D laser cutting of printed circuit board (PCB) substrate.

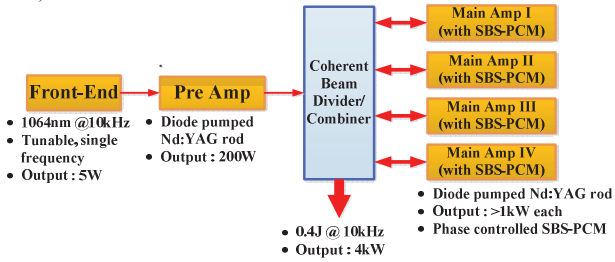

Figure 1: The schematic diagram of the Kumgang Laser.

Figure 1 shows the schematic diagram of the Kumgang laser. The front end consists of a CW laser-diode master oscillator, an acousto-optic modulator (AOM) for 10 kHz pulse generation, fiber-based amplifier(s), and a regenerative amplifier for boosting the power. The average output power of the front end is 5 W [0.5 mJ/10 ns/10 kHz]. Diode-pumped Nd:YAG amplifiers in the pre-amplifier stage amplify the beam in a double-pass configuration. The output beam of the pre-amplifier stage has a power of 200 W [20 mJ/10 ns/10 kHz].

The coherent beam divider/combiner divides the beam from the pre-amplifier stage and combines the beams after amplification through the main amplifier stage. The volume Bragg grating (VBG) is currently being researched. A polarization beam splitter (PBS) will be used before the VBG is developed.

The main amplifier stage is composed of a diode-pumped Nd:YAG amplifier chain and an SC-SBS-PCM. When completed, each divided sub-beam from the coherent beam divider/combiner will be amplified to 1 kW with a double-pass configuration. After the coherent combination, the final output beam will have an energy of 400 mJ per pulse with a pulse width of 10 ns and a repetition rate of 10 kHz, making the average output power 4 kW.

References

[1] H. J. Kong, S. K. Lee, and D. W. Lee, Laser Part. Beams 23 (2005) 107.

[2] H. J. Kong, S. Park, S. Cha, H. Ahn, H. Lee, J. Oh, B. J. Lee, S. Choi, and J. S. Kim, High Power Laser Science and Engineering, to be published.

* Work supported by Republic of Korea, Agency for Defense "Dual-Use Technology Program" (UM12012RD1)

#hjkong@kaist.ac.kr

Short-Pulse Ion Beams for Discovery Science at Berkeley Lab*

P.A. Seidl[1], A. Persaud[1], T. Schenkel[1], W.L. Waldron[1], H. Guo[1], J.J. Barnard[2], A. Friedman[2], D. Grote[2], R. Davidson[3], E. Gilson[3], I. Kaganovich[3]

[1] *Lawrence Berkeley National Laboratory, Berkeley, CA, U.S.A.,*
[2] *Lawrence Livermore National Laboratory, Livermore, CA, U.S.A.,*
[3] *Princeton Plasma Physics Laboratory, Princeton, NJ, U.S.A.*

We have commenced experiments with intense short pulses of ion beams on the Neutralized Drift Compression Experiment (NDCX-II) at Lawrence Berkeley National Laboratory, by generating r < 1 mm beam spots within 2.5 ns FWHM. The Li^+ ion kinetic energy is 1.2 MeV. To enable the short pulse durations and mm-scale focal spot radii, the beam is neutralized in a 1.5-meter drift compression section following the last accelerator magnet. An 8-Tesla short focal length solenoid focuses the beam in the presence of the volumetric plasma near the end of this section before the target.

Results from the initial tuning of the integrated accelerator and drift compression section are shown in Fig. 1.

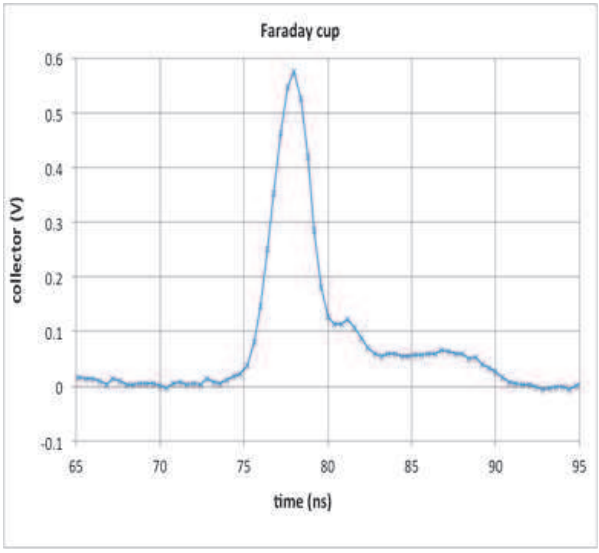

Figure 2: Current collected by the Faraday cup at the focal plane. The peak current is ≈ 0.5 Ampere and the pulse duration is 2.5 ns FWHM. The Faraday cup has a <1 ns time response due to a short transit time through the structure and low stray capacitance.

In the accelerator the line-charge density increases due to the velocity ramp imparted to the beam bunch in the accelerator [1,2]. The transverse distribution is characterized by a thin Al_2O_3 scintillator and gated image-intensified CCD camera. The beam distribution is peaked with 80% of the charge within a radius of 0.8 mm.

To date, the charge in the compressed bunch is only 1-2 nC since the freshly refurbished Li^+ ion source is still conditioning upward toward previously demonstrated emission of ≈50 nC in ≈1 μs [3]. We are aiming for ≥ 30 nC while maintaining a small focal spot and bunch duration. These results show that all the induction accelerator components are functioning as designed. The 28 pulsed, accelerator solenoids operate up to 3 Tesla. The compression and acceleration waveforms of the 12 induction cells are driven by pulse forming networks or Blumlein transmission line pulsers. The Blumleins supply up to 200-kV, 70-ns pulses to the induction cells and associated acceleration gaps, providing most of the acceleration in 5 cells.

The scientific topics to be explored are warm dense matter, the dynamics of radiation damage in materials [4], and intense beam and beam-plasma physics including select topics of relevance to the development of heavy-ion drivers for inertial fusion energy [5].

Since the ion range is short, such beams will push micron-thick targets into the warm-dense matter state on a ns timescale. Below the transition to melting, the short beam pulses offer an opportunity to study the dynamics of radiation-induced damage (ionization cascades) in crystalline materials.

Diagnostics for studying the transient conditions of the bombarded targets may include probe laser transmission and reflection, time resolved spectroscopy of beam-induced emission from the target material, and time of flight and energy analysis of the transmitted ions. The experimental setup is flexible and the facility will be open to outside users in 2015.

References

[1] A. Friedman et al., Phys. Plasmas 17 (2010) 056704.
[2] W.L. Waldron, et al., Nucl. Inst. Meth. A V733 (2014).
[3] P.A. Seidl et al., Phys. Rev. ST – Accel. Beams 15 (2012) 040101; A.I. Warwick, IEEE NS 32 (1985) 1809.
[4] T. Schenkel et al., Nucl. Inst. Meth. B V315 (2013) 350–355
[5] R.O. Bangerter, A. Faltens, P.A. Seidl, Reviews of Accelerator Science and Technology V6, 85-116 (2013).

* This work was supported by the Office of Science of the US Department of Energy under contract no. DE-AC02–05CH11231.

Status of the Figure-8 Storage Ring - F8SR Project

J.F. Wagner[*1], *A. Ates*[1], *M. Droba*[1], *O. Meusel*[1], *H. Niebuhr*[1], *D. Noll*[1], *and U. Ratzinger*[1]
[1]Goethe University Frankfurt, Frankfurt am Main, Germany.

The F8SR project for beam storaging of high currents (1-10A) in the low energy range (150keV-1MeV) is in ongoing development. R&D concentrated on ion filter experiments and beam instrumentation as well as particle simulations in strong longitudinal magnetic fields.

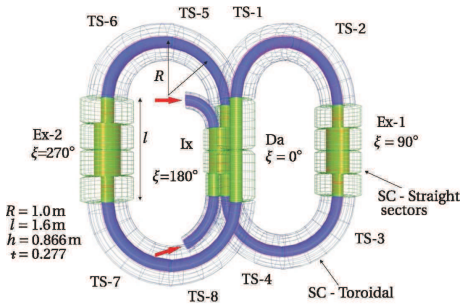

Figure 1: F8SR - latest design.

The scaled down room temperature experimental setup [1] was upgraded with a new type of ion filter system and a second injector [3]. For the filter system a solenoid was combined with a drift tube and an aperture flange at its end. Using the focussing of the solenoid one can adjust the focal point of a desired ion species to match the aperture, e.g. H^+,H^{2+},H^{3+}. The beam loss of the undesired ion species can be measured due to the loss current at the insulated drift channel. Therefore one gets information about the beam constituents comparing these losses with Faraday Cup measurements in front of the ion source and right behind the aperture, see fig. 2. With the second injector and the filter system the objective will be performing injection experiments.

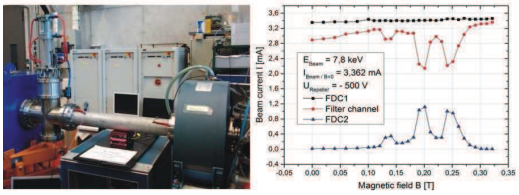

Figure 2: left: Filter channel setup; right: Hydrogen beam current measurements.

The designed non destructive photodiodes detector [2], see fig.3, for high magnetic fluxes was enhanced due to an automized analog-to-digital data aquisition interface (ms range) and a beam reconstruction signal transformation method. Experimental results were able to determine the transverse ion beam position and roughly the size within seconds.

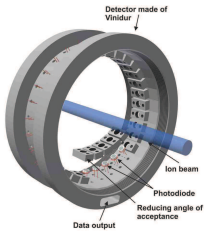

Figure 3: Design view of the photodiodes detector.

The simulation studies for the latest superconducting coil design, see fig.1 adressed the injection concept and higher order field errors. Particle simulations in superposition of the longitudinal magnetic field with multipole fields showed channels of stable beam transport and loss areas.

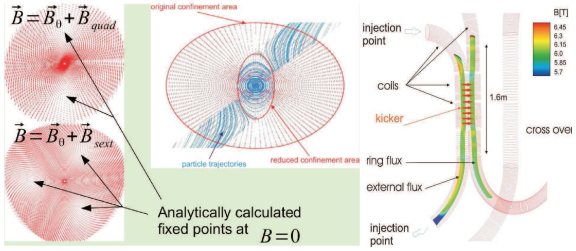

Figure 4: left: Multipole error simulations; right: Proposed injection scheme.

Further more a hyperbolic injection channel was investigated to compensate undesired particle gyrations and drifts. For the injection system simulations of a electromagnetic ExB kicker were performed to estimate the beam behaviour concerning beam shift and beam potential, see fig.5,[3].

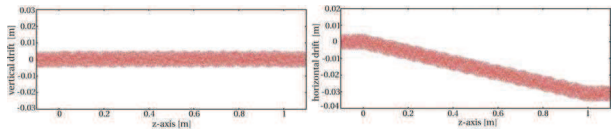

Figure 5: Estimated ExB kicker drifts.

References

[1] N.Joshi et al., Proc. of IPAC'10, Kyoto, Japan, THPEB005.

[2] M.Droba et al., Proc. of IPAC'11, San Sebastin, Spain, WEPS004.

[3] M.Droba et al., Proc. of IPAC'14, Dresden, Germany, TUPRO045.

* j.wagner@iap.uni-frankfurt.de

2 Plasma Physics Experiments with Ion and Laser Beams

Commissioning of the PRIOR prototype*

D. Varentsov[1], *O. Antonov*[2], *A. Bakhmutova*[3], *A. Bogdanov*[3], *C.R. Danly*[4], *S. Efimov*[2], *M. Endres*[5], *A.A. Golubev*[3], *D.H.H. Hoffmann*[5], *A. Kantsyrev*[3], *Ya.E. Krasik*[2], *P.M. Lang*[5], *F.G. Mariam*[4], *N. Markov*[3], *F.E. Merrill*[4], *V.B. Mintsev*[6], *V. Panyushkin*[3], *M. Rodionova*[1,5], *L. Shestov*[1,5], *V. Skachkov*[3], *S. Udrea*[5], *K. Weyrich*[1], *C. Wilde*[4], *and A. Zubareva*[6]

[1]GSI, Darmstadt, Germany; [2]Technion, Haifa, Israel; [3]ITEP, Moscow, Russia; [4]LANL, Los Alamos, USA; [5]TUD, Darmstadt, Germany; [6]IPCP, Chernogolovka, Russia

PRIOR (*Proton Microscope for FAIR*) is one of the three frameworks proposed by the HEDgeHOB collaboration for the future experiments at FAIR. This worldwide unique high energy proton microscopy (HEPM) facility will be integrated into the HEDgeHOB SIS-100 beam line and employ high energy $(3-10\,\mathrm{GeV})$, high intensity $(2.5\cdot10^{13}\,\mathrm{ppp})$ proton beams for fascinating multidisciplinary research such as experiments on fundamental properties of materials in extreme dynamic environments generated by external drivers (pulsed power generators, high energy lasers, gas guns or HE generators) prominent for materials research and high energy density physics as well as the PaNTERA (*Proton Therapy and Radiography*) experiment, with a great relevance to biophysics and medicine.

Recently, as a result of the international effort of a team of scientists from GSI, LANL, ITEP and TUD a PRIOR prototype has been designed, constructed and installed at the HHT area of GSI (Fig. 1(left)). The PRIOR prototype employes high-gradient NdFeB permanent magent quadrupole (PMQ) lenses developed by ITEP and provides a magnification of $\approx4-5$ with a field of view of $\approx15\,\mathrm{mm}$.

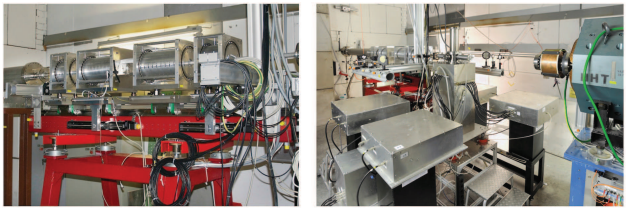

Figure 1: The PRIOR prototype PMQ lenses (left) and the UEWE setup (four high-current generators placed around a small explosion chamber) followed by the four PRIOR lenses (right) installed at the HHT area of GSI.

The detector (image collection) system developed by LANL was installed in the newly constructed concrete-shielded detector room $\approx 9\,\mathrm{m}$ downstream the target location. With a pellicle / mirror arrangement, the system employes two cameras simultaneously: a high resolution (4 Mp) CMOS camera (PCO DIMAX HS) used mainly for static experiments and a fast intensified CCD camera (PCO DICAM PRO) for dynamic measurements. $10\times10\,\mathrm{cm}$ columnar CsI and plastic BC-400 scintillators were installed for static and for dynamic measurements, respectively.

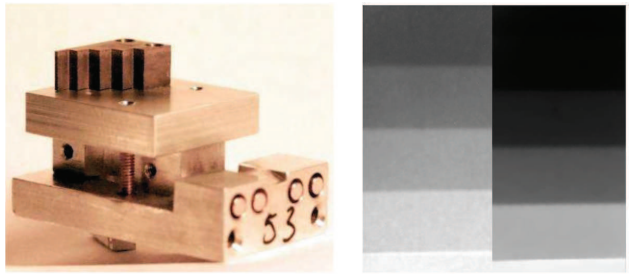

Figure 2: Tantalum step wedge object on a target table (left) and PRIOR proton radiographs (right) of the identical copper and tantalum step wedge objects ($0.56\,\mathrm{mm}$, $2.06\,\mathrm{mm}$, $4.07\,\mathrm{mm}$ and $6.05\,\mathrm{mm}$ step thicknesses).

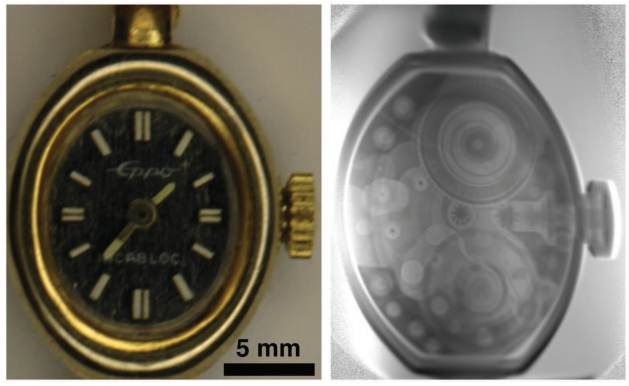

Figure 3: A small women mechanical wrist watch (left) and its proton radiograph (right) obtained with the PRIOR prototype using a 3.6 GeV SIS-18 proton beam at GSI.

In April 2014, an experimental campaign for the commissioning of the PRIOR prototype employing $3.5-4.5\,\mathrm{GeV}$, moderate $(10^8-10^9\,\mathrm{ppp})$ intensity proton beams from the SIS-18 synchrotron took place at GSI. In these experiments a large set of small static objects including step wedges (Fig. 2) and sets of wires made of different metals, resolution and matching tuning targets as well as some fancy objects (Figs. 3 and 4) were used in a vacuum target chamber equipped with a 6-axis manipulator. As a result of these experiments, an rms spatial resolution of the prototype of about $30\,\mu\mathrm{m}$ with a remakrable density sensitivity has been demonstrated. It has also been shown that with

* Work supported by GIF grant No. 1132-11.14/2011, BMBF grants No. 05K10RD1 and 05P12RDRBK, and FRRC research contract No. 29-11/13-17.

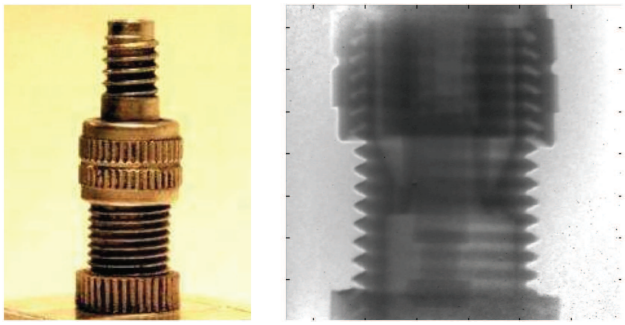

Figure 4: A presta valve from a bicycle inner tube (left) and a PRIOR proton radiograph of its central part (right). One can clearly see the engagement of the threads as well as the valve stem and the details of how this valve is seated.

a sufficient proton beam intensity ($10^{10} - 10^{11}$ ppp) and by using a fast plastic scintillator in the detector system, one can achieve $10\,\mathrm{ns}$ or better temporal resolution without significant degradaton of the imaging properties.

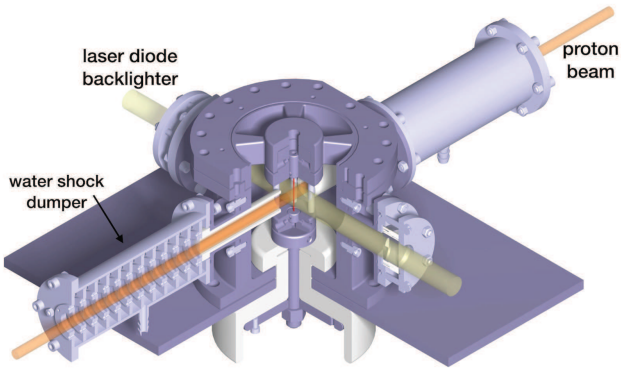

Figure 5: UEWE water filled target chamber. A thin exploding wire (red) in the center of the chamber is illuminated from one side by a proton beam for HEPM measurements, and from the other side — by an optical backlighter for shadowgraphy diagnostics.

For the dynamic commissioning of the PRIOR prototype, a new pulsed power generator had been developed by Technion and GSI (see Fig. 1(right)). This generator (up to $50\,\mathrm{kV}$, $12.5\,\mathrm{kJ}$ stored energy) was designed to generate warm dense matter states of various metals by underwater electric wire explosions (UEWE) for equation of state studies. A metallic wire ($30 - 50\,\mathrm{mm}$ length, $0.1 - 1\,\mathrm{mm}$ diameter) is placed in the middle of a $\approx 11\,\mathrm{cm}$ diameter explosion chamber (Fig. 5). The wire is quickly heated by a pulsed electric current ($\approx 200\,\mathrm{kA}$, $1.5 - 2\,\mu\mathrm{s}$ rise time) to a dense plasma conditions with about $2 - 3\,\mathrm{eV}$ temperature.

In addition to the HEPM measurements with the PRIOR prototype, an optical shadowgraphy setup consisting of a 450 nm, 4 W fiber-coupled laser diode backlighter, two fast intensified CCD cameras and a streak camera has been installed for target diagnostics. A special effort has been taken to design water shock dumpers in order to minimize the amount of material used to separate the UEWE explosion chamber and the vacuum ($10^{-3}\,\mathrm{mbar}$) PRIOR beam line as well as the water layer thickness in the proton beam direction (see Fig. 5).

In July 2014, a new experimental compaign aiming commissioning of the PRIOR prototype for dynamic experiments took place at GSI. In comparison with the April 2014 run, the proton beam intensity has been increased by more than two orders of magnitude (up to 10^{11} protons per pulse) and a new beam diagnostics for high energy protons (scintillator screens and cameras) has been integrated into the HHT beam line to ensure a good beam alignment and matching.

The dynamic PRIOR experiments have been carried out using the developed UEWE setup. In these experiments, a pulsed current ($\approx 40\,\mathrm{MA/cm^2}$, $5\,\mathrm{GW}$ deposited power) run through a tantalum wire ($0.8\,\mathrm{mm}$ diameter and $40 - 50\,\mathrm{mm}$ length) generating this way warm dense matter states charactarized by specific energy deposition level about $10\,\mathrm{kJ/g}$ and $\sim\mathrm{km/s}$ expansion velocities. An example of the proton radiography measurements of an exploding tantalum wire in shown in Fig. 6. In total, about twelve successfull dynamic shots with the PRIOR prototype has been made. In these shots, we have varied the power deposited in the $0.8\,\mathrm{mm}$ Ta wires as well as the time moment of the proton radiography imaging. The obtained data is currently being processed and analyzed.

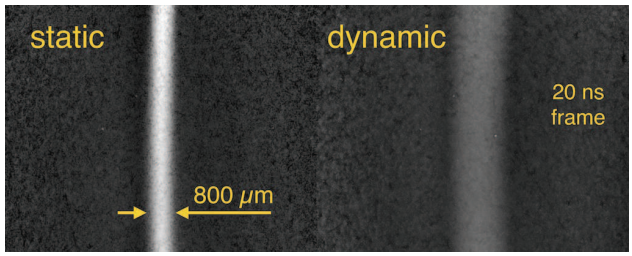

Figure 6: Proton radiographs (20 ns temporal resolution) of a tantalum wire in water before shot (left) and during the explosion (right) driven by the UEWE generator ($\approx 10\,\mathrm{kJ/g}$ specific energy deposition in Ta).

As an unexpected result of the commissioning experiments, we have observed a considerable image degradation caused by the radiation damage of the PMQ lenses (the reduction of the quadrupole strength and increased high-order multipole components) due to large fluences of spallation neutrons which are mainly produced in the tungsten beam collimator located in a close proximity to these permanent magnets. We have also performed special measurements and simulations to study this phenomenon. For the future applications of the PRIOR magnifier at FAIR where much higher proton beam intensities are expected we suggest to either consider using the samarium-cobalt (SmCo) PMQ magnets or, better, to design and employ high-gradient small-apperture radiation-resistant warm electromagnets. The corresponding desing study on the final construction of PRIOR for experiments at FAIR has been started.

The detector setup of the PRIOR proton microscope *

P.-M. Lang[1], *C. Danly*[2], *M. Endres*[1], *D.H.H. Hoffmann*[1], *F. Mariam*[2], *F. Merrill*[2], *M. Rodionova*[1,3], *L. Shestov*[1,3], *S. Udrea*[3], *D. Varentsov*[3], *K. Weyrich*[3], *and C. Wilde*[2]

[1]TU Darmstadt, Darmstadt, Germany; [2]LANL, Los Alamos, USA; [3]GSI, Darmstadt, Germany

Introduction

High energy proton microscopy (HEPM) is an imaging diagnostic technique to probe inner structure of high density materials. To aquire images by HEPM, it is necessary to convert the image information encoded in the proton beam to photons that can be registered by a camera. Moreover, to achieve a nanosecond time resolution, this has to happen on the same timescale.

The common converter in any HEPM setup is a crystal scintillator screen, usually easy to handle cesium iodide (CsI, τ=1000 ns) or lutetium orthosilicate (LSO, τ=50 ns). Each image taken from a faster process will look blurred.

To reach a time resolution below that, plastic scintillators have been studied, which are presumed to be not radiation hard but have a decay time τ on the level of 1 – 4 ns.

Plastic scintillator tests

A test piece of 5 × 5 × 0.1 cm BC–400 plastic scintillator has been irradiated with a 800–MeV proton beam at the proton radiography setup at the Los Alamos National Laboratory. A sequence of more than 400 images was taken, each image roughly corresponding to a incoming pulse of about 10^9 protons.

To quantify degradation during the experiment, light output and spatial resolution on a test object that was imaged on the scintillator have been looked at, both not showing any kind of degradation within the precision of the experiment (see [2] for more details). This lead to the use of plastic scintillators to study dynamic experiments with PRIOR at GSI (see [1]).

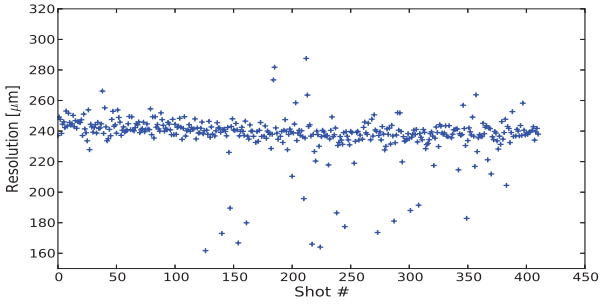

Figure 1: Evolution of spatial resolution of BC–400 under proton irradiation (here only shown along x–axis).

* Work supported by BMBF grants No. 05K10RD1 and 05P12RDRBK, FRRC contract No. 29-11/13-17 and MES of Russia contract No 14.616.21.0023

The PRIOR detector setup

The PRIOR detector setup consists of a 10 × 10 cm CsI or BC–400 scintillator as converter, a pellicle mirror that reflects the light out of the area hit by the beam and two cameras, a PCO DIMAX HS (2016 × 2016 pixels) and a PCO DICAM Pro (1280 × 1024 pixels). Both cameras can take images simultaneously. The DIMAX with its higher pixel number provides better spatial resolution, while the DICAM Pro with its intesified CCD provides the prossibility to take images with high time resolution of down to 5 ns via gating. Fig. 2 gives an overview of the setup at PRIOR.

Probing the bunch structure of the SIS–18

Before starting to set up experiments that require high time resolution, the feasibility to reach this time resolution was demonstrated by catching single bunches (or 10 ns parts of them) as they are extracted from the SIS–18 synchrotron that provides the proton beam for PRIOR (bunch width ≈50 ns FWHM). This lead also to the discovery of what causes the slightly irregular beamshape observed during the first commissioning experiments with PRIOR. Fig. 2 shows an image of each of the 4 bunches, the last one being clearly off axis compared to the others.

Overall it could be demonstrated that PRIOR is capable of recording high resolution images with exposure times of 10 ns and below.

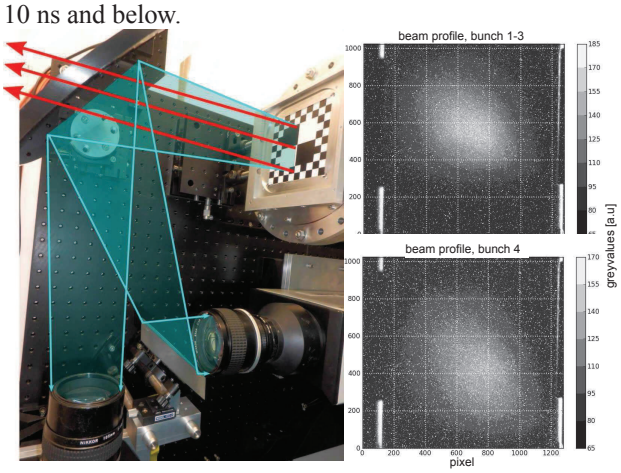

Figure 2: Left: Detector setup with scintillator and cameras. Right: Transversal beam profiles on the scintillator.

References

[1] D. Varentsov et al., "Commissioning of the PRIOR prototype", this report.

[2] P.M. Lang, "Aufbau und Test des Protonenmikroskops PRIOR", PhD thesis, Darmstadt, 2014

High Energy Electron Radiography for Imaging Diagnostic of HED Objects

Y. T. Zhao[1], Z. M. Zhang[1], W. Gai[2], C. X. Tang[3], S. C. Cao[1], Q. T. Zhao[1], R. Cheng[1], J. Q. Qiu[2], Y. C. Du[3], W.H. Huang[3], H. S. Xu[1], and W. L. Zhan[1]
1. IMP, Lanzhou, China; 2. ANL, Argonne, USA; 3. THU, Beijing, China

In general, high energy density matter can only be transiently produced in the laboratory on a time scale of nanoseconds. In addition, the pressure in a high energy density sample exceeds 1 Mbar (100 GPa), thus the hydrodynamic response of the sample is a high expansion velocity in the range of km/s (or μm/ns). Therefore diagnostics which are capable of high time resolution (< ns) and high space resolution (<10μm) are needed. Here we present a scheme that uses a high energy electron beam as a probe for dynamic imaging measurements of high energy density processes in materials with spatial, temporal resolution and frame rate in order of 1 μm, 1ps and 10^{10} FPS, respectively.

The device uses an electron bunch train with a flexible time structure, which can be produced by an e-LINAC (electron Linear Accelerator). A typical electron LINAC (e-LINAC, electron Linear Accelerator) is shown schematically in Figure 1. Beams with bunch intensity ranging from a few pC to 100 nC, and bunch length of 1ps even less can be generated, operating at RF frequencies in the 1-12 GHz range. A mode locked laser is used to produce a train of several electron bunches, with bunch interval as short as 100ps. State of the art technology allows the electron beam timing to be locked to a master clock with a timing jitter less than 1 ps. Normalized emittances from RF guns are typically 1 mm-mR/nC with about 1 % energy spread, which is suitable for high spatial resolution required in radiographic studies. The beam energy can be increased easily from a few MeV to GeV by adding more accelerating sections without any impact on the other beam parameters. Details can be found in [1].

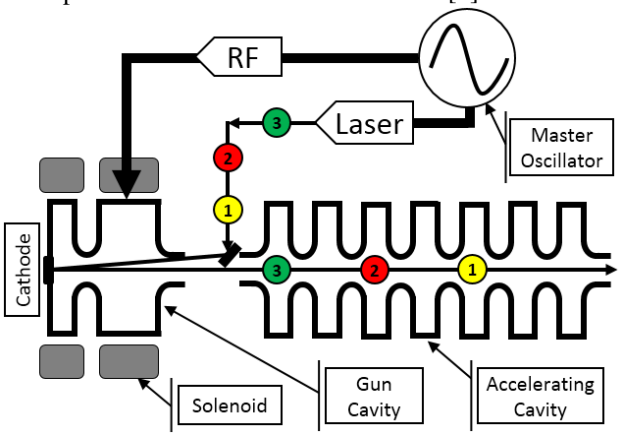

Fig. 1. A typical RF photocathode electron LINAC

With a flexible beam from such an e-LINAC, one can easily generate a bunch group of 3 or more electron beamlets separated by one or more RF periods. As shown in Figure 2, in order to image a target in the 3 orthogonal directions, here 3 beamlets will be set in one bunch group. When the beamlets exit the accelerator, they can pass through a 1/3 harmonic deflecting cavity and separate into three directions. With a septum magnet and achromatic matching beam lines, the three beamlets are then delivered to the target and image it in three orthogonal directions simultaneously. In addition, a second and third bunch group can be generated at arbitrary time delays and used for a time evolution study of the HEDP target to ps accuracy. Since it is not easy to find such a fast imaging screen with reasonable high fluorescence conversion efficiency in addition to such a rapid CCD camera for recording the sequence of the images, a new design similar with a streak camera is proposed as shown in the right hand side of figure 2. An RF deflector could be introduced after the magnet imaging system for spatially separating the images of individual time, sampling electron beamlets to different transverse positions on the screen.

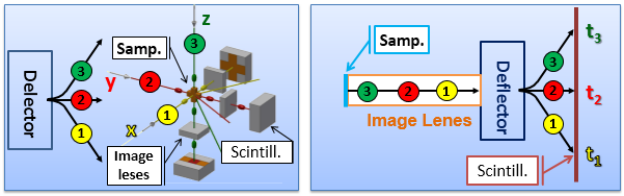

Figure 2. Initiative design for untra-fast 3D or multi-frame imaging system

In order to illustrate the system concept design and to guide a system test experiment, numerical simulations have been carried out, which show that for densities in the range up to 10^2 g/cm^3, or thickness up to several g/cm^2, an electron beam consisting of a train of ~ 800 MeV electron bunchlets with charges of ~ nC is suitable [2]. Successful demonstration of this concept will have a major impact for both future fusion science and high energy density physics research at HIAF (High Intensity heavy-ion Accelerator Facility, see ref. [3]) or elsewhere.

References

[1] J. G. Power, (2010), AIP Conf. Proc. 1299, 20
[2] Zhao Y. T. et al. *A high resolution spatial-temporal imaging diagnostic for high energy density physics experiments* to be submitted.
[3] Y. Zhao, et al, (2014) High Power Laser Science and Engineering, 2, e39 doi:10.1017/hpl.2014.44.

Beam transmission for a plasma stripper device*

G. Xu[1,2,3], J. Jacoby[1], Y. Zhao[2], G. Xiao[2], G. Loisch[1], T. Rienecker[1], A. Fedjuschenko[1], K. Cistakov[1], A. Blazevic[4], K. Weyrich[4], O. Rosmej[4], R. Cheng[2], J. Ren[2,3], A. Schönlein[1], J. Wiechula[1], T. Manegold[1], A. Kutschireiter[1], S. Zähter[1], R. Maeder[1], O. Haas[5], and M. Iberler[1]

[1]Goethe University of Frankfurt, Frankfurt am Main, Germany; [2]IMP, Lanzhou, China; [3]UCAS, Beijing, China; [4]GSI, Darmstadt, Germany; [5]TU-Darmstadt, Darmstadt, Germany

Introduction

For accelerators the traditional stripping methods are gas strippers and foil strippers. Unfortunately, the gas stripper owns a long lifetime but low stripping efficiency whereas the foil stripper exhibits is exact contrary behaviour. Hence, a compromise has to be made between the long lifetime and the high stripping efficiency. However, a plasma stripper is able to posses a long lifetime and a high stripping efficiency at the same time. This huge advantage is of significance for the accelerator, of course also for FAIR (Facility for Antiproton and Ion Research).

Currently, an inductively pulsed device is applied as a plasma stripper. Differing from the Z-pinch, this device has no problems with electrode erosion which reduces the lifetime of the z-pinch. The first inductively pulsed device for us is the theta-pinch manufactured and developed mainly by C. Teske and J. Jacoby[1,2,3,4]. Unfortunately, the beam transmission was poor at the first beam-plasma interaction experiment in 2012[5]. Hence, beside the modified theta-pinch, an alternative inductively pulsed device called the "screw pinch" is also adapted for this year's experiments. In this report, we describe the beam transmission for the "screw pinch" device as a plasma stripper.

Experiment

The configuration of the coils for the "screw pinch" is more complex than the theta-pinch. Imaging the discharge situation, the current in the beginning flows simultaneously from one side of the glass to the other side by three coils in z-direction. Subsequently, the current will flows back via theta-direction. And then, the current again flows to the other side by the other three coils at z-direction. All of coils are wrapped in plastic and are fixed by a plastic support.

For this "screw pinch" device, two groups of two parallel capacities connect in series which results in the capacitance of 25 μF and the maximum operation voltage of 18 kV. In addition, a differential pumping system is installed to match the high vacuum in the beam line. In this report the parameters to produce the plasma are $14\ kV$ as the operation voltage and 20 Pa hydrogen gas pressure.

The pulsed beam of Au^{26+} with the energy of 3.61 MeV/u is adopted for our experiment. The duration for this macro bunch is chosen as around 1 ms comparable to the discharge time. The beam signal after the "screw pinch" device is measured by a diamond detector.

*This work is supported by the BMBF Contract No. 05P12RFRB8; The authors of Ge Xu, Andreas Fedjuschenko and Andreas Schönlein get the scholarships from HGS-HIRe for FAIR.

Results

To determine the beam transmission quality of the plasma stripper, the beam signal after the cold gas target is used as a reference signal as shown in the lower plot in Fig. 1. The gives an impression of the beam signal transmission. For the next shot through the target in the plasma state the obtained beam signal is shown in the upper plot of Fig. 1. The beam signal after discharging does not show the distinct discrete shape as seen in the first theta-pinch experiment[5]. Further, comparing with the benchmark signal, the beam signal after discharging does not decrease significantly which shows the good transmission for the "screw pinch" as a plasma stripper.

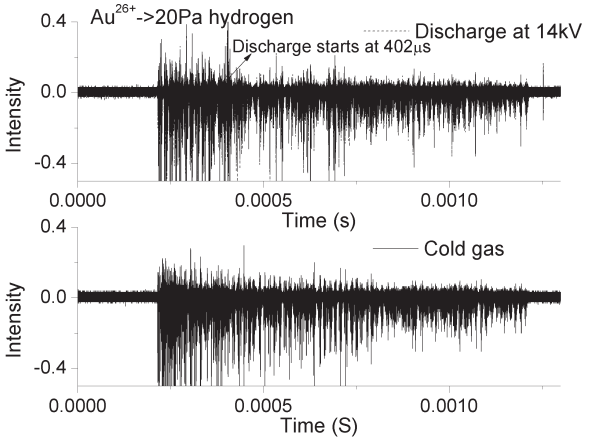

Figure 1: Beam transmissions

References

[1] C. Teske and J. Jacoby, Plasma Science, IEEE Transactions on **36**, 1930 (2008).

[2] C. Teske, J. Jacoby, F. Senzel, and W. Schweizer, Physics of Plasmas (1994-present) **17**, 043501 (2010).

[3] C. Teske, Y. Liu, S. Blaes, and J. Jacoby, Physics of Plasmas **19**, 033505 (2012).

[4] G. Loisch *et al.*, Plasma Science, IEEE Transactions on **42**, 1163 (2014).

[5] G. Xu, J. Jacoby and etc, GSI SCIENTIFIC REPORT 2012, PNI-IONS-EXP-37.

Energy Loss of Low Energy Proton Beam in plasma*

R.Cheng[1], Y.Zhao[1#], X.Zhou[1], Y.Wang[1], Y.Lei[1], S.Liu[1], H.Peng[1], J.Deng[1], G. Xu[1], J. Ren[1], S.Savin[2],R.Gavrilin[2], A.Golubev[2],D.Hoffmann[3], G.Xiao[1]

1 IMP, Lanzhou China; 2 ITEP, Moscow Russia; 3TUD, Darmstadt Germany

Investigation of the interaction processes of ion beams with plasma has attracted a lot of attention during the last decades. Due to the strong non-linear effects and the special importance in ICF research, more and more emphasis has been given to the investigation for ion beams in low energy range and/or for plasma with high intensity. Herein we address the recent progress on the energy loss measurement in case of hundreds keV proton beams passing a gas-discharged plasma target.

The plasma target was produced by igniting an electric discharge of hydrogen gas in two-collinear quartz tubes, each of 5mm in diameter and 78mm in length, the electrical current even up to kA will flow in two opposite directions in either of the two quartz tubes. This device could produce a hydrogen plasma with the line-integrated free electron density of up to 10^{17}- 10^{-18} /cm^2, and with the temperature of around 2 eV when the discharge current was reaching the maximum.

The experiments were carried out at the HV-ECR (High Voltage Electronic Cyclotron Resonance ion source) platform at IMP, where both proton and heavy ion beams with an energy up to 320*q keV (q is the charge-state of the ions) can be provided. After passing through the plasma target, the ion beam is analyzed by a bending magnet and reaches a fast-gated position-sensitive detector with minimum gate of 10 ns (in experiments the gate was set as 100-1000ns to ensure sufficient statistics). The energy resolution of the setup is around 1%, depending on the beam size and the beam divergence (see details in ref [1, 2]).

Figure 1 shows the experimental result of the energy loss for 100 keV proton beam penetrating the hydrogen plasma target (with initial gas pressure of 3 mbar, and discharging high-Voltage of 3 kV) in terms of time after discharging, the calculated energy loss using the Bethe model for the plasma and for the cold gas in initial density were shown as well.

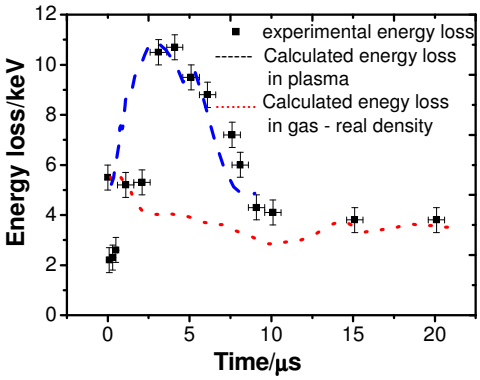

As we can see in the figure, the measurements of energy loss in plasma fit very well with the theoretical predictions after the discharging reaching the maximum, during this period the plasma condition is somehow more stable. However, the measurements were far below the predicted value at the very beginning of the discharging, the reason is still unclear, so far we consider, that the electrons in the target will absorb most part of the discharging power at the beginning so that the electron temperature (or the average velocity of the electrons) will be very high, this may cause a remarkable degradation of the dominating *Se* (electron stopping power).

References

[1] Zhao Y. et al. 2012 Laser and Particle Beams 30 679–706

[2] Cheng R. et al. 2013 Phys. Scr. T156 014074

[3] Y. Zhao, et al, 2014 High Power Laser Science and Engineering, 2, e39 doi:10.1017/hpl.2014.44.

* Work supported by NSFC (11275241, 11375034)

Corresponding author: zhaoyt@impcas.ac.cn

Ion energy loss at the stopping-power maximum in a laser-generated plasma

W. Cayzac[1], V. Bagnoud[1,2], M.M. Basko[3], S. Bedacht[4], A. Blažević[1,2], S. Busold[1,2], O. Deppert[4], M. Ehret[4], A. Frank[2], D.O. Gericke[5], L. Hallo[6], J. Helfrich[4], E. Kjartansson[4], A. Knetsch[7], D. Kraus[8], G. Malka[9], A. Ortner[4], K. Pépitone[6], G. Schaumann[4], T. Schlegel[2], D. Schumacher[1], An. Tauschwitz[10,11], J. Vorberger[12], F. Wagner[4], and M. Roth[4]

[1]GSI; [2]Helmholtz institute Jena; [3]KIAM Moscow; [4]Technical University of Darmstadt; [5]University of Warwick; [6]CEA/CESTA; [7]Department of Experimental Physics, University of Hamburg & CFEL; [8]University of California; [9]Univ. Bordeaux-CEA-CNRS CELIA UMR 5107; [10]University of Frankfurt; [11]HIC for FAIR; [12]MPI for physics of complex systems

Within a collaboration between CEA/CELIA and GSI/TU Darmstadt, measurements of the energy loss of carbon ions at a projectile energy of 0.5 MeV/u in a hot 200 eV fully ionized carbon plasma, i.e at the maximum of the stopping power, have been performed and compared to the predictions of different stopping-power theories [1].
In order to verify and extend these results, another experimental campaign was conducted in 2014 using nitrogen projectile ions with an improved setup, while the simulation and theory tools were refined and extended.
In the second campaign, three potential uncertainties were eliminated. First, the random phase plate of the PHELIX laser beam line, responsible for an intensity spike in the focus profile in the first campaign, was replaced, leading to a more homogeneous plasma. Second, the ablation of the deceleration foil due to the plasma radiation emission was monitored with the help of an optical streak camera, confirming that it does not influence the energy-loss measurements for at least the first 20 ns of the interaction. Third, additional measurements of the non-equilibrium charge-state distribution of the nitrogen beam were performed after interaction with 2-40 μg/cm^2 carbon foils. For the charge state selection and separation, a combination of dipole magnets and slits was used and the data were registered with a scintillator screen coupled to a fast Dicam-pro camera (Fig.1). The obtained data enable a proper scaling of the charge-transfer cross sections at 0.5 MeV/u and hence a more precise calculation of the beam charge-state distribution in plasma than before. The data analysis is in progress.

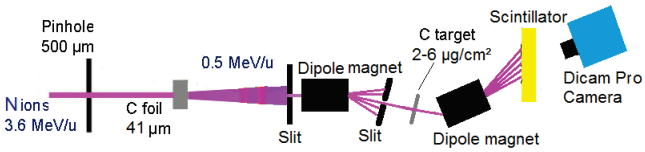

Figure 1: Setup for the charge-state measurements.

Furthermore, the theoretical calculations were extended. First, new hydrodynamic simulations of the plasma were performed with the RALEF2D code using a more realistic laser focus and mesh grid in axisymmetric geometry [2]. Second, for the calculation of the plasma ionization distribution, the equation of state from [3] (in local thermodynamical equilibrium, LTE) as well as the non-LTE FLYCHK code [4] were employed instead of the Saha equation. As shown in Fig.2, the LTE assumption, especially when using the Saha equation, leads to an overevaluation of the plasma ionization and hence of the projectile charge-state value and of the energy loss, even if it does not explain the results of [1].

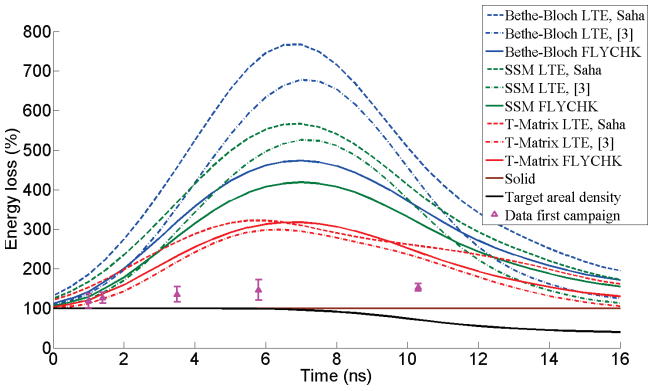

Figure 2: Calculated energy loss of carbon ions as in [1], with the Bethe-Bloch, SSM and T-Matrix schemes, describing plasma ionization with (i) the Saha equation, (ii) the LTE data from [3] and the non-LTE FLYCHK code [4].

Third, the charge calculation is being extended for nitrogen projectile ions and it will benefit from the previously mentioned charge-state measurements. Fourth, additional recent stopping-power descriptions (BPS scheme [5]) are being implemented for a finer theory benchmarking.

This work has been carried out within the framework of the EUROfusion Consortium and has received funding from the European Unions Horizon 2020 research and innovation program under grant agreement number 633053.

References

[1] W. Cayzac et al., GSI report (2013)

[2] An. Tauschwitz et al., High Energy Density Phys. **9**, 158 (2013)

[3] A.F. Nikiforov et al. (2005)

[4] H.K. Chung et al., High Energy Density Phys. (2005)

[5] L.S. Brown et al., Phys. reports **410**, 237-333 (2005)

Energy loss and charge state measurements of heavy ions in dense weakly coupled plasma

A. Ortner[*1], *A. Blazevic*[2], *M. Basko*[7], *S. Bedacht*[1], *W. Cayzac*[2], *A. Frank*[5], *S. Faik*[6], *D. Kraus*[3], *T. Rienecker*[6], *G. Schaumann*[1], *D. Schumacher*[2], *An. Tauschwitz*[6,8], *F. Wagner*[1], *and M. Roth*[1]

[1]Technical University Darmstadt, Germany ; [2]GSI, Darmstadt, Germany; [3]UC Berkeley, USA ; [6]University Frankfurt, Germany ; [7]KIAM Moscow, Russia ; [8]HIC for FAIR, Germany

In october 2014 new experiments measuring the charge state distribution of Ca ions interacting with dense weakly coupled plasma were caried out. These experiments complete the precise energy loss measurements performed 2012.

A 1 ns long, frequency doubled ($\lambda = 527$ nm) laser pulse with a total energy of 150 J is converted in a spherical cavity into X-rays with a radiation temperature of $T_r \approx 100$ eV. This Plackian radiation heats up a secondary cylindrical hohlraum to a radiation temperature of $T_r \approx 30$ eV. These soft X-rays are then used to heat volumetrically two thin carbon foils into a dense plasma state. A weakly coupled carbon plasma with an electron temperature of 5 eV to 15 eV and electron density of up to $5 \cdot 10^{21}$ cm^{-3} and an ionization degree of 2^+ to 4^+ is generated. The properties of the primary as well as of the secondary hohlraum have been extensively studied in the last years and a detailed discussion of the results can be found in [1]. The main finding is, that the cylindrical hohlraum stays free of gold for about 5 ns.

Details about the experimental setup at the Z6 target area at GSI can be found in [2, 3].

Fig. 1 shows the measured energy loss compared to two theoretical models. The scale of the y-coordinate is normalized to the energy loss in cold carbon. As it can be seen on the "empty hohlraum" - measurement, the gold plasma coming from the wall, at earliest affects the ion bunches after 5 ns. In plasma an increase of the energy loss of $+70$ % is observed. Theories like the Standart Stopping Model (SSM) or the Unitary-Convolution-Approximation energy-loss theory (CasP) [4] predict a smaler energy loss than measured in the experiment of only $+50$ % to $+70$ %.

Fig. 2 shows the measured charge state distribution which indicate a small increase of the mean charge state in plasma.

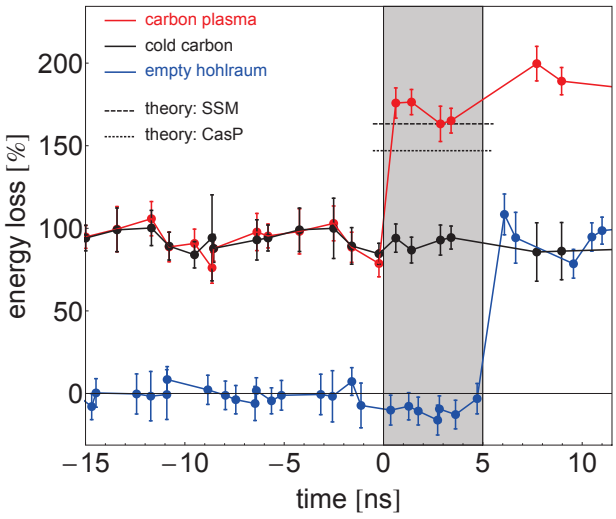

Figure 1: Energy loss results compared with an empty hohlraum, cold carbon and vacuum measurements. $t = 0$ ns indicates the beginning of the laser pulse. The gray area the 5 ns time probing window.

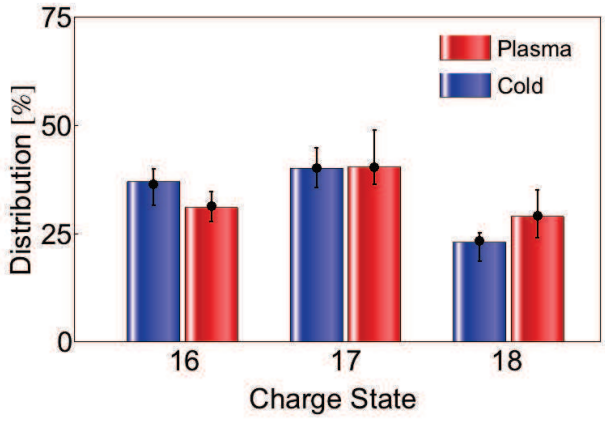

Figure 2: Experimental results of the charge state measurement of Ca^{17+} ion beam in a cold carbon foil and a weakly coupled carbon plasma.

References

[1] A. Ortner et. al., NIMB Volume 343, Pages 123-131 (2015)

[2] A.Ortner et al., GSIReport 2013-1, 374p.(2013)

[3] A. Ortner et al., IFSA 2013 conference proceedings (2014)

[4] G. Schiwietz and P.L. Grande, Phys. RevA 84, 052703 (2011)

* a.ortner@gsi.de

Investigation of Warm Dense Carbon in the 100-200 GPa regime*

J. Helfrich[1], *S. Frydrych*[1], *G. Schaumann*[1], *B. Barbrel*[2], *J. Vorberger*[3], *D. O. Gericke*[4], *B. Bachmann*[5], *L. B. Fletcher*[6], *E. J. Gamboa*[6], *S. Göde*[6], *M. Gauthier*[6], *E. Granados*[6], *H. J. Lee*[6], *B. Nagler*[6], *A. Ravasio*[6], *W. Schumaker*[6], *T. Döppner*[5], *R. W. Falcone*[2], *S. H. Glenzer*[6], *M. Roth*[1], *and D. Kraus*[2]

[1]TU Darmstadt, Germany; [2]UC Berkeley, USA; [3]MPIPKS Dresden, Germany; [4]University of Warwick, UK; [5]LLNL, Livermore, USA; [6]SLAC, Menlo Park, USA

Introduction

Warm dense carbon (i. e. densities around solid density and temperatures from several thousand to several hundred thousand Kelvins) is interesting for the inside of our outer ice giant planets [1] and is also important for inertial confinement fusion (ICF). In ICF experiments, the ablator contains carbon in form of high density carbon [2].

In the laboratory, WDM conditions can be achieved by laser driven shock waves. The final state depends on laser drive intensity, initial carbon structure as well as its density. One of few key diagnostics to measure WDM samples is X-ray Thomson scattering (XRTS) which allows for obtaining information about the microscopic structure [3].

Experiment

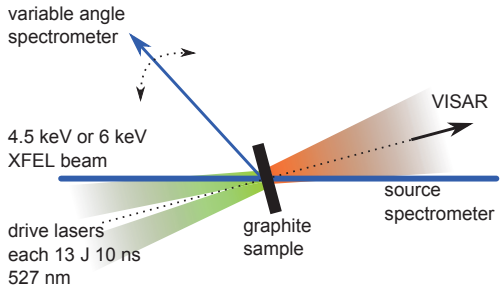

Figure 1: Schematic of experimental setup: The shock wave is driven with two lasers (each deliver 13 J, 10 ns, spotsize 250 µm) into approx.100 µm thick carbon samples. We measured the shock transit time with a VISAR system by the change of reflectivity of the target rear side at the breakout moment. A 50 fs X-ray pulse with 4.5 keV or 6 keV photon energy probes the sample. The scattered radiation is monitored and spectrally resolved by HAPG spectrometers (see Figure 2).

First experiments at GSI with XRTS and laser shock compressed carbon have been done and show that it is possible to produce and characterize high-pressure liquid carbon [4]. Further experiments at the Rutherford Appleton Laboratory have shown that various final states can be achieved by varying the initial density of the graphite sample [5]. Here we present an experiment that has recently been performed at the Linac Coherent Light Source (LCLS). The setup of the experiment is shown in Figure 1. The use of the LCLS brings great benefits to the previous used laser driven X-ray sources. The mayor benefits are the small spectral bandwidth, variable photon energies, the number of photons in a small volume and the 50 fs short pulse. Using XRTS and LCLS as photon source we are able to measure the ion-ion structure factor of carbon for varying initial densities, scattering vectors and allows us to characterize the shock compressed material. With the shape of the inelastic scattering feature the density and temperature can be determined. Figure 2 shows a spectrum of a cold carbon sample with the different scattering features.

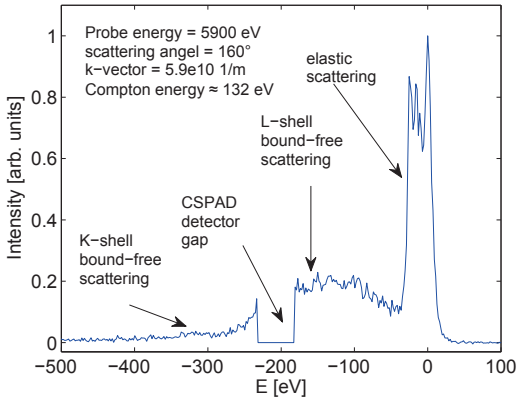

Figure 2: X-ray scattering spectra from cold carbon sample: The elastic scattering profile is given by the LCLS. The inelastic part is bound-free scattering from the K- and L-shell electrons. The ion-ion structure factor can be deduced by determining the ratio of the elastic and inelastic scattering.

References

[1] M. Ross, Nature 292, 435 (1981).

[2] A. J. MacKinnon *et al.*, Phys. Plasmas 21, 056318 (2014).

[3] S. H. Glenzer, R. Redmer, Rev. Mod. Phys. 81, 1625 (2009)

[4] D. Kraus *et al.*, Phys. Rev. Lett. 111, 255501 (2013).

[5] J. Helfrich *et al.*, "Investigation of the solid-liquid phase transition of carbon at 150 GPa with spectrally resolved X-ray scattering" submitted.

* Work supported by BMBF projects 05P12RDFA1 and 06DA9043I. US contracts DEFG52- 06NA26212 and DE-AC02-76SF00515.

Supersonic radiation driven heat waves in foam target heated by X-rays

O. N. Rosmej[1], D. Klir[2], K. Rezak[2], M. Schächinger[3], T. Rienecker[3], G. Vergunova[4], N. Borisenko[4], L. Borisenko[5], A. Malikova[5]

[1]GSI, Darmstadt, Germany; [2] Czech Technical University in Prague; [3]University of Frankfurt, Germany,

[4] Lebedev Physical Institute, Moscow, Russia; [5]Moscow State University, Russia

A combined hohlraum-target concept has been investigated in order to gain a high degree of plasma homogeneity in experiments on the energy loss of heavy ions in ionized matter and approach a plasma with a coupling parameter Γ~0.5-1. In this scheme, low density mm-thick foam layers were heated by means of X-rays generated in the gold hohlraum. The application of low density CHO-foam layers for plasma production has demonstrated a very high hydrodynamic stability of the created plasma and its uniformity [1]. A wide variety of diagnostic methods has been applied for measurements on the thermal wave propagation, plasma opacities and plasma self-radiation.

In Hydrodynamic 1-D calculations, 2 mg/cc cellulose triacetate $C_{12}H_{16}O_8$ of 2 mm thickness was heated from the right side by an X-ray flux with the Planckian spectral distribution at temperature of 30 eV and 10 ns duration (experimental conditions), see Fig.1. For radiation transport in the diffusion approximation $C_{12}H_{16}O_8$ - opacities calculated in [2] have been used.

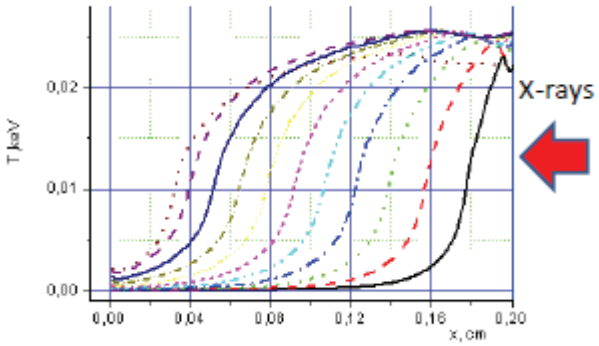

Figure 1: Propagation of the heating front through a 2 mm thick CHO-foam in time window from 1 to 10 ns.

Depending on the hohlraum spectra and foam density two different scenarios of a foam target heating by X-rays can be realized. If the mean photon pass in plasma is shorter than the plasma size, optically thick case, target heating occurs step by step (Fig.1) via propagation of the radiation driven supersonic thermal waves. If the created plasma is optically thin (low target density or more energetic spectra of photons due to higher hohlraum temperature) volumetric heating takes place.

Propagation of the radiation driven supersonic thermal waves has been observed experimentally using a pin-hole camera coupled to the 4-frame gated MCP (microchannel plate) [3] and imaging the CHO-foam at different times of the heating process. An exposition time for every frame, in the experiment 3-5 ns, and time delay between two subsequent frames can be variied. Fig. 2 shows the geometry of the combined target (picture left), the MCP-chip with four imaging areas (right) and a measured time history of the heat-front propagating from the cylindrical hohlraum into the foam (center).

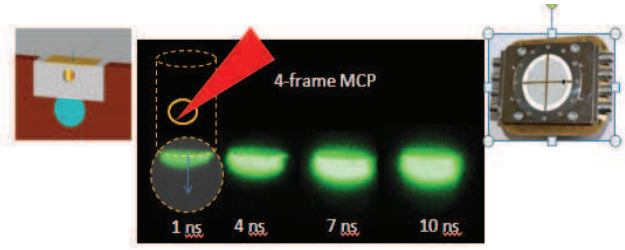

Figure 2: 2-D image of the foam region heated to plasma by hohlraum x-rays in the regime of supersonic radiation driven heat waves, measured at different times.

The supersonic heat wave velocity $V \sim \dfrac{T^{m+4}}{\rho \sim const}$ (1)

is a strong function of the plasma temperature T (in our case m~3) and does not depend on plasma density for hydrodynamic stable plasmas (ρ=const). After analyses of the radiation front position at different times one comes up with the averaged over the exposition time heat wave velocities and corresponding plasma temperatures.

$$V(1ns) = 1.2x10^7\ cm/s \rightarrow T \sim 25\,eV$$

$$V(4ns) = 8.3x10^6\ cm/s \rightarrow T \sim 23\,eV$$

$$V(7ns) = 4.0x10^6\ cm/s \rightarrow T \sim 20\,eV$$

$$V(10\,ns) = 1.4x10^6\ cm/s \rightarrow T \sim 15\,eV$$

In coming experiments this method will be applied for measurements of the plasma temperature in the time window of ion-plasma interaction.

References

[1] G. Vergunova et a,lJournal of Russian Laser Research, Volume 31, Number 5, 2010

[2] N. Orlov et al, LPB 29 (2011), 69–80.

[3] D. Klir, PhD 2005, Czech Technical University in Prague

Comparison of measured time resolved hohlraum radiation temperature with data produced by RALEF II-Code

T. Rienecker[1,2], O.N. Rosmej[1,2], R. Maeder[1,2], D. Martsovenko[3], N. Suslov[3], S. Faik[2], M. Basko[5], An. Tauschwitz[2], L. Borisenko[4], A. Malikova[3], M. Schachinger[2], A. Schönlein[2], S. Zaehter[2], Ge Xu[2] and J. Jacoby[2]

[1]GSI, Darmstadt, Germany; [2]Goethe-University Frankfurt, Germany; [3]VNIIEF-Sarov, Russia; [4]Moscow State University; [5]Keldysh Institute of Applied Mathematics, Moscow

For indirect homogeneous heating of low-Z triacetate-cellulose (TAC) foam targets, used in experiments on ion energy loss in plasma, a large (Ø > 1 mm) soft X-ray source with a Planckian equivalent radiative temperature of 30 to 50 eV is required. In this temperature region soft X-rays are effectively absorbed by low Z low density polymer layers. More energetic radiation above 1 keV passes through the 200 µg/cm^2 TAC-layer without attenuation giving no input into the process of foam heating.

The experiments have been supported by RALEF II simulations, made by S. Faik from University Frankfurt. One important parameter, the hohlraum temperature shows a heating during the shot of the laser in the first ns, it leads to a peak temperature of about 70 eV. After some additional nanoseconds the temperature in the hohlraum is homogenized and stays nearly constant for a longer timespan (>10 ns), see figure 2a.

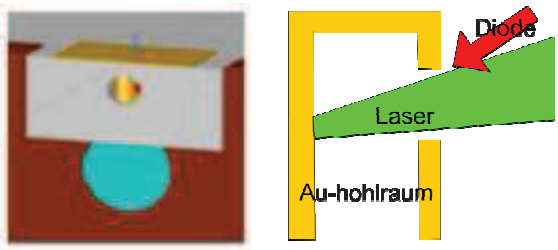

Figure 1(left): The picture shows a scheme of the setup, with a view in the Au-Hohlraum from the same position as the X-ray-diode. Figure 1(right): The scheme shows the laser and the diode, using the same hole for heating and diagnostic.

The temperature in experiment was measured by X-ray-diodes. The X-ray-diodes are composed have either carbon cathodes as well as aluminium cathodes, a grid and a filter. The combination of different filters allow measuring the absolute photon flux in different parts of the hohlraum spectrum and to deduce a time-history of the hohlraum temperature radiation, shown for different wavelength (see Figure 2).

* Work supported by GSI; Extreme Matter Institute EMMI

According to earlier experiments [1,2], we can assume a short time of 5-7 ns after the beginning of the laser pulse of X-ray emission and reemission. After this homogenisation the radiation fits to the normal hohlraum radiation. Folding the this radiation with the filters and the electron efficiency of the cathodes leading to different currents, produced by the X-ray diodes (see Figure 2).

The described measurement assumes an absolute calibrated X-ray-diode, like the one we had. For a better verifiability and a second method, we use a second X-ray-diode, with different filters. In this way it was possible to compare the two signals in a proportional mode, which not necessary needs absolute calibrated X-ray-diodes.

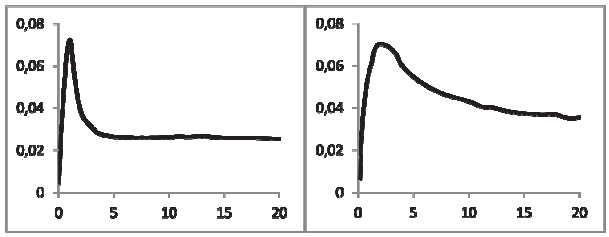

Figure 2 (left): Simulated temperature [keV], time resolved [ns] integrated over a line across the hohlraum. Figure 2 (right): Measured temperature [keV], time resolved [ns] integrated over the view line to the rear wall.

The simulated data (see figure 2) shows a very small peak in the first ns, and a nearly flat temperature curve after 5 ns. The measured curve is some eV higher in the temperature, after the homogenisation. This may be caused by the fact, that the X-ray-diode views a part of the laser spot. The important parameter, the long lasting temperature, is reached in the simulation and the measurement, and both fit together.

References

[1] O.N. Rosmej et al. NIMA 653(2011)52-57
[2] T. Rienecker, et al. GSI-report 2011

Measurements of the Heavy Ion Stopping in X-ray heated low-density nanostructured targets

R. Maeder[2] , T. Rienecker[1,2] , O.N. Rosmej[1] , D. Martsovenko[3] , L. Borisenko[4] , A. Malikova[3], M. Schachinger [2], A. Schönlein[2], S. Zaehter[2] , Ge Xu [2] , J. Jacoby[2]

[1]GSI, Darmstadt, Germany; [2]University Frankfurt, Germany; [3] VNIIEF, Sarov, Russia; [4]Moscow State University

Measurements of the enhanced ion energy loss in plasma compared to those in non-ionized matter have been carried out in the frame of the project U272. The plasma targets were produced via volumetric heating of CHO-foam layers (cellulose-triacetate-TAC; $C_{12}H_{16}O_8$) by soft X-rays. A X-ray source with close to the Planckian spectral distribution was generated by irradiation of a gold cylindrical hohlraum with the PHELIX-laser at 0.54 µm, 150J, 1 ns, 5.10^{14} W/cm^2 [1]. 80% conversion of the laser energy into soft X-rays with $T_{Planck} \sim 45$eV has been reached. Hydrodynamic stable homogeneous plasma with an electron density of $n_e \sim 10^{21}$ cm^{-3} and 20-30 eV temperature is then produced in the state close to the thermodynamic equilibrium. This plasma is partially ionized and contains He-like states of Carbon and Oxygen and fully ionized Hydrogen ions. Calculations of the 4.7 MeV/u Ti-ions energy loss on free and bound target electrons in dependence on plasma temperature/ionization degree (see Fig.1) have been done using a numerical code, described in [2].

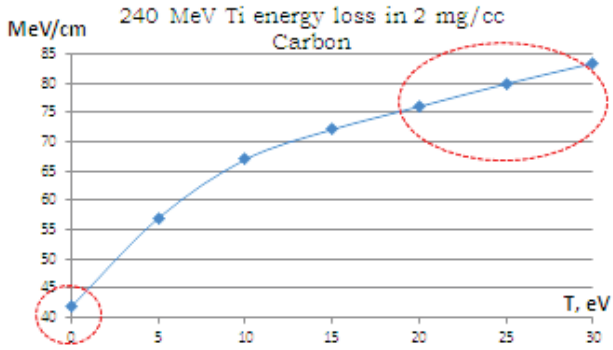

Figure 1: Expected energy loss of 240 MeV Ti-ions in a 1mm thick 2 mg/cm^3 carbon–plasma layer in dependence on plasma temperature.

The experimental set-up for the plasma production and ion energy loss measurements was similar to that used in [3]. The plasma target was probed by Ti-ions with a variable delay between the laser pulse and the ion micro-bunch. The ion velocity after interaction with the target was measured using a Time of Flight method. The results are shown in Fig. 2. Comparison of the TOF data for vacuum and cold target conditions results into a time of flight difference of 6.9 ns. After interaction with plasma layer the ions reached the stop detector 2.8 ns later than in the case of the cold target, this corresponds to1.4-times enhancement of the ion energy loss due interaction with free electrons in plasma. Energy loss of Ti-ions in the plasma was measured for different time-delays and two plasma target densities, the results are presented in Fig. 3. At later times (>10ns) plasma temperature in the interaction region, 0.75mm away from the hohlraum bottom, reached 20-30 eV and for both densities the enhancement of the ion energy loss is between 1.4 – 1.8 in accordance with [2]. The low enhancement factor at earlier times can be explained by lower plasma temperatures (see Fig.1) as a results of the finite time needed for the heating process.

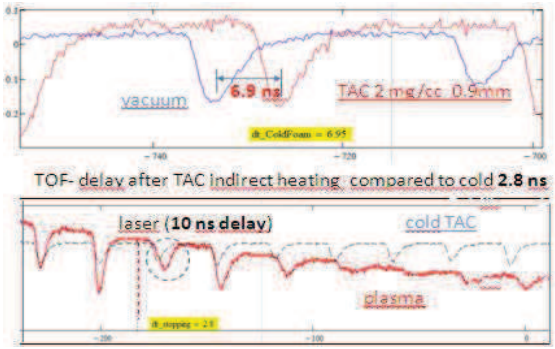

Figue 2: Ti –ion beam micro-bunch structure measured in vacuum and after interaction with foam and plasma.

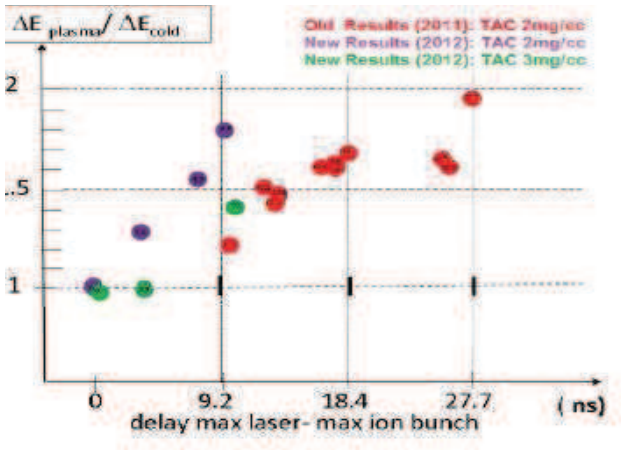

Figure 3: Enhancement of the ion energy loss in plasma depending on the delay between the laser and ion pulses.

References:

[1] O. Rosmej, V. Bagnoud, U. Eisenbarth, et al, "Nucl. Instr. and Meth. A 653 (2011), p.52-57.

[2] M. M. Basko, Ion stopping in dense plasmas, Physika Plazmi, **10**, V6 (1984)1195-1203

[3] R. Maeder, T. Rienecker, et al, Annual GSI-Report 2011, PNI-PP-17, p. 450.

Hard X-Ray backlighting for Warm Dense Matter at FAIR

A. Schoenlein[1], J. Wiechula[1], O. Rosmej[1,2], B. Aurand[2], D. Hochhaus[3], O. V. Chefonov[4], A. V. Ovchinnikov[4], and J. Jacoby[1]

[1]Goethe University, Frankfurt, Germany; [2]GSI, Darmstadt, Germany; [3]EMMI, Darmstadt, Germany; [4]JIHT, Moskau, Russia

FAIR opens new possibilities to study the fundamental properties of matter under extreme conditions. In experiments like HIHEX or LAPLAS [1], Warm Dense Matter will be generated by high-energy, high-intensity ion beams heating large (mm^3) high Z-targets (Al-Pb). For backlighting these targets, it is necessary to generate photons with energies in the keV-MeV range. Hard x-ray and gamma sources can be generated in the processes which occur during interaction of high intensity lasers with matter. When laser pulse impacts onto the target, collective absorption mechanisms transfer up to 20% of the laser energy into hot electrons, which are accelerated to multi-keV and MeV energies. By propagation in the target bremsstrahlung radiation caused by the electron deceleration occurs. Attenuation and scattering of x-rays can be used to determine the electron plasma temperature and density [2]. The advantage of a hard x-ray generation using short-pulse lasers over a common x-ray tube is, that it gives the possibility to generate short bursts of x-rays which provide a possibility to investigate dynamic processes in the plasma.

The experiment was carried out in the frame of the PHELIX-project P42. The laser parameters (E_L=150J, t_p=500fs, focal spot: 15-20μm) lead to a maximum intensity of $3 \cdot 10^{19} W/cm^2$. Ag foils (10 and 100μm) and Ag bulks (3mm) glued on thick PMMA plates, to prevent refluxing of electrons, were used as targets. The experimental setup includes a single hit CCD for the measurement of Ag-Kα radiation, Hard X-ray Detectors (HXRD) for spectral diagnostics and an x-ray knife to determine the energy of hot electrons. The HXRD consists of an image

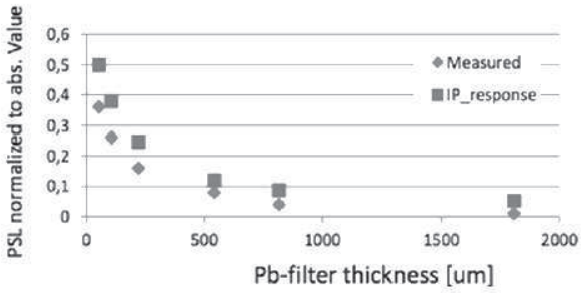

Figure 1: calculated and measured IP response

plate (IP) which is placed behind filters of different thicknesses (Pb 53-1807μm). The x-ray absorption in the filter set takes place in accordance with the Lambert-Beer-Law $I = I_0 e^{-\alpha \rho d}$, where d is the thickness of the filter, α is the attenuation coefficient of the filter material and ρ is the filter density. The bremsstrahlung spectrum will be then reconstructed using a fitting procedure in which a synthetic spectrum with a temperature of hot electrons, defined in a zero approximation by the laser intensity [3], was "sent" through the filter set. Varying the temperature of hot electrons, one tries to achieve the best agreement between theoretical and experimental data.

Fig.1 shows the comparison of calculated and measured IP-responses in the laser-shot at $2 \cdot 10^{19} W/cm^2$. The best fit is achieved for hot electron temperature of $1.5 MeV$.

The X-ray knife diagnostic [4] consists of a $500 \mu m$ thick Au plate placed between the target and IP and allows observing the penetration depth of energetic electrons propagating inside the target using hard x-rays caused by bremsstrahlung radiation with photon energy above $30 keV$. Fig.2 shows that hot electrons are stopped after

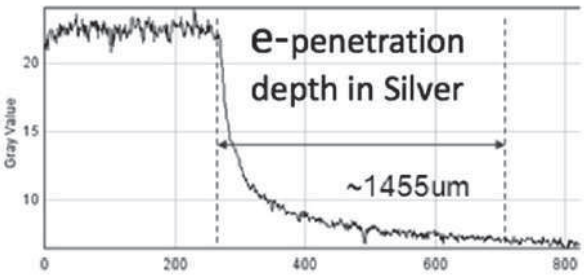

Figure 2: penetration depth of hot electrons in Ag

$1455 \mu m$ propagation in a Ag target. A stopping range of $1.5 mm$ in cold Ag refers to electron energies of $2 MeV$[5].

For backlighting of the $4mm$ thick LAPLAS target tamper [1] made from Nb or W, laser induced photons with energies above 0.5-1MeV, electrons $> 20 MeV$ and protons $> 100 MeV$ are required. The current progress in advanced laser driven sources will allow generating short, quasi-monochromatic bursts of protons, electrons, neutrons and coherent x- and gamma-rays of high energies.

References

[1] N.A. Tahir et al, New J. Phys. 12(2010) 073022

[2] S.H. Glenzer, G. Gregori, R.W. Lee et al. // Phys. Rev. Lett. 90 (2003) 175002

[3] Wilks S.C., Kruer W.L., Tabak M., Langdon A.B. // Phys.Rev. Lett. 69 (1992) 1383-1386

[4] PhD, Daniel Hochhaus 2012

[5] ESTAR http://www.nist.gov/pml/data/star/

Ti-wire isochorically heated by intense short pulse laser*

A. Schoenlein[1], *S. Pikuz*[4], *A. Franz*[1], *J. Jacoby*[1], *O. Rosmej*[1,2], *D. Khaghani*[3], *P. Neumayer*[3], *L. Antonelli*[5], *D. Batani*[5], *J.J. Santos*[5], *and A. Sautery*[5]

[1]Goethe University, Frankfurt, Germany; [2]GSI, Darmstadt, Germany; [3]EMMI, Darmstadt, Germany; [4]JIHT, Moskau, Russia; [5]University of Bordeaux I, France

For the characterization and the investigation of the behavior of warm dense matter, that will be generated at FAIR, it is necessary, to find diagnostics suitable for these tasks and able to operate under extreme conditions. Already, small samples of WDM, with dimension of a few micrometer, can be generated by using intense short pulse lasers like the PHELIX-facility at GSI.

To generate WDM, high energy densities respectively high pressures (>1Mbar) are required. During the interaction between an intense short pulse laser and matter, a part of the energy is transferred to electrons. These electrons are accelerated to energies above a few MeV by the ponderomotiv force of the laser field[1, 2].

The experiment was carried out in the laserbay of the PHELIX-laser facility. The experimental setup consisted of Ti-wires with a diameter of $50\mu m$ and a length of 2-3mm. The PHELIX-laser (E_L=120J, t_p=500fs, λ=1064nm) was focused to the tip of the wires with a focal spot size down to $6\mu m$, leading to intensities of I_L=$10^{21}W/cm^2$ with a ns-contrast up to 10^{-10}. The electrons, accelerated during interaction between laser and wire, penetrate the wire and deposit energy therein, heating the wire up to the plasma state by collisions. Because of the high kinetic energy, the electrons are travelling nearly with the speed of light. This leads to a heating process that is faster then the expansion of the wire, resulting in an isochoric heating [3].

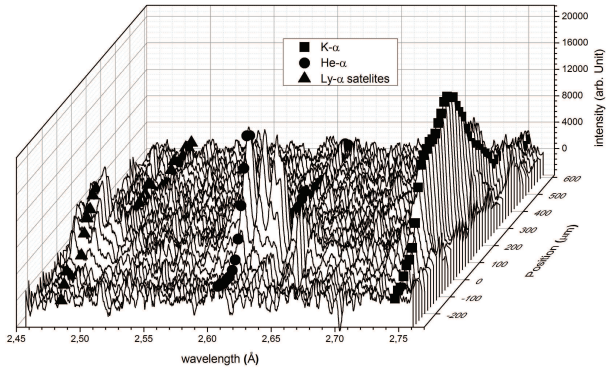

Figure 1: characteristic x-ray spectra along wire axis

While penetrating the wire, the hot electron component ionizes the Ti atoms through K-shell ionisation. As a result, characteristic x-rays are emitted. Outer shell electrons are ionized with high efficiency by electrons with bulk temperatures at tens of eV. The energy of inner shell transitions depends on the effective nuclear charge and thus on the charge state of the ions. This leads to a superposition of Kα transitions from Ti^{+1} up to Ti^{+11}. The characteristic x-rays were measured spatially resolved along the wire axis (fig. 1) with a focusing spectrometer with spatial resolution (FSSR), that consists of a spherical bend crystal as dispersive element and a X-ray film as detector. With the FSSR spectrometer high spectral ($\lambda/\Delta\lambda$=$3 \cdot 10^3$) and spatial resolution ($50\mu m$) can be achieved.

The laser can only penetrate the underdense region of the target. It is mostly absorbed at the critical density of the expanding plasma. At this point, the target is heated to temperatures of keV, resulting in emission of He-like and H-like Kα. The overdense region can only be penetrated by the accelerated particles and is heated to moderate temperatures where a broadened Kα-line is observed (fig.1). The Kα broadening can be calculated by a superposition of emission lines of ionized Ti bulk atoms, weighted by the charge state distribution related to a specific bulk temperature (fig. 2).

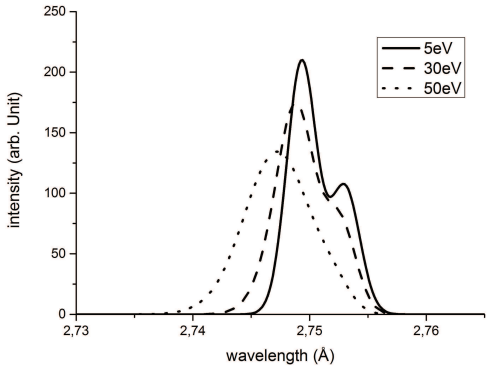

Figure 2: broadening of the Kα-line for different bulk temperatures

It is shown, that WDM can be generated by isochoric heating with hot electrons. Analysis of characteristic x-rays with FSSR provides the possibility to distinguish between direct and particle heated areas and allows a spatial resolved temperature diagnostic which helps to investigate the collisional heating process.

References

[1] S. C. Wilks et al., Phys. Rev. Lett **Vol. 69**, Nr. 9, (1992)

[2] A. J. Kemp and L. Divol, Phys. Rev. Lett **109**, 195005 (2012)

[3] Hochhaus et. al., PHYSICS OF PLASMAS **20**, 062703 (2013)

* Work supported by HGS-Hire, HIC for FAIR and EMMI

Characteristic X-rays from silver foils for backlighting of WDM

O.F. Kostenko[1], *N.E. Andreev*[1], *O.V. Chefonov*[1], *A.V. Ovchinnikov*[1], *O.N. Rosmej*[2], *A. Schönlein*[3], *J. Wiechula*[3], *P. Neumayer*[3], *and J.Jacoby*[4]

[1]JIHT RAS, Moscow, Russia; [2]GSI, Darmstadt, Germany; [3]EMMI, Germany; [4]Goethe Universität, Frankfurt, Germany

The goal of experiments carried out at GSI with high intensity laser system PHELIX is the investigation of mechanisms leading to effective production of photons with energies above 20 keV required for monochromatic backlighting of Warm Dense Matter (WDM). In experiments, 1ω, 500fs, 100J laser pulses were used for irradiation of 3 mm thick Ag targets and thin foils deposited on Al and plastic substrates. The laser intensity was varied between 10^{18} and 4×10^{19} W/cm^2 by changing the laser focal spot size. In this report we present a comparison of numerical simulations of the silver K_α-photon yield with experimental results obtained by means of a single-hit CCD technique [1].

In simulations, the K_α-photon yields from Ag foils in given direction into a unit of solid angle per laser pulse energy, N_k, were calculated according to the model [2], which takes into account dependencies of the conversion efficiency of laser energy into hot electrons $\eta(I_\mathrm{L})$ [1] and average energy of hot electrons $T_\mathrm{h}(I_\mathrm{L})$ [3] on the laser pulse intensity $I_\mathrm{L}(r,t)$, as well as a self-absorption of 22.1 keV K_α photons in a foil of arbitrary thickness. In the case of Gaussian laser pulse, $I_\mathrm{L}(\upsilon) = I_0 \exp(-\upsilon)$, $\upsilon = r^2/r_0^2 + t^2/t_0^2$, we get

$$N_\mathrm{k} = \frac{2}{\sqrt{\pi}} \int_0^\infty \sqrt{\upsilon}\, \mathrm{d}\upsilon \frac{\eta(\upsilon)\, e^{-\upsilon}}{T_\mathrm{h}^2(\upsilon)} \times \times \int_{E_\mathrm{k}}^\infty \mathrm{d}E_0 \exp\left[-\frac{E_0}{T_\mathrm{h}(\upsilon)}\right] \frac{\mathrm{d}N_\mathrm{em}(E_0)}{\mathrm{d}\Omega}\,,$$

were $\mathrm{d}N_\mathrm{em}(E_0)/\mathrm{d}\Omega$ is the number of photons per steradian, emitted by an electron, normally incident with initial energy E_0, from the front side of the foil in given direction.

Theoretical dependencies $N_\mathrm{k}(I_0)$, calculated with the assumption of suppression of hot electron refluxing, describe well features revealed in experiments: sharp increase of K_α-photon yield in the intensity range (1.5–2)$\times 10^{18}$ W cm^{-2}, and then relatively small decrease of N_k with growth of the intensity up to 3.4×10^{19} W cm^{-2} (Fig. 1(a)). The K_α-photon yield increases up to 3 times with increase of foil thickness from 10 to 100 μm (cf. Figs. 1(a) and (b)). The last two features confirm the assumption about suppression of hot electron refluxing in foils deposited on the bulk substrates, even at high laser intensities. The K_α yield from the foil of 10 μm thickness with refluxing electrons, calculated for intensity $I_0 \approx 2.5 \times 10^{19}$ W cm^{-2} [2], exceeds shown in Fig. 1(a) value for the foil with single-pass electrons about 44 times, so only very small input from refluxing electrons could cause insignificant deviations of the experimental value from calculated one (see Fig. 1(a)).

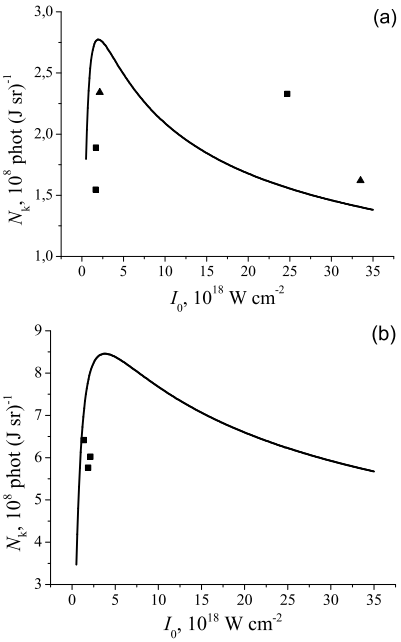

Figure 1: The K_α photon yield vs laser pulse intensity. Solid lines correspond to calculated values with Ag foils of thicknesses: (a) 10 μm and (b) 100 μm. Points correspond to measured values, multiplied by a factor 3: (a) Ag foil of 10 μm thickness deposited on bulk plexiglass (squares) and bulk Al (triangles); (b) Ag foil of 100 μm thickness deposited on bulk plexiglass.

It is important to point out that strong suppression of hot electron refluxing takes place as well for non-conductive substrates like a plexiglass. The last allows supposing the presence of plasma channels in dielectric substrates which occur due to ionization caused by the self-consistent electric field of the electron bunch [4].

The study (OFK, NEA) was performed at the expense of the grant No. 14-50-00124 from the Russian Science Foundation.

References

[1] P. Neumayer *et al.*, Phys. Plasmas **17**, 103103 (2010).

[2] O.F. Kostenko, N.E. Andreev, Quant. Electron. **43**, 237 (2013).

[3] S.C. Wilks *et al.*, Phys. Rev. Lett. **69**, 1383 (1992).

[4] V.T. Tikhonchuk, Phys. Plasmas **9**, 1416 (2002).

Shaping high-current proton bunches in the picoseconds range from a laser-driven source*

S. Busold[1,2], *D. Schumacher*[1], *C. Brabetz*[1], *D. Jahn*[3], *F. Kroll*[4], *O. Deppert*[3], *A. Blazevic*[1,2], *V. Bagnoud*[1,2], *and M. Roth*[3]

[1]GSI Helmholtzzentrum für Schwerionenforschung GmbH, Darmstadt, Germany; [2]Helmholtz Institut Jena, Germany; [3]TU Darmstadt, IKP, Germany; [4]Helmholtz-Zentrum Dresden - Rossendorf, Germany

LIGHT beamline at GSI

The German national collaboration "LIGHT" (Laser Ion Generation, Handling and Transport, [1]) has implemented a worldwide unique laser-driven proton beamline at GSI. The compact acceleration up to nearly 30 MeV proton energies is driven by the PHELIX laser via the TNSA mechanism and a pulsed high-field solenoid provides for beam collimation and energy selection [2].

A radiofrequancy (rf) cavity is implemented in the beamline at 2 m distance to the source for phase rotation of the created single bunch, which shows a typical energy spread of around 20% (FWHM around central energy) and high particle numbers of up to 10^9. Energy compression of the bunch below 3% was demonstrated in an experimental run in 2013 [3].

For the 2014 campaign, the beamline has been extended by a diagnostic chamber at 6 m distance to the source, two quadrupole doublets for beam transport and a third doublet for final focusing of the bunch. The additional space behind the cavity, which is again used at -90 deg synchronous phase but this time at higher rf power to 'over-focus' the bunch in longitudinal phase space, is necessary as drift space for phase focusing experiments.

Results on temporal compression via phase focusing

Proton bunches with a central energy of 7.8 MeV were selected from the source and propagated through the beamline, containing typically particle numbers in the range of 2×10^8 to 5×10^8 within FWHM. The temporal bunch profile measurement was done by two independent and parallel working diagnostics: on the one hand the emitted radiation of a fast plastic scintillator (BC422Q with 1% benzene quenching from Saint Gobain), temporally resolved by a streak camera; and on the other hand a specially developed diamond detector (constructed by GSI's detector laboratory).

Both detectors yield consistent results, with the accuracy of the streak suffering from the still large decay time of the scintillator of 700 ps and thus only setting an upper limit of the bunch length. Figure 1 shows the signal of both detection systems for the shortest measured bunch with a FWHM bunch length of τ=(462±40) ps. This minimum is obtained by injection at a synchronous phase of Φ_s=-90 deg into the rf field and scanning the rf power (indicated by the normalized rf amplitude $U_{rf,n}$) for the optimum working parmeters (see figure 2).

* This work is supported by the Helmholtz Institute Jena.

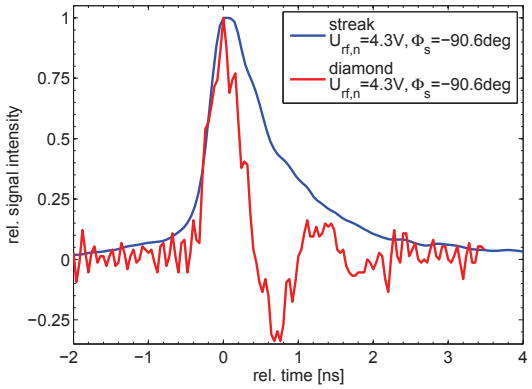

Figure 1: Measurement of the temporal profile of the proton bunch. While the scintillator of the streak camera image suffers from a slow decay time, the diamond detector provides a high temporal resolution.

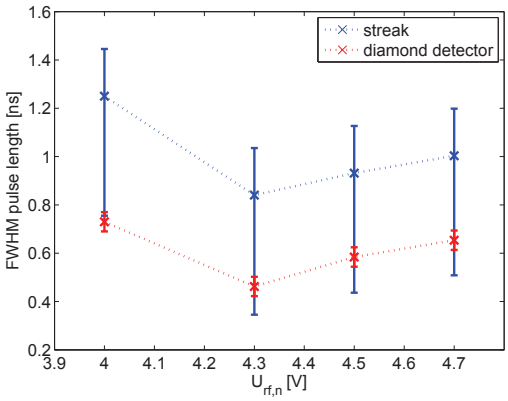

Figure 2: Scan of the applied rf power $U_{rf,n}$ at Φ_s=-90 deg synchronous phase to achieve the shortest bunch length. The streak data represents the upper limit and the diamond detector provides a high-precision measurement.

References

[1] S. Busold *et al.*, NIMA **740**, 94-98 (2014)

[2] S. Busold *et al.*, PRSTAB **16**, 101302 (2013)

[3] S. Busold *et al.*, PRSTAB **17**, 031302 (2014)

Laser-driven ion acceleration at PHELIX with targets made from cryogenic hydrogen and plastics*

S. Bedacht† [1], *F. Wagner*[1,2], *O. Deppert*[1], *S. Geschwind*[1], *R. Jaeger*[1], *A. Kleinschmidt*[1], *F. Mertins*[1], *A. Ortner*[1], *V. Schanz*[1], *G. Schaumann*[1], *A. Tebartz*[1], *B. Zielbauer*[2,3], *V. Bagnoud*[2,3], *M. Roth*[1], *and D.H.H. Hoffmann*[1]

[1]Technische Universität Darmstadt, Germany; [2]GSI, Darmstadt, Germany; [3]Helmholtz-Institut Jena, Germany

Abstract

We successfully demonstrated laser-driven ion acceleration with cryogenic hydrogen targets and plastic targets with energies up to 65 MeV/nucleon for protons, setting a new record for laser-driven ion acceleration at *PHELIX*.

Introduction

For laser-driven ion acceleration the mechanism of *Target Normal Sheath Acceleration* (*TNSA*) has been dominant for the last ten years. Typical experiments at *PHELIX* involving metal targets made from aluminum, copper, and gold with thicknesses in the range of 5 μm to 50 μm yielded proton energies of up to 40 MeV/nucleon. In order to achieve higher particle energies new mechanisms of laser-driven ion acceleration need to be exploited such as the *Laser Breakout Afterburner* (*BOA*) [2] scheme. This scheme relies on a phase of relativistic transparency of the target during the interaction with the laser, thus making high demands on both the driving laser pulse in terms of energy and temporal contrast as well on the target in terms of composition and thickness.

Setup

The experimental campaign *P060* was carried out in two runs of 10 and 20 shifts of *PHELIX* beam time in April and August of 2013, respectively. It made use of the *uOPA* high contrast option [1] of the short pulse frontend and an off-axis parabolic mirror with an f/1.7 opening. With pulses delivering 200 J in 500 fs the peak intensity on target was on the order of 5×10^{20} W/cm^2. For the production of hydrogen targets a custom made cryogenic target mount cooled by a cold head down to temperatures as low as 8 K was used. [3] The cryogenic hydrogen targets were produced just prior to the actual laser shot at the laser interaction point with a thickness of few μm to 100 μm. Additionally, thin plastic targets made from polymethylpentene with thicknesses in the range of 200 nm up to 1100 nm were used.

Results

For the very first time pure cryogenic hydrogen targets and combinations of plastic substrates with layers of cryogenic hydrogen were employed for laser-driven ion acceleration. The pure cryogenic hydrogen targets yielded energies of up to 41 MeV/nucleon. Adding cryogenic hydrogen layers to 200 nm plastic substrates significantly improved the smoothness of the spatial profile of the accelerated ions and yielded higher ion energies of up to 57 MeV/nucleon. The shots at pure plastic targets yielded ion energies of up to 65 MeV/nucleon for a target thickness of (745 ± 67) nm.

By tilting the target with respect to the laser propagation axis by 10° two spatially separated ion beam profiles could be obtained. [4] The ion beam along the target normal direction can be attributed to *TNSA* while the beam profile along the laser propagation axis corresponds to an acceleration via *BOA* [2]. The particle distribution function dN/dE of these two beams is shown in figure 1.

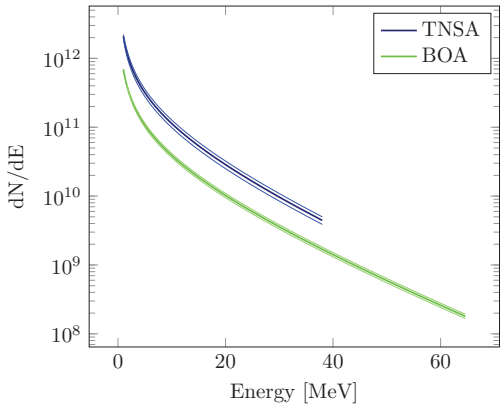

Figure 1: Particle distribution function dN/dE of laser-driven protons obtained from a (745 ± 67) nm thick plastic target at *PHELIX* using radiochromic film. The blue and the green lines correspond to protons accelerated via the *TNSA* and *BOA* acceleration schemes, respectively.

References

[1] F. Wagner et al., *Applied Physics B*, DOI 10.1007/s00340-013-5714-9 (2013)

[2] L. Yin et al., *Laser and Particle Beams*, DOI 10.1017/S0263034606060459 (2006)

[3] S. Bedacht et al., *GSI Scientific Report 2011*, PNI-PP-25, page 458 (2012)

[4] F. Wagner, S. Bedacht et al., *Physics of Plasmas*, submitted (2014)

* Work supported by TU Darmstadt, GSI(PHELIX), BMBF, HiPER

† s.bedacht@gsi.de

Pre-plasma characterization at PHELIX *

F. Wagner[1,2], *S. Bedacht*[3], *A. Ortner*[3], *M. Roth*[3], *A. Tauschwitz*[4], *B. Zielbauer*[1,2], *and V. Bagnoud*[1,2]

[1]GSI, Darmstadt, Germany; [2]Helmholtz Institut Jena, Germany; [3]TU Darmstadt, Germany; [4]Goethe Universität Frankfurt, Germany

Introduction

Modern high intensity laser systems suffer from imperfections of the pulse shape. Typical features of the temporal pulse profile such as compressed prepulses, a pedestal which is due to amplified spontaneous emission (ASE) as well as a slowly rising slope lead to pre-ionization of the targets used in an experiment before the impact of the pulse maximum. In general an uncontrollable pre-plasma is generated which strongly influences the experiment and complicates the interpretation of the results.

The objective for well-controlled experimental conditions implies two aspects: first an adjustable contrast level needs to be established, second the influence of different contrast levels on the properties of the pre-plasma must be characterized. The former requirement has been fulfilled at the PHELIX laser using a technique based on an ultrafast optical parametric amplifier (uOPA) as described in [1]. This technique enables a tunable ASE level between 6 and 11 orders of magnitude.

The evaluation of the dependence of the pre-plasma parameters on the temporal contrast is described in the following. For a more detailed description see reference [2].

Pre-Plasma characterization

The pre-plasma was explored experimentally as well as by using computer simulations. For the experimental investigation we have developed a pre-plasma diagnostic based on a pump-probe setup: The fully amplified PHELIX pulse was focused on flat metal targets to achieve peak intensities around 10^{20} W/cm^2 while a small fraction of this pulse was used as a probe beam to take shadow images of the targets during the interaction with the main beam. By changing the delay between both beams the plasma expansion could be evaluated at different times before and after the impact of the pulse maximum. This measurement was repeated for different ASE levels which are achievable exploiting the uOPA technique. For an ASE intensity of $5 \cdot 10^{13}$ W/cm^2 we could indentify a shadow of a widespread pre-plasma while for an ASE intensity of $2.5 \cdot 10^{10}$ W/cm^2 no pre-plasma was detected. These results qualitatively show the influence of temporal contrast on the pre-plasma dimension and confirm the high contrast achieved with the uOPA.

In order to gain quantitative information the measured shadow images were linked to computer simulations. For this purpose we used the 2-dimensional radiation hydrodynamics code RALEF-2D [3] which provided quantitative information on the plasma parameters like electron density and plasma temperature. The simulation results reproduced our measured plasma dimensions and thus are regarded suitable to describe the experimental conditions. An example is shown in figure 1. The figure shows the 2-dimensional electron distributions of initially flat Cu targets after beeing irradiated by the lowest (left) and the highest (right) used ASE intensity.

While with the low ASE intensity just a minor pre-plasma is generated, the high ASE intensity leads to a pre-plasma with an electron density above 10^{19} cm^{-3} extending up to several tens of micrometers from the target surface. For the higher ASE level the shape of the pre-plasma deviates from a half-sphere geometry. The electron density is lower along the laser axis which acts on the laser beam like a convex lens. Additional simulations show an increase of the laser intensity at focus by a factor of two (for more details see reference [2]).

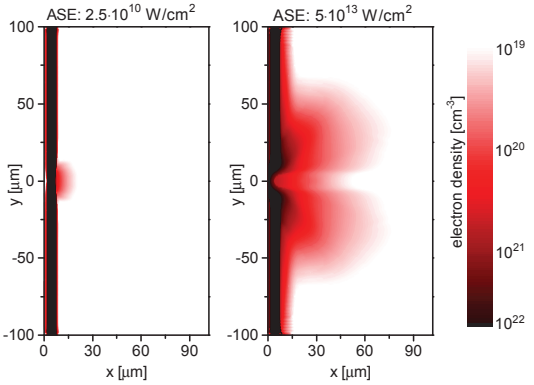

Figure 1: Simulated 2-dimensional electron density distributions for two different ASE levels

The parameters of the generated pre-plasma define the initial condition for experiments done with ultra-intense lasers. For this reason our results could improve the interpretation of experimental data obtained with the PHELIX laser or comparable laser systems. Furthermore the obtained electron distribution could be used as an initial configuration for simulations aiming at exploring the interaction of ultra-intense lasers with matter.

References

[1] F. Wagner et. al., Appl. Phys. B **116**, 2014.

[2] F. Wagner et. al., Opt. Express **22**, 2014.

[3] M. M. Basko et. al., GSI report 2010-1, p. 410.

* This work was supported by the BMBF 05P12RDFA1 and it has been carried out within the framework of the EUROfusion Consortium and has received funding from the European Unions Horizon 2020 research and innovation programme under grant agreement number 633053.

Electric field measurement of laser-produced plasma in a tenuous, current-free large plasma*

B.R. Lee[1,#], S.E. Clark[2], A. Bondarenko[2], C. Constantin[2], E. Everson[2], D.H.H.Hoffmann[1], D. Schaeffer[2], and C. Niemann[2]

[1]Technische Universität Darmstadt, Germany; [2]University of California, Los Angeles, CA, U.S.A.

Collisionless shocks are ubiquitous in space plasmas, however it is beyond our limit to control plasma parameters to study shock physics in this regime. To complement *in-situ* spacecraft measurements, laboratory experiments are performed to create scalable conditions for shock formation [1,2]. Two dimensional hybrid code simulations are used to study debris-ambient coupling in magnetized collisionless shocks [3], in which ions are treated kinetically and electrons as fluid. Recently, a two-electron fluid model has been used in the simulation to study the effect of various electron pressure models and how increasing polytropic coefficient in the electron temperature equation in the code affects the pressure gradients. A correlation between the shock dynamics of the ions and the electric field is found and in the last experiment at University of California, Los Angeles (UCLA), the electric field development of plasma expansion was also measured in addition to the magnetic field measurement.

The experiment has been performed with the Raptor kJ-class laser at a wavelength of 1053nm and a 20ns pulse width [4], coupled to the LArge Plasma Device (LAPD) [5] at UCLA, which creates a tenuous, uniform, current-free plasma at a peak density of $n_i \sim 10^{13}$ cm^{-3} and a background magnetic field that can vary between 200 and 1400 G. The laser irradiates a carbon or polyethylene target and through collisionless coupling mechanisms between the ablated debris ions and the ambient ions, the background magnetic field is expelled and compressed into a thin layer generating a diamagnetic cavity. If the cavity size exceeds the directed debris Larmor radius, the interaction of the debris plasma with the ambient plasma and the magnetic field acts as a piston and collisionless shocks can be launched [6].

Figure 1a) shows the temporal evolution of the electric field measured by the heated emissive Langmuir probe. The radial electric field (solid) has its peak at ~0.5µs when the unmagnetized debris ions reach the probe. As electrons are tied to the magnetic field, a radial electric field is induced generating azimuthal current in conjunction with the magnetic field in z-direction. This current is strongest at the cavity edge (dashed) and it explains the following peak in the azimuthal electric field (long dashed). A similar trend can be seen in the hybrid simulation (Figure 1b). However, disagreements between the experiment and simulation results, such as different magnitude or duration of peaks, field fluctuation etc., should be studied more in detail.

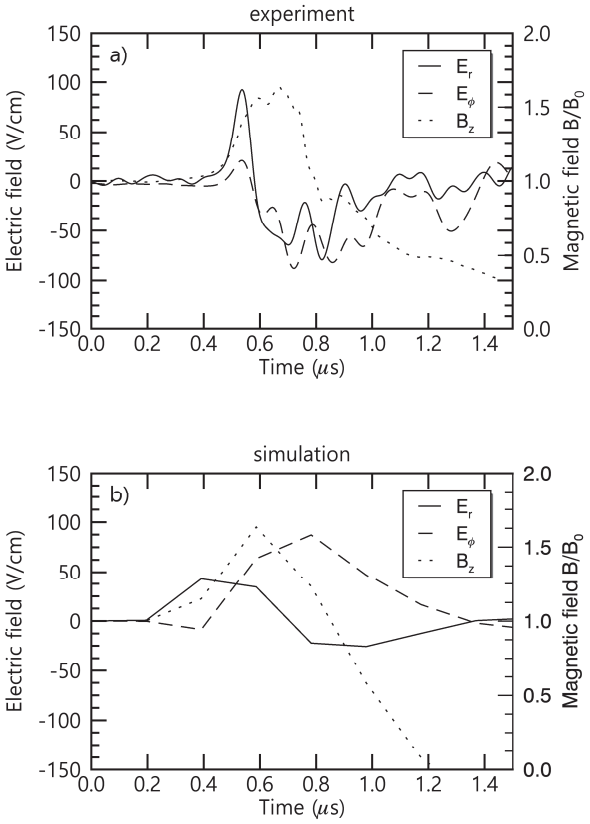

Figure 1: Electric field development in radial (solid) and azimuthal (long dashed) direction a) in experiment measured by a heated Langmuir probe and b) in hybrid simulation, both 30cm away from the target on the target-normal axis.

In summary, a correlation of the electric field with the magnetic compression in the experiment has been observed and in the computer simulation, as well. Further investigation will be needed in the future for deeper understanding of field development and ion dynamics during plasma expansion, especially at the cavity edge.

* This work has been financially supported by the Deutsche Forschungsgemeinschaft in the framework of the Excellence Initiative, Darmstadt Graduate School of Excellence Energy Science and Engineering (GSC 1070) and the US Department of Energy.

#boramlee@skmail.ikp.physik.tu-darmstadt.de

References

[1] C. Niemann *et al*., Phys.Plasmas, **20** 1 012108 (2013)
[2] D. Schaeffer *et al*., Phys.Plasmas., **21** 5 056312 (2014)
[3] S. Clark *et al.*, Phys.Plasmas, **20** 8 082129 (2013)
[4] C. Constantin *et al.*, Astrophys.&Space Sci., **322** 155 (2009)
[5] W. Gekelman *et al*., Rev.Sci.Instrum., **62** 2875 (1991)
[6] C.Niemann *et al*., Geophys. Res. Lett., **41** 21 7413 (2014)

Nonlinear increase of X-ray intensities from thin foils irradiated with Petawatt-class femtosecond laser

A.Ya. Faenov[1,2], J. Colgan[3], S.B. Hansen[4], A. Zhidkov[5], T.A. Pikuz[2,5], M. Nishiuchi[6], S. A. Pikuz Jr.[2], I.Yu. Skobelev[2], J. Abdallah, Jr.[3], H. Sakaki[6], A. Sagisaka[6], A. S. Pirozhkov[6], K. Ogura[6], Y. Fukuda[6], M. Kanasaki[6], N. Hasegawa[6], M. Nishikino[6], M. Kando[6], Y. Watanabe[7], T. Kawachi[6], S. Masuda[5], T.Hosokai[5], R. Kodama[1,5,8], K. Kondo[6]

[1]*Institute for Academic Initiatives, Osaka University, Suita, Osaka, 565-0871, Japan*
[2]*Joint Institute for High Temperatures, Russian Academy of Sciences, Moscow 125412, Russia*
[3]*Theoretical Division, Los Alamos National Laboratory, Los Alamos, NM 87545, USA*
[4]*Sandia National Laboratories, Albuquerque, New Mexico 87123, USA*
[5]*PPC Osaka University and JST, CREST, 2-1, Yamadaoka, Suita, Osaka 565-0871, Japan*
[6]*Quantum Beam Science Directorate, Japan Atomic Energy Agency, Kizugawa, Kyoto, Japan*
[7]*Interdisciplinary Graduate School of Engineering Sciences, Kyushu University, Japan*
[8]*Graduate School of Engineering Sciences, Osaka University,,Suita, Osaka 565-0871, Japan.*

Powerful x-ray sources can produce and probe exotic material states with high densities and multiple inner-shell electronic excitations. X-ray free-electron lasers have achieved ultra-high intensities, which were successfully used for different applications. However, they require large accelerator facilities, their energies are not sufficient to compress high-Z materials, and this energy cannot be easily increased in the near future. Recently we demonstrate via high-resolution x-ray spectroscopic measurements that the energy E of femtosecond optical laser pulses with relativistic intensities $I>10^{21}$ W/cm^2 is efficiently converted to x-rays with an extremely non-linear growth ~ E^5, reaching intensities above ~10^{17} W/cm^2 [1]. Femtosecond laser-produced plasmas may thus provide unique ultra-bright x-ray sources, for future studies of matter in extreme conditions, material science studies, and radiography related to FAIR experiments

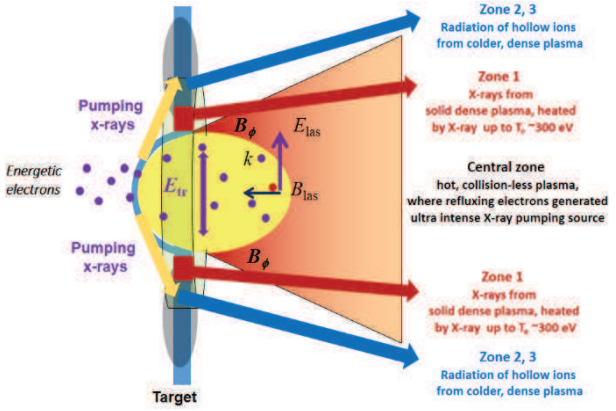

Figure 1 Scheme of generation of ultra-intense x-ray source in relativistic laser-produced plasma. Relativistic laser beam focuses on the foil (central zone) and generates very intense bunches of fast electrons, which, due to strong refluxing in expanded plasma, produce ultra-bright x-rays with a duration comparable to the laser pulse duration or slightly longer. Such transient RDKR x-ray source heats periphery of plasma up to hundreds eV temperature keeping it solid (zone 1). At a greater distance from the center of the plasma (zones 2 and 3) electron temperature drops to a few eV, and due to efficient pumping by x-ray source hollow ions generated.

Fig. 1 demonstrates principles of X-ray generation when laser intensity reaches Radiation Dominant Kinetic Regime [2,3]. Experiments provided in Kansai Photon Science Institute, JAEA Japan with Ti:Sa 40 fs laser facility

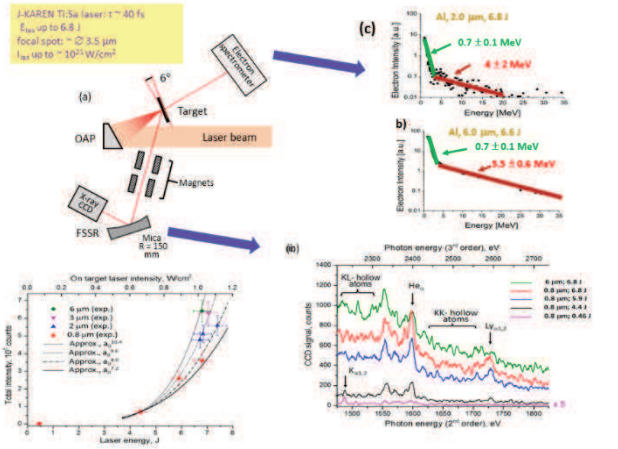

Figure 2 Scheme of observation and results. a) Experimental set up. Laser beam focused by off-axis parabola practically perpendicular to the surface of foil and heat plasma. Produced plasma generated x-ray emission, which was measured by X-ray high luminosity spectrometer with high spectral resolution placed at 45° to the target surface. Electron spectra were measured by electron spectrometer placed from rare side of plasma perpendicular to the target surface; **b)** Single shot, spatially- and temporally averaged Al ions K-shell spectra (raw data) emitted from foil targets with different thickness and laser energies **c)** Experimentally measured electron energy distribution in the case of irradiation 2 and 6 μm thickness Al foils by maximum laser intensity of 10^{21} W/cm^2. Increasing of electron temperature of hot electrons $T_{e,hot}$ with the thickness of Al target is clear seen. Nonlinear increase of X-ray intensities from thin foils irradiated with Petawatt-class femtosecond laser is obviously seen.

clearly demonstrated (See Fig.2) strong non-linear growth of x-ray intensity when laser flux exceeds of 6x10^{20} W/cm^2. The central part of laser plasma rapidly becomes an efficient x-ray source with non-linear power growth, as ~E^5 and such bright x-rays, generated over the laser pulse duration, heated a dense plasma from its initial cold state to a final thermal temperatures of ~300 eV. Simultaneously x-ray source with intensity exceeded ~ 10^{17} W/cm^2 pumping of atomic and ion transitions in the periphery of such plasma resulting in the appearance of hollow atom lines.

This work was partly supported by the Russian Science Foundation grant # 14-50-00124 and #14-02-91171

References

[1] A.Ya Faenov et al. (2014) to be submitted
[2] Zhidkov, A. *et al. Phys. Rev. Lett*. **88**, 185002 (2002).
[3] Colgan, J. *et al., Phys. Rev. Let.* **110**, 12501 (2013)

3 New Diagnostic Methods, Target Fabrication and Plasma Sources

Development of a CVD diamond detector for temporal profile measurements of intense sub-nanosecond ion bunches

D. Jahn[1], *S. Busold*[2,3], *D. Schumacher*[2], *C. Brabetz*[2], *M. Träger*[2], *M. Kis*[2], *M. Ciobanu*[4], *A. Blazevic*[2,3], *and M. Roth*[1]

[1]Technische Universität Darmstadt, Darmstadt, Germany; [2]GSI Helmholtzzentrum für Schwerionenforschung, Darmstadt, Germany; [3]Helmholtz-Institut Jena, Jena, Germany; [4]Institute of Space Science, Bucharest, Romania

Within the Laser Ion Generation Handling and Transport (LIGHT) research project at GSI laser-driven ion acceleration and, especially, ion beam shaping with conventional accelerator technology are explored using the LIGHT test beamline in the Z6 experimental area [1,2,3]. In the LIGHT experimental campaign in 2014, protons were accelerated via the TNSA mechanism resulting in a continuous energy spectrum up to a maximum energy of 28.4 MeV. 45 mm behind the gold target, a pulsed high-field solenoid was used to select a specific proton energy range via chromatic focusing. The resulting bunch was then phase-rotated inside a rf cavity. As a result, temporally refocused proton bunches were generated at a distance of 6 m from the target through phase focusing. TraceWin simulations predicted bunch durations in the sub-nanosecond regime.

In order to measure the temporal profile of these proton bunches with up to 10^9 protons and a central energy of 7.8 MeV, a diamond detector with a time resolution below 50 ps (FWHM) was developed. To improve the time resolution through diamond capacity reduction, an area of 1 mm diameter with 100 nm chrome/100 nm gold was metallized on a 3 mm quadratic polycrystalline chemical vapour deposited (pcCVD) diamond. The 13 μm thick diamond was placed on a conductive plate in a Faraday housing. Moreover, the input resistance of the detector was set to a value of 7.5 Ω and the output resistance to a value of 50 Ω through impedance matching with a so-called T attenuator, a specific resistive circuit based on rf resistors. Figure 2 shows a photograph of the diamond detector.

During the LIGHT experimental campaign in 2014 this diamond detector was positioned at a distance of 6 m from the source and connected via SMA cables to a 8 GHz oscilloscope. A voltage of 30 V, leading to a field gradient of 2.31 V/μm within the diamond, was applied on the detector. The shortest measured duration of an ion bunch was (462 $\pm$ 40) ps (FWHM). Figure 2 shows the temporal bunch profile. The signal drop below zero and the oscillating behaviour at the end of the proton bunch can be explained with the partly frequency dependent T attenuator in the design of the detector, thus an artefact of the detector. As a result, this diamond detector with an optimized time resolution was developed and successfully tested.

For future experiments a new conductive plate design based on a similar T attenuator will be designed to eliminate the artefact. Moreover, the detector will be based on a single crystal diamond membrane with a thickness of 5-7 μm so that higher electric field gradients can be applied and charges can be collected faster.

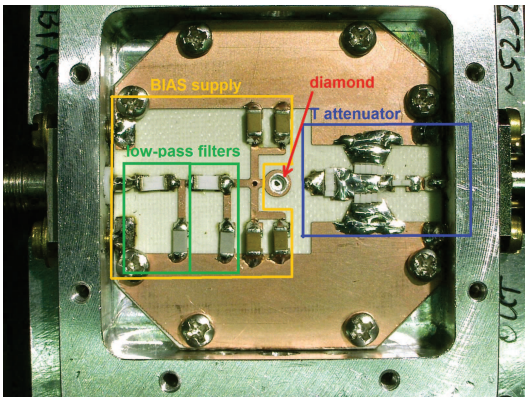

Figure 1: Photograph of the diamond detector: The pcCVD diamond is in the center of the housing. On the right-hand side of the diamond is the T attenuator. Around the diamond are several capacitors of 220 nF as fast charge providers. On the left-hand side of the diamond detector are two low-pass filters.

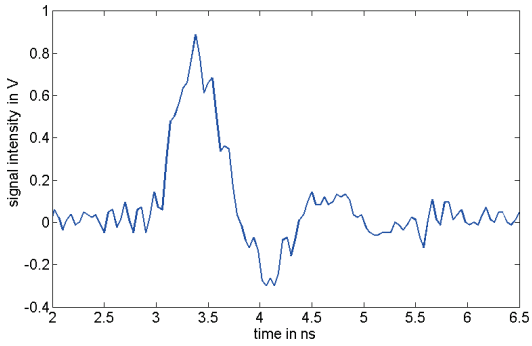

Figure 2: Temporal profile of the shortest measured proton bunch with a duration of (462 $\pm$ 40) ps at FWHM.

References

[1] S. Busold et al., *Shaping laser accelerated ions for future applications – The LIGHT collaboration*, NIM-A **740**, 94-98 (2014)

[2] S. Busold et al., *Focusing and transport of high-intensity multi-MeV proton bunches from a compact laser-driven source*, PR-STAB **16**, 101302 (2013)

[3] S. Busold et al., *Commissioning of a compact laser-based proton beamline for high intensity bunches around 10 MeV*, PR-STAB **17**, 031302 (2014)

Survey of Fabrication Methods for Sensors for the Determination of the Electrical Conductivity of Warm Dense Plasmas

F. Fülbert[1], *D.H.H. Hoffmann*[1], *G. Schaumann*[1], *and S. Udrea*[2,3]

[1]Technical University Darmstadt, Germany; [2]GSI, Darmstadt, Germany; [3]Goethe University Frankfurt am Main, Germany

Introduction

One of the basic properties of matter is its electrical conductivity. Yet, there is still no complete working theory, especially for warm dense and high energy density matter. Therefore extended theoretical and experimental work is still needed. One possibilty to measure the electrical conductivity is by inducing eddy currents and sensing their variable magnetic field [1]. Foregoing work performed at TU and GSI Darmstadt [2] showed that one of the main challenges is the production of a large number of appropriate sensors, having well defined parameters. Hence different means for manifacturing these sensors are presently investigated at TU Darmstadt. In this contribution we briefly present the sensor design, different ways for producing the sensors and show the results of first investigations performed on prototypes.

Design of the Sensor

The sensor consists of metallic, planar structure of about 0,7 mm width on a saphire substrate with a saphire layer on top for protecting it during the measurement from the plasma in its proximity, see figure 1. By driving HF currents through this structure, one eventually induces eddy currents in the sample under investigation. Their variable magnetic field is also inducing a current in the sensor. Hence the inductance of the structure is changing in the presence of the sample. This can be measured and is directly related to the sample's electrical conductivity [1,2].

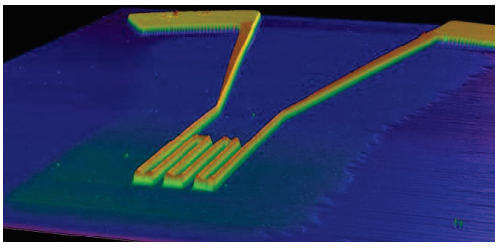

Figure 1: The sensor used in [2] and imaged by a Dektak profilometer. The metallic structure is shown in yellow (light grey) in this image.

Sensor fabrication methods

At the Target Laboratory of the Institute of Nuclear Physics, TU Darmstadt, three different fabrication methods were analyzed: sputtering of the metall on the substrate through a mask, photolithography and stripping of unneeded material by a fs-laser from the substrate. Prototypes realised by this methods have been investigated with a SENSOFAR PLu neox confocal microscope. In the case of the sputtering method penetration of the material between substrate and sputter mask was observed. Samples prepared by photolithography didn't show a very good reproducibilty. By using the fs-laser system, relatively good results have been achieved, nevertheless the main problem is the erosion of the substrate by the laser radiation. Three test structures are shown in figure 2.

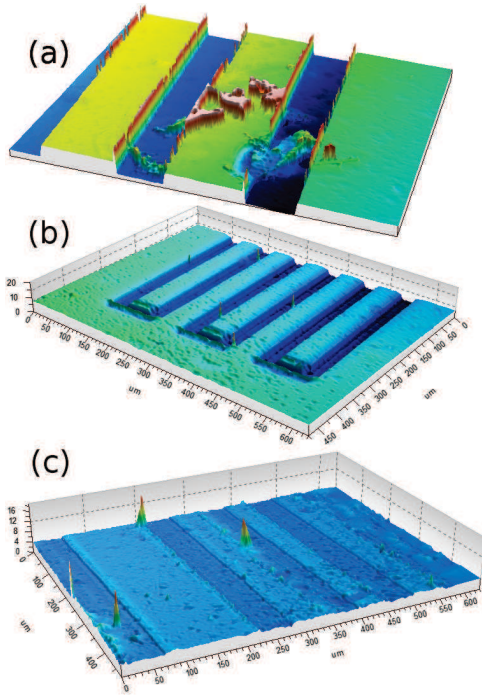

Figure 2: Three test structures: (a) sputtered structure (b) photolithographic structure (c) laser ablated structure

Thus none of the methods showed especial advantages and more experimental work is necessary to decide about the best way of producing a large number of suitable sensors.

References

[1] Yu. B. Kudasov, High-Frequency Conductivity Measurement by a Contactless Method in Superhigh Magnetic Fields, Instruments and Experimental Techniques 42, 1999 , p. 527-530.

[2] J. Ling, Entwicklung, Aufbau und Test eines kontaktfreien Messverfahrens zur Bestimmung der elektrischen Leitfähigkeit dichter Plasmen, TU Darmstadt, 2011

Optical Spectra from Beam Induced Fluorescence (BIF) Profile Monitor*

Y. Shutko[1#], D.H.H. Hoffmann[1], P. Forck[2,3], T. Sieber[2], B. Walasek-Höhne[2], S. Udrea[3], J. Wieser[4], A. Ulrich[4]

[1]TUD, Darmstadt, Germany, [2]GSI, Darmstadt, Germany; [3]Goethe-Universität, Frankfurt am Main, Germany,[4]TUM, München, Germany.

The development of non-interceptive beam diagnostics methods is of high relevance for the future FAIR accelerator facilities. One of these methods is based on Beam Induced Fluorescence (BIF). Such monitors are already in operation at GSI's LINAC since some years [1]. However, further BIF-monitor developments are required for applying this method to high energy beams, as those to be delivered by FAIR's SIS-100 synchrotron.

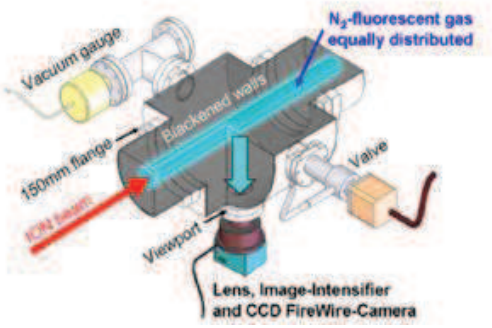

Figure 1: Typical set-up of a BIF profile monitor [2].

For this purpose beam profile and spectroscopic investigations have been performed with different gases in the pressure range from $1{\cdot}10^{-3}$ to 2 mbar with heavy ion beams at energies between 100 and 900 MeV/u for slow and fast extraction mode.

A typical experimental set-up is showing in Fig.1. The gas chamber is mounted on the beam line and has blackened inner walls to avoid light reflections. The chamber can be filled by different gases through a needle valve regulated by a vacuum gauge. Single photons emitted by the excited gas molecules are detected by low light cameras, either by an image intensified ICCD equipped by MCPs in chevron geometry (Proxivison) or an emCCD (Princeton Instruments ProEM+ 512B).

During the experiments performed in 2014 three different set-ups have been used: beam transverse profile set-up with the ICCD camera, beam transverse profile set-up with the emCCD camera and spectroscopy set-up with a CP 140-202 spectrograph coupled to the ICCD camera. The grating of the spectrograph operates in the 190-800 nm wavelength range with 50 nm/mm average dispersion The ICCD camera has at least 40% of its peak sensitivity in the 200 to 600 nm wavelength range. To increase the light throughput of the system, the spectrometer's entrance slit has been set to 400 µm which resulted in a spectral resolution of about 12 nm.

As shown in Fig. 2, in the case of nitrogen the measurements reveal no significant differences between the slow and fast extraction mode. Moreover, the spectra are consistent with previous results obtained at low ion energies [3].

The measured spectra obtained with Argon at pressures between 0.1 and 1 mbar showed different spectral compositions for the slow and fast extraction mode. This is shown in Fig. 3 for measurements performed at 0.4±0.1 mbar N_2 equivalent. The additional, strong emission at 285 and 310 nm, significant only in the case of slow extraction, may be attributed to OH radicals excited by Ar* atoms [4].

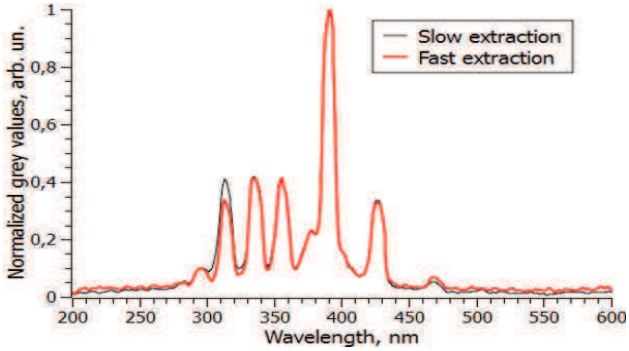

Figure 2: Nitrogen spectra for slow and fast extraction at 0.45±0.02 mbar, U^{73+} 300MeV/u beam.

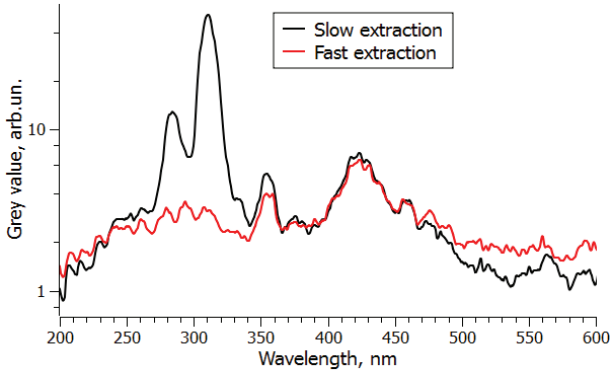

Figure 3: Argon spectra for slow and fast extraction at 0.4±0.1 mbar N_2 equivalent, U^{73+} 300MeV/u beam.

References

[1] C.A. Andre, et al, DIPAC2011 proc., p.185
[2] P. Forck et al, HB2010 proc., p. 497
[3] F. Becker, et al, IPAC2012 proc., p. 798
[4] A. Morozov, et al, Appl. Phys. Lett., **86**, 011502, (2005)

* Work supported by BMBF project No. 05P12RDRBN and Graduate School of Excellence ESE TU- Darmstadt.
#y.shutko@gsi.de

Temperature and Energy Effects on Secondary Electron Emission

L. Zeng[1,2,4], X. Zhou[3], R. Cheng[3], X. Wang[1,2], L. Zhang[1,2], J. Ren[3], Y. Lei[3], Y. Sun[3], S. Liu[3], L. Ma[3], Y. Zhao[1,3], X. Zhang[3,4] and Z. Xu[1,2,3,#]

[1]HCI Joint Center of Xi'an Jiaotong University and the National Laboratory for the Heavy Ion Research Facility in Lanzhou, Xi'an, China

[2]Department of Applied Physics, Xi'an Jiaotong University, Xi'an, China

[3]Institute of Modern Physics, Chinese Academy of Science, Lanzhou, China

Electron emission from solid surfaces under bombardment by charged particles is a well-known emission phenomenon, which is usually described by the mean number of emitted electrons per incident projectile, the electron emission yield γ. The knowledge of electron emission yield gives important information about the basic interaction mechanism between projectiles and solids and contributes to the understanding of impact phenomena like ion-track production.

Secondary electron emission yield from the surface of SiC ceramics induced by Xe^{17+} ions has been measured as a function of target temperature. The experiment was performed with the 320kV electron cyclotron resonance ion source (ECRIS) platform at the Institute of Modern Physics, Lanzhou[1]. A large number of experiments on interaction of highly charged particles with solid surfaces have been performed on this platform. In our experiment, Xe^{17+} ion beams, with ion current in the range of 80-480nA, are focused and collimated to a diameter of 3mm. The experimental setup in our experiment has an UHV heater, which is different from the previous equipment.The pressure in the target chamber is maintained at about 10^{-8} mbar. Through experimental results, we find that the electron emission yield is hardly affected by ion current, or the effect can be neglected in our experiment.

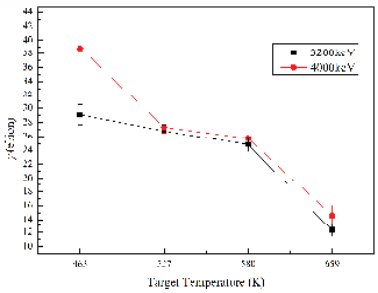

Figure 1: Total electron yield as a function of target temperature for 3200keV and 4000keV Xe^{17+} ions impacting on SiC ceramics in normal incident case.

Figure 1 shows the total yield gradually decreases with increasing target temperature in the temperature range of 463-659 K. The decrease is about 57.48% for 3.2 MeV Xe^{17+} impact, and about 62.49% for 4.0 MeV Xe^{17+} impact, which is much larger than the decrease observed previously for ion impact at low charged states[2,3]. That is to say, the temperature effect on electron emission is obvious for highly charged ions impacting. The result is discussed in terms of work function changes, because the work function of target, which determines the threshold energy, may depend on temperature and could be responsible for the observed temperature effect. That is to say, both kinetic electron emission and potential electron emission is influenced by temperature.

In addition, our experimental data show that the total electron yield gradually increases with projectile energy, when the target is at a constant temperature higher than room temperature. We have done some work about it at room temperature[4]. This result can be explained by electronic stopping power which plays an important role in kinetic electron emission. The electronic stopping power *Se* for Xe^{17+} impacting on SiC ceramics surface can be calculate by SRIM2008. The dependence of the electron emission yield on projectile energy for high target temperature is consistent with the results at room temperature.

The probably most important effect is the temperature dependence of the Fermi distribution of target electrons, which, for sufficiently high temperatures, can even result in thermal emission. However, it is noteworthy that this should increase the yield with increasing temperature, in contrast to our measurements. Further studies are in progress.

Our research will supply useful data to the studies about secondary electron emission and researches on SiC ceramics.

References

[1] Y. Zhao, G. Xiao, H. Xu, H. Zhao, J. Xia, G. Jin, X. Ma, Y. Liu, Z. Yang, P. Zhang, Y. Wang, D. Li, H. Zhao, W. Zhan, Z. Xu, D. Zhao, F. Li, and X. Chen, Nucl. Instr. and Meth. B 267 (2009) 163.

[2] A. Stacey, S. Prawer, S. Rubanov, R. Ahkvlediani, Sh. Michaelson, and A. Hoffman, Appl. Phys. Lett. 95 (2009) 262109.

[3] O. Benka, and M. Steinbatz, Nucl. Instr. and Meth. B 201 (2003) 396.

[4] Z. Xu, L. Zeng, Y. Zhao, J. Wang, X. Zhang, G. Xiao, and F. LI, Laser Part. Beams 30 (2012) 319.

Heavy Ion Induced Desorption Measurements on Cryogenic Targets *

Ch. Maurer† [1,2], *L.H.J. Bozyk*[1], *P.J. Spiller*[1], *and D.H.H. Hoffmann*[2]
[1]GSI, Darmstadt, Germany; [2]TU Darmstadt, Institut für Kernphysik, Germany

Abstract

Heavy-ion impact induced gas desorption is a key process that drives beam intensity limiting dynamic vacuum losses in heavy ion synchrotrons. Minimizing this effect, by providing low desorption yield surfaces, is an important issue for maintaining a stable ultra high vacuum during accelerator operation with medium charge state ions. Measurements with the prototype cryocatcher for SIS100[1] showed a deviation from the previously observed scaling of the desorption yield η (number of desorbed molecules per impacting beam ion) with the electronic energy loss at the surface[2], which needs to be explained. An experimental setup for systematic examination of this behaviour is presented. The cryogenic beam-induced desorption yield of several materials at different temperatures and for different beam parameters is examined.

Experimental Setup

The experiment described in this article has been set up at the SIS18 at GSI. Its approach is rather straightforward: a cold target is hit by a (heavy) ion beam pulse of $\approx 1\,\mu$s length, while the resulting pressure peak is recorded.

A sufficiently low pressure background is provided through a partly bakeable setup including a differential pumping line with a conductance limiting pipe between target and accelerator. This pipe establishes a defined volume for the desorbed gas to disperse. Separating the target area from rest of the beamline with a small diameter pipe establishes a defined volume for the desorbed gas to dissipate in. This pressure peak is measured by an extractor gauge. Cryogenic temperatures are provided by a coldhead (surrounded by a thermal shield). The SIS100-like target is mounted electrically insulated. A more detailed description is given in[3].

Measurement Methodology

The impacting beam opens a measurement window of $\approx 10\,$s. During that time, the pressure evolution is recorded with 10 Hz to resolve the desorption peak. Several combinations of target- and insulating plate materials were measured for varying temperatures. Due to the waiting time for pressure relaxation after beam impact, the repetition rate was limited to roughly one shot per minute. After the first beamtime, data taken on the falling temperature slope proved to be much more stable than on the rising slope. Therefore, the measurement strategy for the second beamtime was adapted accordingly.

Results

The measured desorption yield η as a function of beam energy is shown in fig. 1.

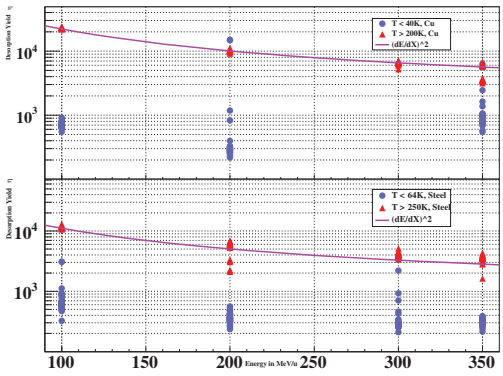

Figure 1: Comparison between the energy dependance of η at cryogenic and room temperature for a gold cotaed copper target (upper panel) and a stainless steel target (lower panel).

While the desorption yield scales quite nicely with the electronic energy loss at the surface for both targets at room temperature, the copper target exhibits a different behaviour at cryogenic temperatures. The steel target does not exhibit this scaling.

Summary and Outlook

An experimental test setup to systematically investigate heavy ion impact induced gas desorption from cryogenic surfaces has been built and experiments have been performed. The previously observed change of behaviour at cryogenic temperatures could be seen here, too, as well as the $(\mathrm{d}E/\mathrm{d}x)$-scaling at room temperature. Gas dynamics and finite element simulations, in combination with further data analysis will be done to gain further insights.

References

[1] L.H.J. Bozyk., "Entwicklung und Test eines Kryokollimator-Prototypen zur Kontrolle des dynamischen Vakuums im SIS100", PhD thesis (2012)

[2] H. Kollmus et al., "Measurements of Ion-beam Loss Induced Desorption at GSI", in AIP Conf. Proc. **773**, p. 207 (2005)

[3] Ch. Maurer et al., "Heavy Ion Induced Desorption Measurements on Cryogenic Targets," in Proc. of IPAC 2014, p. 867

* This project is funded by the german ministry for education and research (FKZ 06DA7031)

† C.Maurer@gsi.de

Design and feasibility study on fabrication and manipulation of HEDgeHOB cryogenic targets*

E.R.Koresheva#, I.V.Aleksandrova, E.L.Koshelev, A.I.Nikitenko, T.P.Timasheva, S.M.Tolokonnikov

Lebedev Physical Institute of RAS, Moscow, Russia

This report addresses the feasibility study and preliminary designing of a specialized cryogenic system (SCS) for fabrication, delivery and positioning of multi-layer cylindrical cryogenic targets at the chamber center for the LAPLAS scheme experimentation.

The HEDgeHOB collaboration plans to carry out a set of experimental projects in the field of High Energy Density (HED) matter generated by the interaction of intense heavy ion beams. One of the approved experimental projects is called LAPLAS (Laboratory PLAnetary Science). This scheme proposes low-entropy compression of a material like frozen hydrogen or deuterium ice that is enclosed in a cylindrical shell of a high-Z material like gold or lead [1]. Such type of experiment is suitable for studying the problem of hydrogen metallization or for creating physical conditions that are expected to exist in the interiors of the giant planets.

According to the FAIR/GSI request, the rate of the target delivery at the chamber center is no less than 1 target per hour. For this reason, in this report we have considered the fabrication and delivery methods related only to free-standing targets (so-called, un-mounted approach) [2]. The study is performed in the following directions:

1.Target fabrication: For the first time there was considered a possibility of cryogenic cylindrical target fabrication with a parameter $L/\varnothing$ = 5.00÷6.25 (where L *and* $\varnothing$ are the length and the diameter of the cryogenic target core, respectively). There were also investigated different technical approaches for designing the target elements, such as cryogenic core from solid H_2 and D_2 and cylindrical shell from the lead.

2. Target manipulation: Different variants for the target elements assembly, target delivery and positioning were investigated. The result of the gravitational delivery is shown in Figure 1. A thorough analysis of diagnostics possibilities for a cryogenic cylindrical target placed inside the target chamber was made.

3. Target survival: A modeling of the target heating process up to the triple point of solid H_2 or D_2 under different heat-exchange conditions was made. There was given an estimation and an optimization of the cryogenic target lifetime inside the chamber with a hot wall has been made.

As a result of our analysis the main functional modules of the SCS have been determined, the technical requirements to the modules have been formulated, possible variants of the SCS arrangement have been analyzed, and two conceptual designs of the SCS have been proposed.

The Project for the construction, installation and commissioning of the SCS has been proposed. The time schedule and approximate cost of the Project realization have been estimated.

Studies carried out have shown that there is a set of open questions, answers which determine the final choice of SCS design have to be found. These questions remain to be answered by GSI in the Agreement stage. After the Agreement stage will be completed it is possible to start the next stages of the Project, namely the Baseline design stage and the stage of SCS construction, installation and commissioning.

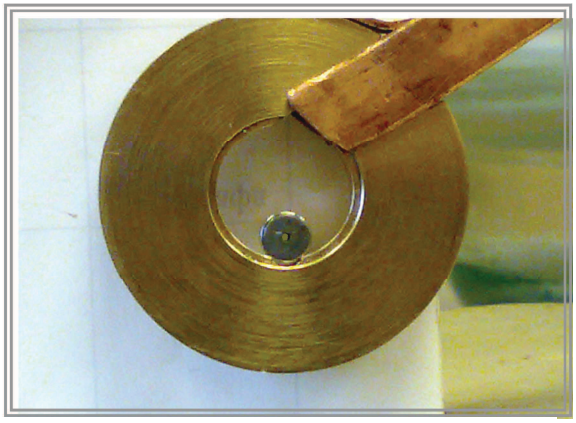

Figure 1: Gravitation delivery of the cylindrical lead target to the test chamber

[1] N.A.Tahir, et al.Phys.Rev. E **63**, 016402, 2000

[2] E.R.Koresheva, I.V.Aleksandrova, A.I.Nikitenko, et al. Laser Part. Beams **27**, 255-272, 2009

Work supported by the R&D contract of 2007 between LPI-GSI-HEDgeHOB collaboration entitled "Design and feasibility study on fabrication and manipulation of HEDgeHOB cryogenic targets"

#elena.koresheva@gmail.com

Development of a light-gas driver for studies on matter properties at FAIR*

M. Endres †[1], *S. Udrea*[2], *Y. Hitzel*[1], *and D.H.H. Hoffmann*[1]
[1]Technische Universität Darmstadt, Germany; [2]Goethe-Universität Frankfurt, Germany

Introduction

For fundamental research on matter properties within the framework of the HEDgeHOB Collaboration with the proton microscope PRIOR the design and realization of a light-gas accelerator as external driver is ongoing. A PRIOR prototype was commissioned at GSI in 2014. At FAIR, PRIOR will use protons from the APPA SIS-100 beamline for radiography. Since SIS-100 is going to be used for diagnostics, external drivers for creating high energy density states will be needed.
One of these possible drivers is the planned light-gas driver. The device will accelerate flyer-plates to velocities of up to 3 km/s. On impact, the flyer-plate shockloads the targets. For first-day experiments at FAIR it is proposed to investigate the resulting material states by proton radiography.

Design

The device will consist of two stages. In the first stage, a light-gas, here Helium, is compressed. In the second stage, the expanding light-gas accelerates a projectile.
To fit into the cave, the length of the first stage needed to be minimized. Therefore the Helium is compressed from the sides, comparable to an opposed-piston car engine (as seen in figure 1). The first stage consists of three major parts, the central block containing the compression chamber and two outer blocks, each containing two combustion chambers. The methane combustion in these chambers will force 4 pistons in the direction of the central block, thus, compressing the helium.

To achieve the maximum velocity the helium is compressed by a factor of 24 leading to a final temperature in the gas of about 2500 K and a pressure of about 1600 bar. Helium was chosen as it is simpler to handle as hydrogen. For later applications a use of hydrogen is also possible.
The pistons are also mechanically synchronized. All parts of the chambers and the pistons are constructed to be easily renewable, also the pistons are not supposed to get destroyed after a shot. The repetition rate is expected to be one shot every 15 to 30 minutes.
In the second stage, the expanding helium accelerates the projectile in the barrel. This barrel has an inner diameter of 12.7 mm and a length of 2 m. The compression chamber of the first stage contains 6 l. With this setup 3 g loads can be accelerated to about 3 km/s. The loads could be made for example of a 10 mm diameter and 4 mm thick Al-flyer and a corresponding sabot.

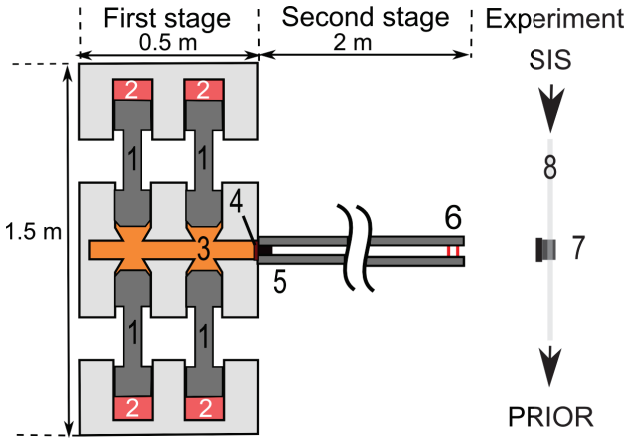

Figure 1: Not to scale scheme of the proposed setup. First stage: (1) pistons, (2) methane combustion chambers, (3) Helium compression chamber,(4) rupture disc. Second stage: (5) barrel with projectile, (6) velocity sensor. Experiment: (7) pusher and target irradiated by (8) proton beam.

Outlook

A pending issue is the synchronization of the device with the proton beam. Since such devices have a ms jitter it is not possible to synchronize the ignition of the device itself with the synchrotron. Instead, the velocity of the projectile is measured at the end of the barrel. Considering the velocity measurement and the flight-length between the end of the barrel and the target a trigger pulse is generated. The detailed setup for the synchronization will be developed in the years of GSI shut-down. Discussions with the developers of the future timing system at GSI and FAIR are already under way.
Choosing methane as the propellant the exhaust fumes (CO_2 and H_2O) of the combustion process are safe and not harmful to the environment. Using helium instead of hydrogen also means there are less safety issues. Because of that and due to the the compact dimensions of the driver the device can easily be transported and installed at different laboratories and other facilties, such as synchrotron radiation sources. Thus the driver can also be tested and used while the GSI accelerator is shut-down in preparation for FAIR. The construction will take place in 2015 at TU Darmstadt. After its commissioning the transportation to GSI for further tests is planned.
Once set up at FAIR, the light-gas accelerator can serve as a relatively simple and cheap driver for first-day experiments at the APPA Cave. In conjunction with PRIOR, it is possible to study a wide range of shock-induced states and other phenomena related to extreme conditions in matter.

* Work supported by BMBF
† m.endres@gsi.de

Suppression of Liquid Metal Flow by Supersonic Free Jet toward Intense and Point X-ray Source

D. Takewaki, Y. Homma, K. Takahashi, T. Sasaki, T. Kikuchi, and Nob. Harada
Nagaoka University of Technology, 1603-1, Kamitomiokamachi, Nagaoka 940-2032, Japan

X-rays and EUV sources [1-5] are applied to observations of hydrodynamic behavior in dense plasma and bio-tissue, and lithography. A small size plasma light source with intense emission is expected to apply the applications, and we focus on an X-pinch [3-4]. The load consists of two or more fine wires, which cross and touch at one point. To apply high current flow into the load, the point grows up to the high temperature and dense plasma by pinch effect. However, it is difficult to generate a high repetitive and intense X-ray source due to reloading thin wire.

We proposed a novel X-pinch load using a liquid metal and a nozzle corn electrode. In this study, reducing pressure gradient between the liquid metal flow and a vacuum, we investigate a suppression of liquid metal by supersonic free jet.

The experimental setup for a liquid metal injection device is shown in Fig. 1. Figure 1 (a) shows a schematic diagram of liquid metal injection. The used liquid metal is Galinstan, which is liquid state at room temperature. An aerospike nozzle [6] with the diameter of 2 mm introduces a coaxial supersonic free jet to the outer surface of the liquid metal flow. The coaxial supersonic free jet suppresses the expansion of the liquid metal by reducing pressure gradient on the surface of the liquid metal flow. Helium gas is used for optically thin in short wavelength regime. The experimental setup of observing liquid metal behaviors is shown in Fig. 1(b). The liquid metal injection device is placed in the vacuum chamber. The image of the liquid metal flow was taken after the supersonic free jet had reached the chamber. The image was exposed by camera using a single focus lens for 20 μs that the high pressure Xe flash ramp had emitted. The pressure in the chamber was 10^2 Pa.

From the observation of the liquid metal flow with the supersonic free jet generated by the aerospike nozzle, the liquid metal diameter as a function of the direction of the liquid metal flow is shown in Fig. 2. In this result, the liquid metal diameter without the supersonic free jet is 55 μm at the liquid metal injection distance of 1 mm. On the other hand, the liquid metal diameter with the supersonic free jet is 48 μm at the liquid metal injection distance of 1 mm. These results indicated that the liquid metal expansion can be suppressed by the supersonic free jet.

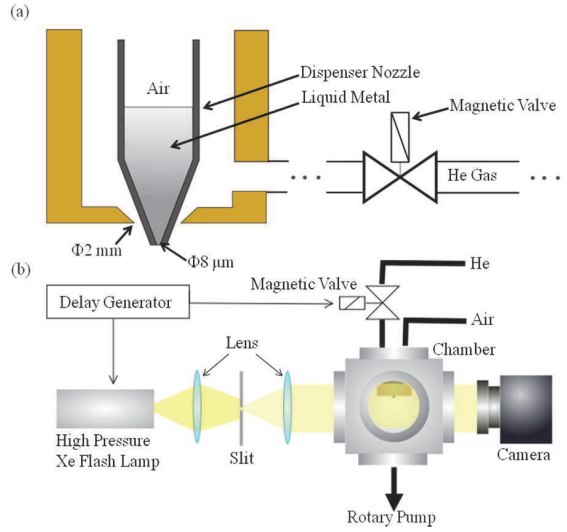

Fig. 1. Experimental setup of liquid metal injection

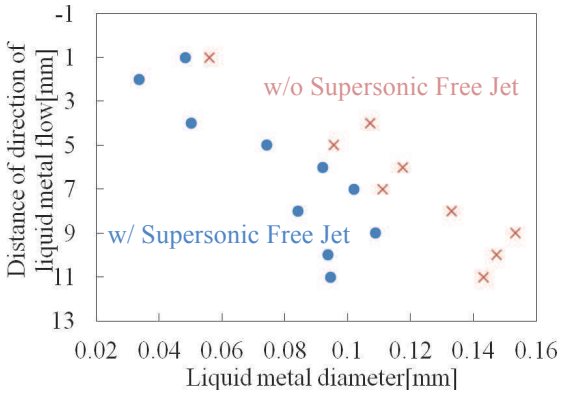

Fig. 2. Liquid metal diameter with and without supersonic free jet

References

[1] T. Higashiguchi, *et al.*, J. Appl. Phys. **96** (2004) 6147.
[2] M.A. Klosner and W.T. Silfvast, Appl. Optics **40** (2001) 4849.
[3] T.A. Shelkovenko, *et al.*, Phys. Plasmas **8** (2001) 1305.
[4] F. Tachinami, *et al.*, Nucl. Instrum. Methods Phys. Res. A**733** (2014) 25.
[5] T.A. Shelkovenko, *et al.*, Phys. Plasmas **17** (2010) 112707.
[6] T.T. Bui and J.E. Murray, *41st AIAA/ ASME/ SAE/ ASEE Joint Propulsion Conference & Exhibit*, AIAA-2005-3797 (2005).

Study on Optical Measurement System for Warm Dense Matter Generation using Intense Pulsed Power Generator

Ryota Hayashi[1)], *Tomoaki Ito*[1)], *Fumihiro Tamura*[1)], *Takahiro Kudo*[1)], *Naoto Takakura*[1)], *Shoma Horinouchi*[2)], *Kenji Kashine*[2)], *Kazumasa Takahashi*[1)], *Toru Sasaki*[1)], *Takashi Kikuchi*[1)], *Nob. Harada*[1)], *Weihua Jiang*[1)], *and Akira Tokuchi*[1),3)]

[1)] *Nagaoka University of Technology, 1603-1, Kamitomioka, Nagaoka, 940-2188, Japan*

[2)] *National Institute of Technology, Kagoshima College, 1460-1, Shinkou, Hayato, Kirishima, 899-5193, Japan*

[3)] *Pulsed Power Japan Laboratory Ltd., 2-3-16, Oji, Kusatsu, Shiga, 525-0032, Japan*

In order to obtain property data of the warm dense matter (WDM) in inertial confinement fusion (ICF), an evaluation method with isochoric heating [1,2] on the implosion timescale using an intense pulsed power generator ETIGO-II (~1 TW, ~50 ns) [3] has been proposed [4]. Foamed metal is considered as structural materials in the fuel pellet [5]. The properties in WDM should be clear to design the ICF fuel pellet.

We studied the measurements of the internal energy and the temperature for the estimation on a specific heat at constant volume of the WDM. In this study, an optical measurement system with a spectroscope is considered for the temperature evaluation of a foamed metal sample.

Figure 1 shows a concept of the experimental setup. Foamed copper is used as a sample, which is packed into a hollow sapphire capillary (∅5 mm × 5 mm). The density of the foamed copper sample is 0.1 times the solid density. The temperature of the sample is increased due to Joule heating with intense pulsed power discharge. To determine the feasibility of generating WDM state using ETIGO-II, the input power was measured [4].

The temperature of the sample is estimated with the measured power and the conventional thermodynamic properties. The achievable temperature of sample is estimated ~10000 K in several-10 ns.

To estimate the requirements for the temporal and the wavelength resolutions, the time evolution of emission intensity is estimated from numerical simulation [6,7]. Figure 2 shows the emission intensity. The temporal resolution and the wavelength interval are defined as 1 ns and 10 nm, respectively. Squared points in the figure indicate the peak emission intensity. The wavelength of peak emission intensity shifts from 750 nm to 400 nm during 22 ns. The peak shift is obtained over 10 nm up to 18 ns. From above estimations, total sweep time of streak camera and the wavelength resolution of spectroscope are required to 100 ns and 5 nm with the equipment specification. It indicates that the temporal resolution of 1 ns and the wavelength resolution 10 nm are enough to evaluate the temperature of the sample with wavelength.

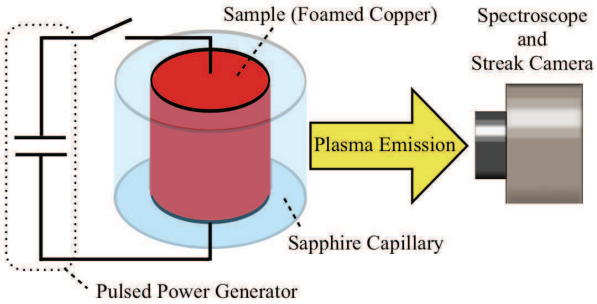

Fig. 1 Concept of experimental setup

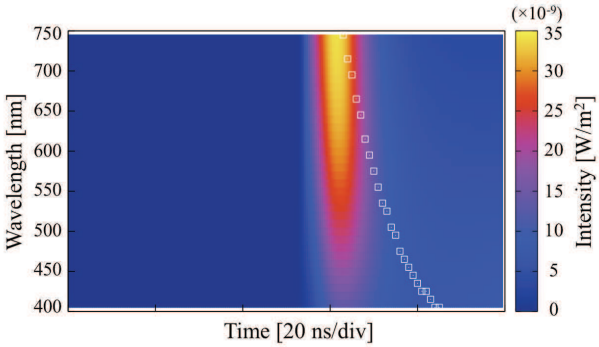

Fig. 2 Emission intensity estimated by numerical result

References

[1] Y. Amano, *et al*., Rev. Sci. Instrum. **83** (2012) 085107.

[2] T. Sasaki, Y. Miki, *et al*., Nucl. Instr. Meth. Phys. Res. A **733** (2014) p. 28.

[3] W. Jiang, *et al*., Jpn. J. Appl. Phys. **32** (1993) L752.

[4] R. Hayashi, *et al*., *12th Symp. Heavy-Ion Inertial Fusion, Lanzhou, 2014*, P15.

[5] M. Tabak and D. C. Miller, Nucl. Instr. Meth. Phys. Res. A **415** (1998) p. 75.

[6] T. Kikuchi, *et al*., NIFS-PROC **94** (2013) p. 80.

[7] T. Kikuchi, *et al*., Trans. GIGAKU **2(1)** (2014) 02010/1-10.

4 Theory for HEDP/WDM in Plasma-, Laser- and Atomic Physics

Application of the energy principle of magnetohydrodynamics to fusion and lightning plasmas *

C.-V. Meister[1,2], *Th. Haase*[1], *B.R. Lee*[2], *and D.H.H. Hoffmann*[1,2]

[1]Institut für Kernphysik, Schlossgartenstr. 9, 64289 - Darmstadt; [2]Graduate School of Excellence Energy Science and Engineering, Jovanka-Bontschits-Str. 2, 64287 - Darmstadt, Germany

Introduction

In nuclear fusion systems, plasma instabilities getting unstable for different reasons interrupt the fusion process and make the application of nuclear fusion for an energy gain in reactor systems up to now unachievable. In the Earth's magnetosphere, plasma instabilities modify the physical parameters and vary the transport of solar energy and radio signals from vertical sounding stations. Thus, it is essential to study plasma instabilities in both nuclear fusion and magnetospheric systems. Using the energy principle of magnetohydrodynamics (MHD), this all can be done without knowing the exact values of growth rates of unstable waves. According to [1], the growth rates of MHD instabilities in inertial fusion plasmas are, anyway, on the order or smaller than 5 percent of the possible observation times. And if even shorter observation times will be possible in future, the application of the MHD energy principle will often be much easier as a kinetic calculation of the growth rate.

Applying the MHD energy principle means to analyse, if the potential energy of the plasma system may decrease for any of its allowable small displacements. If this is the case, the system is unstable. Thus, applying the MHD energy principle, one has to solve variational problems for the potential energy.

The present work considers instabilities in plasmas which are described within the frame of ideal MHD, that means the system has an infinite electrical conductivity (see e.g. [2-4]). The energy principle is applied to an internally homogeneous pinch. Indoing so, an analytical equation is derived to describe axial fluid displacements in systems with non-cylindrical disturbances [3]. Numerical applications are performed for systems with cylindrically symmetric disturbances for ITER-type [4-6] and lightning [4, 6] plasmas. Thus, with respect to the general plasma phase diagram, the applications here considered are located in the electron density-temperature region of the future FAIR experiments, which is presented by a black triangle in Fig. 1. Figure 1 shows the locations of different space and laboratory plasmas with respect to electron density n_e and plasma temperature T. Lightnigs (L) and the inner parts of the fusioning sun are situated in the black triangle, as do also plasmas generated by the GSI laser PHELIX and heavy ion beams (HI).

* Work financially supported by the Excellence Initiative Darmstadt Graduate School of Energy Science and Engineering (GSC1070)

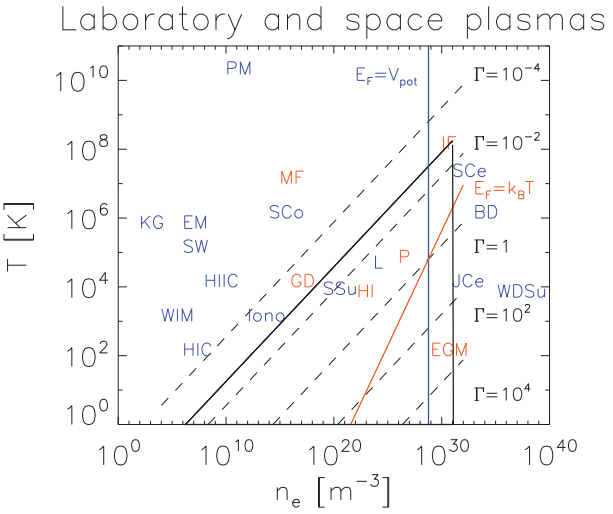

Figure 1: Location of different space and laboratory plasmas in the plasma phase diagram. n_e - electron density, T - plasma temperature. $\triangle$ - FAIR region, dashed lines - plasma parameter Γ. BD - brown dwarf, EGM - electron gas in metals, GD - gas discharge, HI - heavy ion heated gas targets, HIC - interstellar HI cloud, HIIC - interstellar HII cloud, I - ionosphere, IF - intertial fusion, JCe - Jupiter center, KG - interstellar coronal gas, L - lightning, MF - magnetic confinement, P - PHELIX, PM - pulsar magnetosphere, SCe -sun center, SCo - sun corona, SSu - sun surface, WDSu - white dwarf surface, WIM - warm partially-ionised interstellar matter. [4]

Plasma model

It is assumed that the plasma is located in a cylinder in the equilibrium state. In the plasma, an axial magnetic field $B_z(\vec{r})\vec{n}_z$ exists. Further, it is supposed that the plasma is surrounded by a vacuum region, and in the vacuum only an azimuthal magnetic field $B_\varphi(r)\vec{n}_\varphi$ is located. The whole system consisting of the cylindrical plasma core and the surrounding vacuum is contained in a cylindrical conducting shell. That means, the plasma does not contact the shell at all, there is a vacuum boundary between the plasma and the shell.

In the plasma core along the symmetry axis $\vec{n}_z$. $\nabla \times$

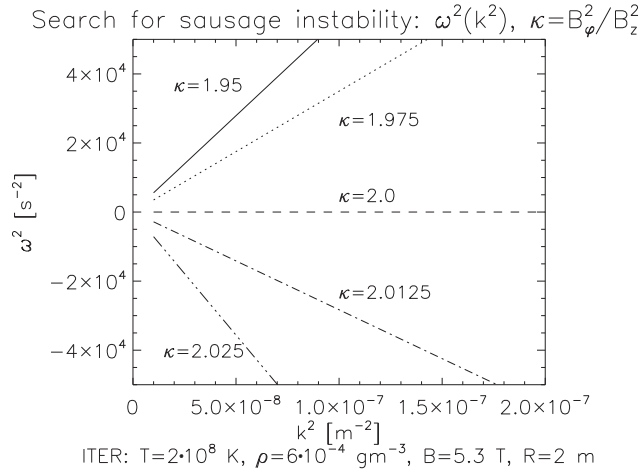

Figure 2: Dispersion relation of waves in an ITER-type plasma at different ratios of azimuthal to axial magnetic field B_φ/B_z. Solution for $\alpha R < 1$. At $\omega^2 < 0$, the sausage instability is excited. [4]

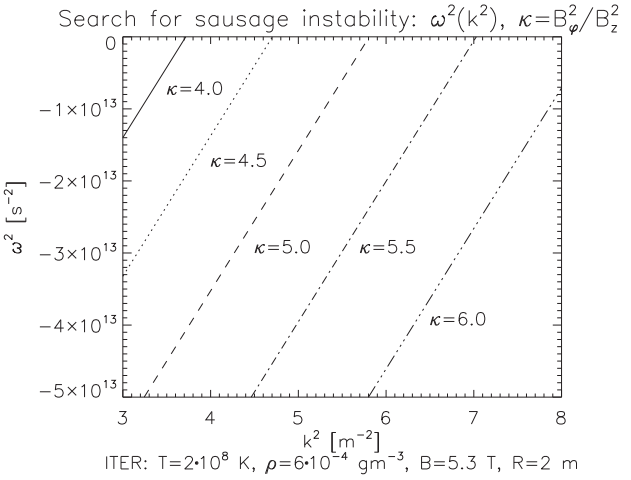

Figure 3: Dispersion relation of waves in an ITER-type plasma at different ratios of azimuthal to axial magnetic field B_φ/B_z. Solution for $\alpha R > 1$. At $\omega^2 < 0$, the sausage instability is excited. [4]

$\vec{B}_z = 0$ and $\nabla p_o \approx 0$. The approximation $\nabla \times \vec{B}_z = 0$ means that no current exists in the inner part of the plasma (i.e. along the z-axis). Indeed, in the case of the θ-pich with an axial magnetic field in the plasma core, the currents are almost negligible along the symmetry axis.

The method applied to derive the dispersion relation of waves excited in the plasma model is decribed in detail in [4,6]. There it is shown, that the solutions of the derived dispersion relations depend on a parameter

$$\alpha^2 = \frac{(v_s^2k^2-\omega^2)(v_A^2k^2-\omega^2)}{v_s^2v_A^2k^2-(v_s^2+v_A^2)\omega^2}, \quad v_A^2 = \frac{B_z^2}{\mu_o\rho_o}, \quad v_s^2 = \frac{\gamma p_o}{\rho_o}.$$

ω and k are wave frequency and wave number, v_A and v_s Alfvén und sound velocity. γ describes the polytropic index of the plasma, and ρ_o and p_o are its mean mass density and mean pressure, respectively. Studying magnetohydrodynamic waves within the frame of the chosen pinch model, one obtains always at least two modes. One is a stable pure Alfvén wave, and the second is an Alfvén-type mode, which may be instable.

ITER-type plasmas

Since 2005 in Caderache, France, the International Thermonuclear Experimental Reactor ITER is under construction. ITER is a Tokamak-type reactor with a total radius of 10.7 m and a height of 30 m. It is designed to deliver a fusion power of 500 MW and contains 18 superconducting toroidal and 6 poloidal field coils. The strength of the ITER toroidal magnetic field will be about 5.3 T (here locally described by B_z). It can reach up to 11.8 T. A device volume of 840 m^3 will contain a plasma of 0.5 g at mean temperature of $2 \cdot 10^8$ K. Thus, in case of ITER, one has to consider a plasma with a mass density of about $\rho_o = 6 \cdot 10^{-4}$ gm^{-3}. The Alfvén and sound velocities of the plasma amount to $v_A = 6 \cdot 10^6$ m/s and $v_s = 1.2 \cdot 10^6$ m/s, respectively.

Results for the frequency of the Alfvén-type mode ω^2 in the ITER plasma at $\alpha R > 1$ (plasma radius $R = 2$ m) are presented in Fig. 2. It is to be seen that the strength of the instability, i.e. the region with $\omega < 1$, grows monotonically with increasing $\kappa = B_\varphi^2/B_z^2$ at small wave numbers k. Generally, instabilities occur at $\kappa > 2$. Having found an instability for a given κ and a special wave number k, the system is obtained to be unstable for the κ at any wave number. But the wave numbers studied in Fig. 2 are not of real importance for ITER. They are too small. Nevertheless, the obtained results are very helpful as limiting cases for numerical analyses, when the nonlinear dynamics of ITER-type plasma instabilities at smaller wavelengths is studied.

Considering large $\alpha R > 1$, instabilities in ITER-type plasmas should occur at wavelengths $\lambda > 2\pi R/\kappa = 4\pi/\kappa$ m. For $\kappa = 2$, unstable waves have much smaller wavelengths, but they are larger than 6 m. And if κ increases, the wavelength will further decrease. In Figure 3, results of the numerical calculation of ω^2 as function of the square of the wave number k^2 are presented for different values of the parameter κ. To describe smaller wavelengths than that considered in Fig. 2 for $\alpha R < 1$, much larger k^2-values are chosen. They correspond to wavelengths of about 3 m. Results are only shown for $\omega^2 < 0$, as then also $\alpha^2 > 0$. Indeed for the k^2-interval studied, $\alpha R = 1$ is satisfied at $\omega^2 \approx 10^{12} - 10^{15}$ s^{-2}. For stable plasmas with $\omega^2 > 0$, values of α^2 below zero occur. From Figure 3 follows, that, in contradiction to the case $\alpha R < 1$, under the condition of $\alpha R > 1$ instabilities may be obtained for all considered κ-parameters, but they do not occur at any wave number k. The smaller the wave number the stronger the instability.

Lightnings

In nature, pinches occur very often in connection with the appearance of lightnings. There, temperatures of up to some 30000 K are found, and electrical currents are of the order of 40 kA [7]. The lifetime of lightnigs amounts to 1 ms. The discharge radii with values of a few centimeters are rather small. This results into magnetic fields of about 0.4 T and a magnetic pressure of 0.6 atm (60795 Pa). Thus, at MHD pressure balance, the pinch pressure is about 1.6 atm (162120 Pa) and the pinch Alfvén speed has a value of 4000 m/s [7].

Concerning the plasma model considered in the present work, the $\vec{B}_z$ in the inner plasma core, i.e. the hot lightning plasma, equals 0.4 nT. Of course, the hot lightning plasma is not surrounded by a vacuum, but by a plasma with much lower ionization intensity, which is here approximated by a vacuum. The magnetic field of the surrounding plasma is the geomagnetic one with an intensity of $5 \cdot 10^{-5}$ T. In the Earth's lower atmosphere, always an electrical field exists, which is directed vertically to the Earth's surface. It causes field-aligned electrical currents which may generate azimuthal magnetic fields. It is known that thunderclouds mainly help to conserve the vertical electrical field of the Earth's atmosphere. But lightnings may be indeed directed to the Earth or in the opposite direction, so they may increase or decrease the normal electric field locally. In the Earth's atmosphere also horizontal electric fields are observed. But these fields are not taken into account in the present model. Besides, the gravitational acceleration is neglected.

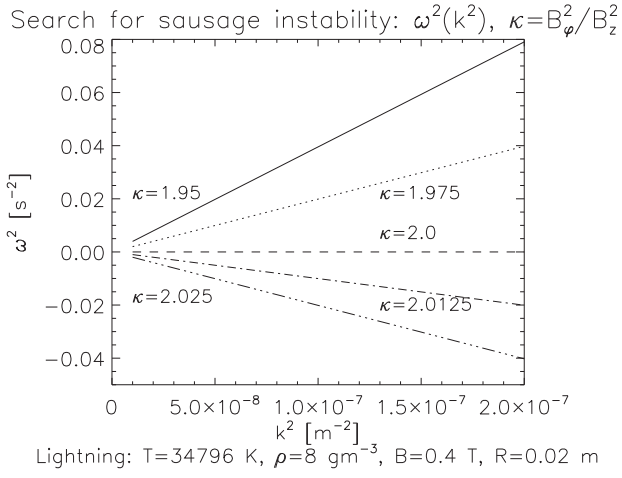

Figure 4: Dispersion relation of waves in an lightning plasma at different ratios of azimuthal to axial magnetic field B_φ/B_z. At $\omega^2 < 0$, the sausage instability is excited. [4]

For the above mentioned plasma parameters in a lightning, the dispersion equation of Alfvén-type waves is solved for $\alpha R < 1$ and the results are presented in Fig. 4 for the same κ-parameters and wave numbers k as have been chosen for the ITER study at $\alpha R < 1$. It is to be seen, that again under the condition $\kappa > 2$, the plasma becomes unstable. But the square of the frequencies of the waves ω^2 is about 6 orders of magnitude smaller than in the case of the ITER plasma. Besides, ω^2 increases more slowly with the wave number than in the ITER case. The numerical analysis of radial displacements of the plasma fluid in the lightning shows, that the displacement amplitudes grow with increasing wave number k. In the studied plasma parameter region they have a maximum value of 10 m [4,5].

Conclusions

The magnetohydrodynamic energy principle is derived for an internally homogeneous pinch and applied to ITER-type and lightning systems. In comparison to former works it is shown, that the dispersion relation of waves in the chosen model describes a stable pure Alfvén wave. This wave is also stable under the condition that other unstable modes are generated in the system. The results for the instability of the Alfvén-type waves strongly depend on the ratio of the azimuthal to the axial magnetic fields in the system. Consequently, one may use this dependence to avoid such instabilities in technical devices like ITER.

References

[1] A.N. Simakov, "Formal theory of MHD stability: Energy principle" CMPD & CMSO Winter School 2008, http://home.physics.ucla.edu/calendar/conferences/cmpd /talks/simakov.pdf (downloaded 01.01.14)

[2] J.P. Freidberg, Ideal magnetohydrodynamics, Springer, New York (1978).

[3] C.-V. Meister, D.H.H. Hoffmann, "Application of the MHD energy principle to pinch plasmas", 33dr Int. Workshop on Physics of High Energy Density in Matter, 13-18.01.13, Waldemar-Petersen-Haus, Hirschegg, Austria.

[4] C.-V. Meister, Theoretical plasma physics, chapter: Magnetohydrodynamic energy principle, Lecture notes, winter semester 2013/2014 and summer semester 2014, University of Technology Darmstadt.

[5] C.-V. Meister, B. R. Lee, D.H.H. Hoffmann, The influence of boundary conditions on the excitation of instabilities in magnetohydrodynamic systems, 17th Int. Conf. on Recent Progress in Many-Body Theories (MBT17), 8.-13.09.2013, Rostock, Germany; Journal of Physics: Conference Series, Vol. 529 (2014) paper 012018, doi: 10.1088/1742-6596/529/1/012018.

[6] Th. Haase, "MHD-Instabilitäten im homogenen linearen Pinch. Dimensionsanalyse für ideale ITER-typ Plasmen", Bachelor thesis, University of Technology Darmstadt, August 2014.

[7] W.M. Manheimer, M. Lampe, J.P. Boris, Effect of a surrounding gas on magnetohydrodynamic instabilities in Z pinch, Phys. Fluids ,16 (1973) 1126-1134.

On the way to study ballooning modes

C.-V. Meister[1,2], P. Zourchang[1], and D.H.H. Hoffmann[1,2]

[1]Institut für Kernphysik, Schlossgartenstr. 9, 64289 - Darmstadt; [2]Graduate School of Excellence Energy Science and Engineering, Jovanka-Bontschits-Str. 2, 64287 - Darmstadt, Germany,

The ballooning mode is an internal pressure-driven mode of plasmas. It occurs in planetary magnetospheres (e.g. of the Earth), but also in Tokamak fusion devices. Therefore, its excitation mechanism has to be studied very carefully.

In 2014 at the University of Technology Darmstadt, the study of ballooning modes began within the frame of the energy principle of ideal magnetohydrodynamics [1-3]. These investigations are mainly based on the works by Freidberg [1] and Cooper [2,4] considering such modes in two- and three-component plasma systems.

Using the principle of ideal magnetohydrodynamics means to apply the variational principle to the potential energy of the plasma system. Mathematical expressions for the variation of the potential energy in an ideal plasma are well-known [1-3]. So, it is very easy to derive the formula for the variation of the potential energy in dependence on the displacements $\vec{\xi}$ of the fluid elements because of a force $\vec{F}(\vec{\xi})$,

$$\delta W = -\frac{1}{2}\int \vec{\xi}^{*}\cdot\vec{F}(\vec{\xi})\,d\vec{r} = -\frac{1}{2}\int d\vec{r}\vec{\xi}^{*}\Big[\frac{1}{\mu_o}(\nabla\times\vec{Q})\times\vec{B} + \frac{1}{\mu_o}(\nabla\times\vec{B})\times\vec{Q} + \nabla(\gamma p\nabla\vec{\xi}+\vec{\xi}\cdot\nabla p)\Big]d\vec{r}. \tag{1}$$

In equation (1), $\vec{B}$ ist the vector of the mean magnetic induction, $\vec{Q} = \nabla\times(\vec{\xi}\times\vec{B})$, and p_o as well as γ describe the mean plasma pressure and the polytropic coefficient of the matter, respectively. However, in works concerning ballooning modes, the starting expression for the variation of the potential energy is often a relation where $|Q|^2$ occurs, which is presented without (detailed) derivation. For instance, the relation

$$\delta W = \frac{1}{2}\int d\vec{r}\Big[\frac{|\vec{Q}|^2}{\mu_o} - \frac{\vec{\xi}^{*}}{\mu_o}\Big((\nabla\times\vec{B})\times\vec{Q}\Big) + \gamma p|\nabla\vec{\xi}|^2 - \vec{\xi}^{*}\nabla(\vec{\xi}\cdot\nabla p)\Big] - \frac{1}{2}\int d\vec{S}\left[\frac{(\vec{\xi}^{*}\times\vec{B})\times\vec{Q}}{\mu_o} + \gamma p\nabla\vec{\xi}(\vec{n}\vec{\xi}^{*})\right] \tag{2}$$

for plasmas with $\vec{B}$ locally parallel to the plasma surface $d\vec{S}$ is to be found. $\vec{n}$ is a unity vector which is directed perpendicularly to the surface $d\vec{S}$. In the lecture notes [4], now a detailed derivation of the formula (2) is given. Equation (2) is used in [1] to express δW only by the displacements of the fluid elements perpendicular to the magnetic field $\xi_\perp$. In doing so, the original 3D-problem is tranferred to a series of independend 1D-problems.

Introducing in eq. (2) a curvature vector of the magnetic field line $\vec{\kappa} = (\vec{b}\cdot\nabla)\vec{b} = -\vec{R}_c/R$, $\vec{b} = \vec{B}/B$, the relation

$$\delta W_V = \frac{1}{2}\int d\vec{r}\Big[\frac{|\vec{Q}_\perp|^2}{\mu_o} + \frac{B^2}{\mu_o}|\nabla\cdot\vec{\xi}_\perp + \xi_\perp\cdot\vec{\kappa} + \vec{b}(\vec{\xi}_\perp\cdot\nabla)\vec{b}|^2 + \gamma p|\nabla\cdot\vec{\xi}|^2 - (\vec{\xi}_\perp\cdot\nabla p)(\vec{\xi}_\perp^{*}\cdot\vec{\kappa} + \vec{b}(\vec{\xi}_\perp^{*}\cdot\nabla)\vec{b}) - j_\parallel(\vec{\xi}_\perp^{*}\times\vec{b})\cdot\vec{Q}_\perp\Big] \tag{3}$$

is found for the volume-dependent part of (2) in [3]. Here $\vec{R}_c$ designates the vector of the curvature radius of the magnetic field. The result (3) is reproduced in [5].

Relation (3) is indeed nonlinear with respect to the gradients of the thermal pressure. So, it might happen in Tokamak devices, that the ballooning instability gets strengthened at decreasing thermal plasma pressure gradient - a problem which was under discussion in 2014. Further, it is shown in [3,5], that the growth rate of a ballooning instability is strongly determined by the ratio of the perpendicular to the parallel components of additional hot anisotropic electrons which may be generated in a Tokamak plasma. The works [3,5] contain some first analyses of ITER-type plasmas with respect to ballooning instabilities. Numerical results for growth rates of ballooning waves in the MAST tokamak are presented in [6].

References

[1] J.P. Freidberg, Ideal magnetohydrodynamics, Springer, New York (1978).

[2] W.A. Cooper, Variational formulation of the linear MHD stability of 3D plasmas with noninteracting hot electrons, Plasma Phys. Control. Fusion, 34(6) (1992), 1011-1036.

[3] C.-V. Meister, Theoretical plasma physics, chapter: Magnetohydrodynamic energy principle, Lecture notes, winter semester 2013/2014 and summer semester 2014, University of Technology Darmstadt.

[4] W.A. Cooper, D.B. Singleton, R.L. Dewar, Spectrum of ballooning instabilities in a stellarator, Phys. Plasmas, 3(1) (1996), 275-280.

[5] P. Zourchang, Anwendung des MHD-Energieprinzips auf die Ballooning-Instabilität, Bachelor-Arbeit, University of Technology Darmstadt, October 2014.

[6] A. Kleiner, Finite toroidal mode number ideal MHD instabilities in Tokamak plasmas with externally applied magnetic perturbations, Master thesis, University of Technology Darmstadt, October 2014.

Collisionless absorption and hot electrons in intense laser-target interaction

P. Mulser
TQE: Theoretical Quantum Electronics, Tech. Univ. Darmstadt, Germany

Intense and superintense laser beam interaction with dense matter is characterized by the generation of superthermal high energy electrons.

The focus of the present contribution is on the physics of collisionless absorption of intense laser beams in dense targets in the intensity domain I = 10^{18} - 10^{22} W/cm^2 for optical wavelengths, on the variation of the spectral composition of the energetic electrons with intensity and on their scaling with the latter. Most remarkable results are the Brunel-like spectral hot electron distribution at the relativistic threshold [1], the minimum of absorption at a = 15 - 30, the drastic reduction of the number of hot electrons in this domain and their reappearance beyond, the strong coupling with the return current beyond expectation, and a strong hot electron scaling in a = 1-10, a scaling in vague accordance with current published estimates in a = 10 - 50 and a strong increase beyond. a = eA/m_ec, a laser vector potential.

On a fundamental level understanding collisionless absorption is equivalent to the search for the non-orthogonality of induced current density to the laser field. The answer is found in the interplay of the laser field with the space charge E-field induced by it. The idealized model of Brunel works already on this basis. It is capable of explaining important effects at the relativistic intensity threshold and below, like the generation of two groups of electrons, a hot and a cold component. The non-Maxwellian spectrum predicted by the model is found in our simulations [2] at the relativistic threshold and below; with increasing a it is washed out. By following test orbits we are able to localize absorption at the vacuum-target interface and in the skin layer for all intensities below the radiation reaction limit at I = 10^{22} W/cm^2 in linear polarization, in agreement with Brunel for non relativistic intensities. If therefore the ominous "vacuum heating" is invoked as responsible for absorption this is correct if it is identified with Brunel's mechanism. What it does not explain in terms of physics, and Brunel does not either, is the underlying principle, i.e. the phase shift and, in concomitance, orbits crossing. An explanation in terms of physics has to show that (i) such a breaking of flow is not by accidence and (ii) a hot Maxwellian tail in the spectrum is a natural outcome from strong drivers. Anharmonic resonance [3] is currently the best model explaining both aspects. It rules stochastic heating and "weave breaking" out automatically. Anharmonic resonance constitutes an attractor (fix point).This kind of resonance always happens in presence of a sufficiently strong driver at any laser frequency and any target density, in contrast to harmonic resonance which is bound to the plasma frequency, i.e., $\omega = \omega_p$. When crossing resonance the momentum of an electron undergoes a phase shift by π or a fraction of it with respect to the bulk of the plasma. Wave breaking, here more appropriately called breaking of flow owing to profile steepening on lengths of a small fraction of a laser wavelength, from 1/10 to 1/30, is a consequence of absorption and energetic electron generation, not its origin. From I = 5* 10^{21} W/cm² on anharmonic resonance is strengthened by the generation of runaway electrons due to trapping in both, the incident and the reflected laser wave. The reduction up to nearly disappearance of hot electrons of energies $E \geq E_{os}$ is attributed to oscillation inhibition by the ponderomotive space charge field. In the whole intensity domain considered the major fraction of laser energy is deposited in the hot and moderately hot electrons. The next significant portion goes into Cherenkov plasmons excited by the periodic plasma jets. From the analysis of test trajectories their coupling to the neutralizing return current is apparent. We consider it as an important aspect when modeling anomalous transport of heat and fast electrons in compressed matter.

Finally, we reexamined the hot electron scaling in 1D, perhaps the most controversially discussed subject in the pertinent literature. Acceptable coincidence with the leading approximations, see Refs. in [2], is only found in the intensity range 10^{20} - 10^{21} W/cm^2. The deviations below a = 10 are to be attributed mainly to the imprecise proportionality between E_{os} and I ~ a^2. In the runaway absorption regime the governing scaling law is still to be discovered. The main reason for the current misunderstandings and disagreements have to be attributed to the poor knowledge of the electron energy spectrum f(E). What is missing most at present in the experiment and in the theory is a clear definition of what means "hot" and "cold" electrons. In order not to fall into this deficiency here electrons are defined "hot" and moderately hot" if their energy is higher than E_{os} and $(0.5 - 2/3)E_{os}$. It is approximately the range of the Maxwellian tail. The commonly used terminology "Maxwellian" is misleading because it refers to the electron velocities or momenta with a distribution law df (E) = v^2 $\exp(-E/k_BT_{hot})dv$ ~ $E^{1/2}$ $\exp(-E/k_BT_{hot})$ dE. This differs from our findings (and, implicitly, of others) of a Boltzmann 3 nn distribution df (E) = $\exp(-E/k_BT_{hot})$ dE for the relevant restricted phase space of total energies $\mathcal{E} = \Sigma E_i$.

References

[1] P. Mulser, S.-M. Weng, and Tatyana Liseykina, Phys. Plasmas **19**, 043301 (2012)
[2] Tatyana Liseykina, P. Mulser, and M. Murakami, arXiv 1412.7233, submitted to Phys. Plasmas
[3] P. Mulser, D. Bauer, H. Ruhl, PRL **101**, 225002(2008)

Nonequilibrium electron-lattice relaxation in ultrashort laser-excited solids

N. Brouwer[1], *B.Y. Mueller*[2], *and B. Rethfeld*[1]

[1]Fachbereich Physik und Landesforschungszentrum OPTIMAS, Technische Universität Kaiserslautern, Germany;
[2]Max Planck Institute for Intelligent Systems, Stuttgart, Germany

After excitation with an ultrashort laser pulse, the electronic system of a solid is in a state of strong thermodynamic nonequilibrium. Its thermalization occurs on a femto- to picosecond timescale; on a similar timescale energy is transfered to the lattice. The coupling strength of the electron-lattice relaxation depends on the particular electron distribution and differs for the nonequilibrium case as compared to a thermalized electron distribution. Moreover, in dielectrics, the electron excitation from the valence band to the conduction band leads to an increase of the density of the electron-hole plasma, which also influences the energy transfer to the lattice. Here, we show our studies on electron-lattice coupling in dependence on laser parameters for different materials.

Usually the laser energy is absorbed by the electrons of the material. After ultrashort laser pulse irradiation, the conduction band electrons thus have a higher energy density u_e than the phonons u_{ph}. In case an electron temperature T_e and a phonon temperature T_{ph} can be defined, the cooling of the electronic system can be described by

$$\frac{\partial u_e}{\partial t} = \alpha \left(T_{ph} - T_e\right) \quad , \tag{1}$$

where α denotes the electron-phonon coupling parameter. In dielectrics, high intensity pulses promote electrons from the valence band to the conduction band, thus increasing the density of the electron-hole plasma n_e to densities much higher than the equilibrium density.

Fig. 1 shows the coupling parameter α, determined by Eq. (1), for laser-excited fused silica. Two electron temperatures are assumed and the dependency on electron density is shown. The phonon temperature is at room temperature. The curves show an increase for low densities and a transition to an asymptote or shallow decrease for higher densities, respectively. This shape and its origin is discussed and explained in Ref. [1], where also the calculation of $\partial u_e/\partial t$ with the help of Boltzmann collision integrals is introduced.

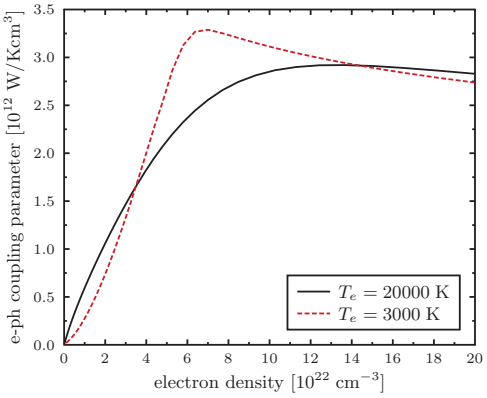

Figure 1: Coupling parameter α in fused silica.

Kinetic equations also open the way to determine a coupling strength for systems in nonequilibrium. The distribution function of electrons f may be strongly disturbed and deviate from a Fermi distribution after excitation. Also the phonon distribution g may be disturbed. It is, however, possible to determine a unique Fermi and Bose distribution, respectively for electrons and phonons, which obey the same internal energies u_e and u_{ph} as f and g. The temperatures of these corresponding equilibrium distribution are called corresponding temperatures and serve as a possibility to determine an electron-phonon coupling parameter in nonequilibrium

$$\alpha_{\mathrm{neq}}[f,g] = \frac{du_e[f]/dt}{T_{ph}[g] - T_e[f]} \quad . \tag{2}$$

Fig. 2 shows this parameter α_{neq} in gold in dependence on the corresponding temperature $T_e[f]$ for different wavelengths of the exciting laser. It can be seen that the coupling deviates from the equilibrium case, which is also shown in the figure. The details of the calculation as well as an intensive discussion is presented in Ref. [2].

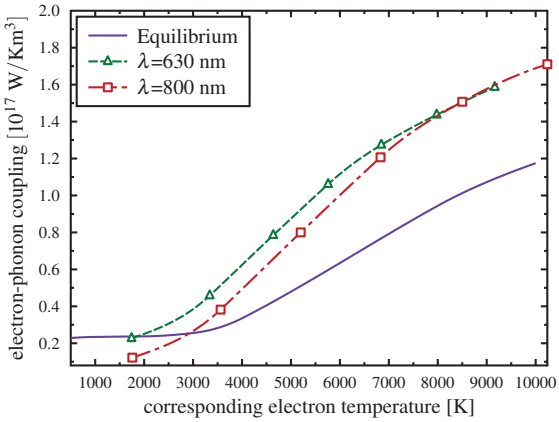

Figure 2: Coupling parameter α_{neq} in laser-excited gold, in dependence on laser wavelength and excitation strength.

References

[1] N. Brouwer and B. Rethfeld. *JOSA B*, 31:C 28, 2014.

[2] B. Y. Mueller and B. Rethfeld. *Appl. Surf. Sci.*, 302:24, 2014.

Electron acceleration at grazing incidence of an intense laser pulse*

N. E. Andreev† [1,2], *L. P. Pugachev*[1,2], *M. E. Povarnitsyn*[1], *P. R. Levashov*[1], *and O. N. Rosmej*[3]
[1]JIHT RAS, Moscow, Russia; [2]MIPT, Dolgoprudny, Russia; [3]GSI, Darmstadt, Germany

In this paper, the generation of hot electrons at grazing incidence of a subpicosecond intense laser pulse onto the plane solid target is analyzed for the parameters of the petawatt class laser system PHELIX using 3-D PIC modeling [1]. The typical time structure of the petawatt class laser pulse can be found in Fig. 2 of the paper [2], where the pulse shape of the PHELIX laser is shown for different parameters of the contrast boosting module. While nanosecond ASE prepulse can be substantially reduced by different measures, the prepulse emission on the timescale of a few tens of picoseconds is present practically in any case. In our modeling of the plasma formation we analyzed first the bulk Al target heating by the picosecond prepulse only for the time interval $[-100, -5]$ ps, as shown in Fig. 2 of paper [2] for high contrast level $\sim 10^{-10}$ at time less than -100 ps (zero time moment correspond to the maximum of the laser pulse intensity). The basic features of the model used for simulation of the laser-matter interaction at the nonrelativistic prepulse intensities are described in our recent paper [3]. The electron and ion densities distributions at $t = -5$ ps are demonstrated in Fig. 1 for the P-polarized PHELIX laser pulse with the angle of incidence 80 degrees and maximum intensity 4×10^{19} W/cm^2. For the electron densities less and about the reflection point

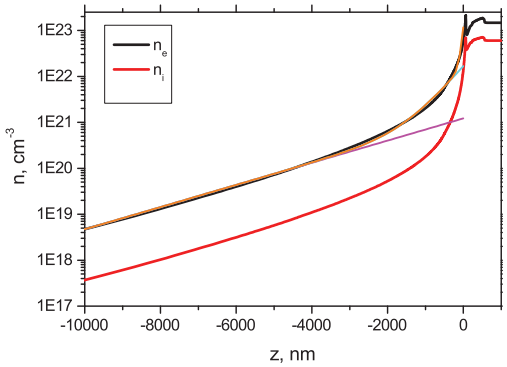

Figure 1: The electron and ion densities distributions at $t = -5$ ps (before the main pulse).

($n_e \approx 0.03 \times n_{cr} \approx 0.03 \times 10^{21}$ cm^{-3}) the density profile can be well approximated by the rarefaction wave exponent with characteristic scale length $L_r = 1.8$ μm. This density profile was used in PIC simulations as the initial density distribution for the main P-polarized pulse interaction at the pulse duration 400 fs with the angle of incidence 80 degrees and maximum intensity 4×10^{19} W/cm^2. Figure 2 shows the energy spectra of accelerated electrons for the initial density scale lengths $L_r = 1.8$ μm and 3.6 μm, and also the spectrum with a hot temperature $T_h = 3.73$ MeV predicted by the ponderomotive electron energy at pick laser intensity [4]. With an increase of the plasma density scale within a few micrometers the number of accelerated electrons drops for energies higher than 30 MeV. But this dependence takes place for the plasma density scales less than 10 μm only. For longer pre-plasma density scales that can be produced by the nanosecond ASE pedestal of the laser pulse, the accelerating mechanism changes and the maximum energy of accelerated electrons growth up to 300 MeV for the density scale $L_r = 20$ μm (at the expense of the number particles decrease in the energy range 50–100 MeV). Obtained results indicate the substantial in-

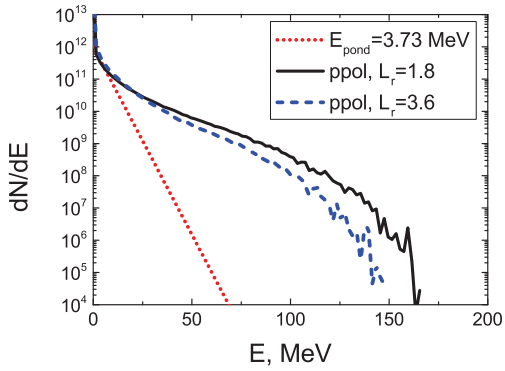

Figure 2: Electron energy spectra for the initial density scale length $L_r = 1.8$ μm (solid line) and $L_r = 3.6$ μm (dashed line). Dotted line sows the spectrum for a hot temperature $T_h = 3.73$ MeV predicted by the ponderomotive electron energy.

crease of the characteristic energy and number of accelerated electrons for the grazing incidence of a subpicosecond intense laser pulse onto the plane solid target in comparison with the laser interaction at normal (not grazing) incidence. It should be noted that at grazing incidence of the laser, the accelerated electrons are directed mainly along the target surface with a rather small divergence.

References

[1] A. Pukhov, J. Plasma Phys. 61, (1999) 425.

[2] F. Wagner, S. Bedacht, A. Ortner, *et al.*, Opt. Express. 22, (2014) 29505.

[3] M. E. Povarnitsyn, N. E. Andreev, P. R. Levashov, *et al.*, Las. Part. Beams. 31, (2013) 663.

[4] S. C. Wilks, W. L. Kruer, M. Tabak, A. B. Langdon, Phys. Rev. Lett. 69, (1992) 1383.

* Work is partially supported by the Program of RAS No 43.
† andreev@ras.ru

Wide-range models for hydrodynamic simulation of laser experiments*

M. E. Povarnitsyn†[1], *N. E. Andreev*[1,2], *and P. R. Levashov*[1]
[1]JIHT RAS, Moscow, Russia; [2]MIPT, Dolgoprudny, Russia

Ultrashort subpicosecond laser irradiation of targets with relativistic pulse intensities $\geq 10^{19}$ W/cm^2 is used in many applications, in particular, for the development of X-ray sources and warm dense matter production, particle acceleration, and fast ignition. In these experiments, a very important laser facility parameter is the pulse contrast ratio (the ratio of the prepulse intensity to the peak laser intensity of the main pulse). Laser systems based on the chirped pulse amplification technique usually produce two types of prepulses: a relatively low-intensity nanosecond pedestal due to the amplified spontaneous emission, and temporal structures on a sub-100 ps time scale. Typically, the contrast ratio at $\sim$ 1 ns before the main pulse is about 10^{-6}, and it can be diminished using the plasma mirror technique or frequency doubling by a few orders of magnitude. But even for improved contrast less than 10^{-7}, which can be produced by modern setups [1], for the laser pulses of peak intensities $\geq 10^{19}$ W/cm^2 the energy contained in the nanosecond prepulse is sufficient to generate a plasma at the surface of a solid target, well before the main pulse. This changes a lot the dynamics of high-intensity laser-solid interaction and hampers in the application of thin foils and nano-structured targets, which can be destroyed completely by the prepulse action.

For simulation of laser experiments, we have elaborated and used a two-temperature single-fluid radiation hydrodynamic model [2, 3, 4]. This wide-range model describes the laser energy absorption, electron-ion coupling and two-temperature effects, radiation transport, thermodynamic properties of materials and ionization from normal conditions at room temperature to weakly non-ideal high-temperature plasma. Using the model we have studied pump–probe experiments [2] as well as the action of a nanosecond prepulse on thin films [3, 4].

Thin foil dynamics under the prepulse action is especially important for the promising design of targets for the laser ion acceleration and effective X-ray generation. On the other hand, a thin foil can be arranged to shield the main target from the laser prepulse impact. In the latter case the shielding foil of a proper thickness can totally absorb the prepulse till the moment specified. Indeed, the heating of the foil material results in its subsequent rarefaction. This process leads eventually to the electron density drop below the critical value so the plasma shield becomes transparent for the laser beam. The moment of the foil material transparency depends on the laser pulse intensity profile, foil thickness, material used etc. In the best case this moment corresponds to the main pulse arrival time.

* Work partially supported by RFBR Nos. 13-08-01179, 14-02-01077.
† povar@ihed.ras.ru

As an example of modeling, we present here the dynamics of thin Al and CH_2 films irradiated by long nanosecond prepulse with 10^{13} W/cm^2. The balance between the incident laser intensity, transmitted laser intensity and radiation flux is investigated. The fraction of the laser energy transmitted through the film is determined together with the determination of emitted thermal radiation flux. The spectrum for Al and CH_2 films after 1 ns prepulse action is presented in Fig. 1. On can see a tenfold decrease in radiation flux for CH_2 film in comparison with Al one.

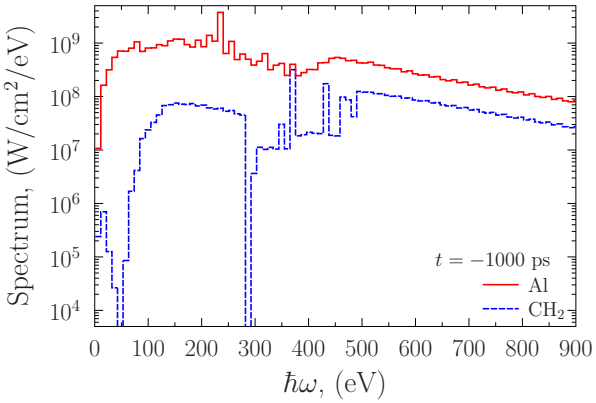

Figure 1: Spectrum of re-emission from the back side of the films after 1 ns prepulse action: Al — solid (red) curve; CH_2 — dashed (blue) curve.

We have found out that there is an "optimal" film thickness that can totally diminish the prepulse energy transmittance and become transparent by the moment of the main high-intensity subpicosecond pulse arrival. At the same time the re-emission of the prepulse energy by the shielding film can be significant for Al films producing an undesirable preheating and rarefaction of the main target placed behind the film. Fortunately, for a CH_2 film it is observed a tenfold reduction of the re-emission flux which does not produce an essential target disturbance. Thus, films composed of light elements can be effective in the cutting off of the nanosecond low-intensity prepulses.

References

[1] F. Wagner, S. Bedacht, A. Ortner, *et al.*, Opt. Express. 22, (2014) 29505.

[2] M. E. Povarnitsyn, N. E. Andreev, E. M. Apfelbaum, *et al.*, Appl. Surf. Sci. 258, (2012) 9480.

[3] M. E. Povarnitsyn, N. E. Andreev, P. R. Levashov, *et al.*, Phys. Plasm. 19, (2012) 023110.

[4] M. E. Povarnitsyn, N. E. Andreev, P. R. Levashov, *et al.*, Las. Part. Beams. 31, (2013) 663.

Deep plasma channels for high quality electron acceleration *

A. Pukhov[1], *O. Jansen*[1], *T. Tueckmantel*[1], *J. Thomas*[1], *and I. Yu. Kostyukov*[2,3]
[1]Uni Düsseldorf, Germany; [2]NNSU, Nizhni Novgorod, Russia; [3]IAP RAS, Nizhni Novgorod, Russia

We study hollow plasma channels with smooth boundaries for laser-driven electron acceleration in the bubble regime. Contrary to the uniform plasma case, the laser forms no optical shock and no etching at the front. This increases the effective bubble phase velocity and energy gain. The longitudinal field has a plateau that allows for mono-energetic acceleration. We observe as low as 10^{-3} r.m.s. relative witness beam energy uncertainty in each cross-section and 0.3% total energy spread. By varying plasma density profile inside a deep channel, the bubble fields can be adjusted to balance the laser depletion and dephasing lengths. Bubble scaling laws for the deep channel are derived. Ultra-short pancake-like laser pulses lead to the highest energies of accelerated electrons per Joule of laser pulse energy.

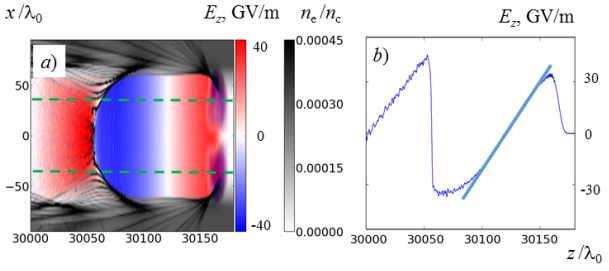

Figure 1: Simulation results for the case $R = 32\,\mu$m.

Here, we consider the bubble regime of electron acceleration, but in a deep plasma channel rather than in a uniform plasma. This allows for a significant improvement of the acceleration . We demonstrate that (i) the effective bubble phase velocity and energy gain increase in the channel; (ii) the longitudinal field has a plateau that allows for mono-energetic acceleration; (iii) the focusing force acting on the accelerated bunch is strongly reduced; (iv) the bubble scaling laws and the bubble field distribution for the deep channel are derived; (v) according to the new scaling laws, ultra-short pancake-like laser pulses match the dephasing and depletion length in the channel and thus lead to the highest energy gains of accelerated electrons per Joule of laser pulse energy. In simulations, we observe as low as 10^{-3} r.m.s. relative witness beam energy uncertainty in each cross-section and 0.3% total energy spread. The lack of focusing in the channel eliminates the very possibility of a betatron resonance and leads to much sharper beam energy distributions.

To check the theory, we perform a 3d PIC simulation using the code VLPL [1]. In the simulation, we take a laser pulse with 141 J energy and 16 fs duration that is very closed to the designed parameters of the Apollon laser [2]. The laser pulse was focused down to 32 μm spot radius in a plasma channel of 24 μm radius with soft exponential walls [3]. We observe very little or no self-injection in the bubble when an empty on-axis channel is used. Thus, we inject an external co-propagating witness electron bunch at the end of the bubble.

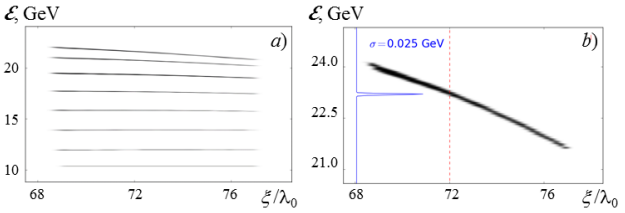

Figure 2: a) Longitudinal phase space of the witness bunch at different propagation distances. b) The final phase space of the bunch zoomed. The local energy uncertainty is 10^{-3}.

The bubble generated by the laser pulse of radius $R = 32\,\mu$m is shown in Fig.1. The accelerating field, Fig.1(a), is transversely uniform. It allows for mono-energetic acceleration of wide electron bunches. This transverse field uniformity is also observed in homogeneous plasmas. The on-axis profile of the accelerating field in the channel, Fig.1(b), however, differs from that in the uniform plasma case. There is a region of flat accelerating field at the very back of the bubble. This region can be used to accelerate reasonably long witness bunches mono-energetically. We inject a witness bunch that occupies about 10% of the bubble length. The longitudinal phase space of the accelerated bunch is shown in Fig.2(a) at different times. The bunch stays very monoenergetic for the first 30 cm of acceleration, because it was injected in the flat accelerating field part of the bubble. The relative r.m.s. energy spread $\sigma_\mathcal{E}/\mathcal{E}$ of the bunch is merely 0.3% when it gains 7.5 GeV energy. This is much better than the ratio of the bunch length to the bubble length that is 10%. Later, the bunch slowly leaves this flat $E-$field region and advances into the region with linearly growing E_z-field. Finally, it gains a positive energy chirp as seen in Fig.2.

In conclusion, the deep plasma channels allow for high quality acceleration of a witness bunch.

* Work supported by DFG TR18, EU FP7, EUCARD2 and by BMBF

References

[1] A. Pukhov Journal of Plasma Physics **61**, 425 (1999).
[2] F. Giambruno et al., Appl. Opt. **17**, 2617 (2011).
[3] A. Pukhov et al., PRL **113**, 245003 (2014)

Voronoi Particle Merging for PIC Codes*

P. T. Luu[1], *T. Tückmantel*[1], *and A. Pukhov*[1]
[1]Heinrich Heine Universität, 40223 Düsseldorf, Germany

Introduction

The particle-in-cell (PIC) method has been used to simulate a wide varieties of physical problems, ranging from electrical discharge to particle acceleration. However, in several situations, e.g. pair production or ionisation, the number of particles grows exponentially in the simulation box. As a consequence, the memory is easily overflowed and thus the performance drops drastically.

Usually, the blind merging method is employed in order to combine particles in the phase space. However, by picking up particles randomly, this method can easily distort the physical description of the system. In this work, we present a new method, so named Voronoi particle-merging algorithm. Our algorithm partitions the phase space of one simulation cell into smaller subgroups such that each group will consist particles that are close to each other. Firstly, the algorithm measures which axis has the largest standard deviation and then makes a hyperplane cut through that axis. The hyperplane cut will reduces the deviation on that axis. The algorithm continues until the deviation on each axis reaches a certain value.

Simulations

We test our algorithm in the case of magnetic shower. Due to the radiation reaction, an energetic electron propagating in a strong magnetic field will emit a hard photon. This photon, after interacting with the strong magnetic field, will in turn decay into an electron - positron pair through the Breit-Wheeler process. The whole event repeats itself and leads to the avalanche of pair production.

Fig. 1 shows the evolution of the total energies of electron, positron, and photon in time. It can be seen that the total energies for electron and photon with Voronoi merging algorithm (purple lines) are equivalent to those with no merging. We see that there is a small loss in the total energy of positron and thus the total energy of the system decreases by the same margin. On the contrary, for blind merging method (red line), not only we observe that there is a huge drop in the total energy of positron after the first merging event, but also the total energy of photon behaves in a strange way. To point out the performance of our algorithm, we plot the number of particles in fig. 2. At the beginning, we have only 40 electrons in the simulation box. When the simulation ends, without merging (blue line) the number of particles for both electrons and positrons are 34000 and that of photon rises up to 400000. The Voronoi merging algorithm (purple line) reduces the number of particles in the simulation box by a factor of 7. Even though this performance is humble compared to that of blind merging method (red line), the physical description of the system is still equivalent to without merging.

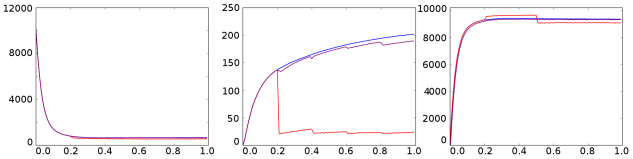

Figure 1: (From left to right) The total energies of electron, positron, and photon in the simulation without merging (blue), with blind merging (red), and with Voronoi merging (purple).

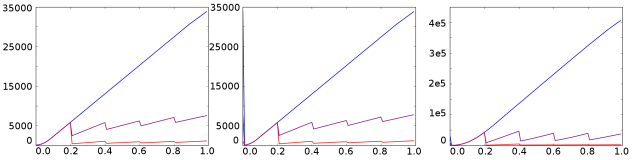

Figure 2: (From left to right) The total numbers of particles for electron, positron, and photon in the simulation without merging (blue), with blind merging (red), and with Voronoi merging (purple).

Summary

We have presented the Voronoi particle-merging algorithm, in which only particles which are close to each other in the phase space are allowed to merge together. The simulation results have shown that the current implementation of the algorithm conserves perfectly momentum and a good energy conservation is achieved. Future effort will be focused on the improvement of the enegy conservation and the merging performance.

References

[1] T. Schreiber, "A Voronoi Diagram Based Adaptive K-Means-Type Clustering Algorithm for Multidimensional Weighted Data", Lecture Notes for Computer Science 553, Computational Geometry - Methods, Algorithms and Applications (H.Bieri, H. Noltemeier (Eds.)), 1991.

[2] V. Anguelov and H. Vankov, "Electromagnetic Showers in a Strong Magnetic Field", J. Phys. G: Nucl. Part. Phys., 25 (1999), p. 1755 - 1764. (1997) 56.

[3] A. Pukhov, "Three Dimensional Electromagnetic Relativistic Particle-in-cell code VLPL (Virtual Laser Plasma Lab)", Journal of Plasma Physics 61 (1999), p. 425-433. (1997) 56.

* Work supported by DFG TR18, EU FP7, EUCARD2 and by BMBF

Dynamic control of laser-accelerated protons from a guiding cone *

D. B. Zou[1,2], *A. Pukhov*[1], *H. B. Zhuo*[2], *and F. Q. Shao*[2]

[1]Heinrich Heine Universität, 40223 Düsseldorf, Germany; [2]National University of Defense Technology, 410073 Changsha, China

Introduction

Radiation pressure acceleration (RPA) has been proposed as an alternative method of ion acceleration at ultrahigh laser intensities. It allows a better control of the ion energy distribution and the acceleration of a much larger number of ions from a smaller target area. However, this mechanism is not stable due to the excitation of transverse instabilities on the laser-foil interface. This is a hotly debated question that what conditions should be required to preserve a good beam quality during acceleration for these thin targets. Besides, for target normal sheath acceleration (TNSA), the angular divergence of the ions measured in experiment ranges from 20° to 60°. Therefore, it is also essential to improve the spatial properties of the ion beam for practical applications.

Control of the RPA protons

A foil-in-cone target, by using a guiding cone to encircle the mass-limited foil, is proposed to enhance stable laser-radiation-pressure-driven proton acceleration by avoiding the beam degradation in whole stage of acceleration. While an ultraintense circularly polarized laser pulse is incident onto the cone, the laser radiation pressure pushes the entire foil forward. During the foil acceleration, a radial sheath electric-field is formed on the inner walls of the cone because the skin-layer electrons are dragged out by the oscillating electric-field of the laser wings. This sheath electric-fields, accompanying with conical electrons propagation, act as a dynamic lens to focus the proton beams and suppress undesirable transverse explosion of the foil. It is shown that, by using a transversely Gaussian laser pulse with intensity of $\sim 2.74 \times 10^{22} W/cm^2$, a quasi-monoenergetic proton beam with a peak energy of $\sim$1.5GeV/u, density $\sim 10 n_c$ and transverse size $\sim 1\lambda_0$ can be obtained at the tip of the cone as shown in Fig. 1.

Control of the TNSA protons

For TNSA, such a hollow cone is used to encircle a thicker solid target and a *p*-polarized laser pulse with a Gaussian profile is incident along the axial direction of the cone from the left boundary. It is found that a part of target hot electrons propagate along the conical inner surfaces due to the confinement of self-generated electromagnetic fields, and a radial electric-field around the conical inner surfaces is thus induced by these moving electrons. Its intensity is even comparable with the pure coulomb explosive field in the limit case and is strong enough to transversely focus these expanding protons. As a result, most of the rear accelerated protons with use of the guiding cone are confined within the conical channel as shown in Fig. 2. Besides, the divergence of the proton beam can be significantly reduced and the number density is substantially enhanced.

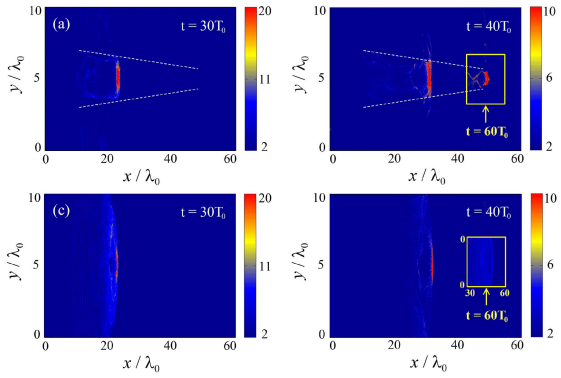

Figure 1: The evolution of the foil proton density n_i^H for cases with [(a) and (b)] and without cone [(c) and (d)].

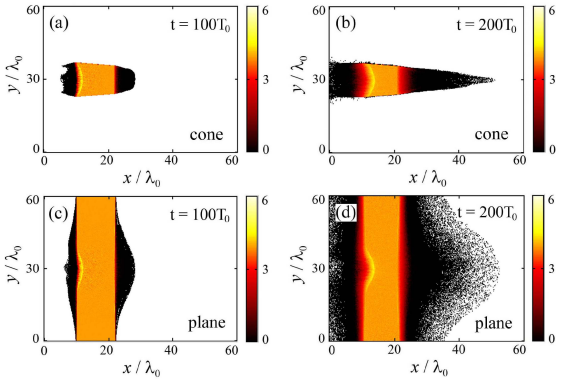

Figure 2: Density distribution of the protons for both cone [(a) and (b)] and plane [(c) and (d)] target cases at $t = 100T_0$ and $t = 200T_0$, respectively.

Summary

It is demonstrated by particle-in-cell simulations that the laser-accelerated energetic protons in both TNSA and RPA can be dynamically controlled by using a guiding cone.

References

[1] A. Macchi, M. Borghesi, and M. Passoni, "Ion acceleration by superintense laser-plasma interaction", Rev. Mod. Phys. **85**, 751 (2013).

* Work supported by EU, EURONS contract No. 506065.

Raman amplification in the strong wavebreaking regime*

J. P. Farmer† *and A. Pukhov*
Heinrich Heine Universität, Düsseldorf, Germany

Introduction

Raman amplification in plasma is a potential method for the creation of the next generation of ultrashort, ultraintense laser pulses. One of the most attractive aspects of using plasma as a gain medium is the absence of a damage threshold, which acts as a limiting factor in conventional, solid-state gain media. However, while the plasma itself has no damage threshold, the generated plasma wave which acts to couple the pump and probe may only grow to finite amplitude before breaking. Whether the excited plasma wave reaches the cold wavebreaking limit depends only on the pump amplitude[1].

Results

Simulations are carried out using the Leap model[2], a fast multidimensional code for the simulation of Raman amplification. The pump and probe are described through their envelopes, while the plasma susceptibility and the excited plasma wave amplitude are calculated from a particle-in-cell treatment. A 800 nm pump of intensity of 1×10^{15} W cm^{-2} is used to amplify a probe of initial intensity 1×10^{16} W cm^{-2} in plasma of density 4.4×10^{18} cm^{-3}. These parameters correspond to a pump intensity 50 times above the threshold for the wavebreaking regime.

While the presence or absence of wavebreaking depends only on the pump amplitude, we find that amplification depends strongly on the initial probe. Two-dimensional simulations were carried out for an initial probe FWHM intensity duration of 83 and 50 fs, as shown in Fig 1. Fig. 2 shows that, while the peak amplitude grows roughly linearly with propagation distance in both cases, the growth rate is lower for the initially longer pulse. This is attributed to self-steepening of the probe, leading to a maximum final amplitude at a point corresponding to a much lower initial probe amplitude. This lowering of the effective initial amplitude reduces the final amplitude.

Conclusions

It is clear from these simulations that in order to maximise amplification, the initial probe should be chosen carefully. Indeed, a more energetic probe does not guarantee better amplification. Future experiments may benefit from simulations scanning the possible parameter space to find the optimal probe parameters for the experimental setup.

* Work supported by DFG TR18, EU FP7, EUCARD2 and by BMBF
† farmer@hhu.de

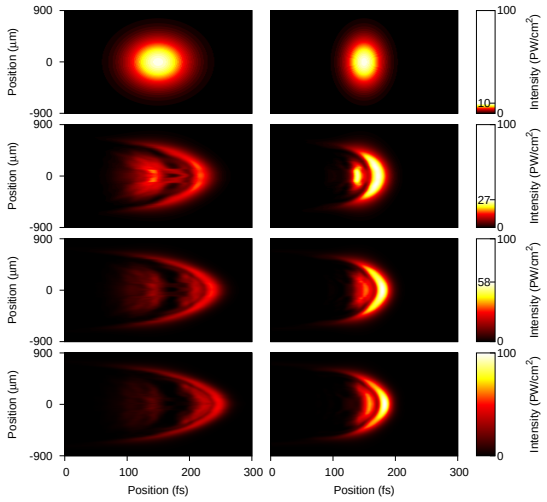

Figure 1: Evolution of the probe pulse intensity as it is amplified, shown (from top to bottom) after 0, 2, 4 and 6 ps interaction with the pump. Figures to the left show a probe with an initial FWHM of 83 fs, those to the right for 50 fs.

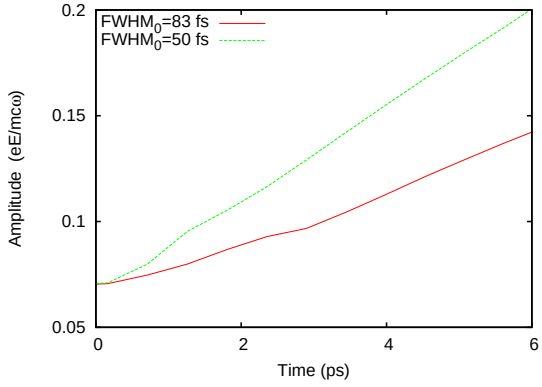

Figure 2: Plot of peak probe amplitude over time for an initial pulse duration of 83 and 50 fs.

References

[1] V. M. Malkin, G. Shvets, and N. J. Fisch, "Fast Compression of Laser Beams to Highly Overcritical Powers", Phys. Rev. Lett. (1999).

[2] J. P. Farmer and A. Pukhov, "Fast Multidimensional Model for the Simulation of Raman Amplification in Plasma", Phys. Rev. E (2013).

Calculation of ion structure factors in warm dense matter *

C.-V. Meister, B. Jiang, and D.H.H. Hoffmann
Technische Universität Darmstadt, Germany

Introduction

Transport properties in solid and fluid phases of matter are strongly determined by the disposition of their atoms, molecules, ions and electrons. In case of solids and plasmas, this disposition is theoretically recorded by the structure factor of the charged particles, which may be expressed by Fourier transforms of two-particle correlation functions.

In weakly nonideal plasmas with plasma parameters, i.e. ratios of the potential interaction energies of the charges to their kinetic energies, smaller than 0.1, the correlation functions may be well estimated in Debye approximation [1-3]. There the particle interaction is described by the Debye potential considering electrostatically screened point particles. But with increasing density of the matter, also the dimension of the ions has to be taken into account. Here the calculation of the structure factors within the frame of the mean spherical approximation is promising. Within the mean spherical approximation, the ions are considered to be charged hard spheres located in a homogeneous neutralizing electron background [4]. Using the mean spherical approximation, rather good results were obtained for alkali plasmas at the melting point [1, 2]. Furthermore, recently models of structure factors are being developed extending the Debye approximations to quantum physical problems. In doing so, the dielectric functions of the matter have to be calculated, at least, in random phase approximation [3]. The authors of [3] concluded that their quantumphysical model is in correspondence with hypernetted chain approximations (HNCA) provided one neglects local field correlations. The University of Technology Darmstadt (TUD) began to deal with HNCA in 2014.

Structure factor in mean spherical approximation

In accordance with the long-time experience concerning the MSA [1, 2], in 2014 at the TUD also first MSA calculations were performed for chemical elements foreseen as target materials in present and future FAIR experiments. Particularly, the newly developed numerical programmes of the structure factor will also be used to calculate electrical and heat conductivities of the Super Fragment Separator of FAIR.

In this report, only the ion structure factor is considered, which takes the distribution of the ions in the plasma, or the lattice of a solid, into account. The Fourier transform of the square of the absolute value of the interaction potential $V_{ei}(\vec{q})$ of N electrons and N ions in matter can be decomposed into the single ion scattering part $|v_{ei}(\vec{q})|^2$, i.e. the form factor, and an ion distribution factor $\hat{S}(\vec{q})$, so that

$$|V_{ei}(\vec{q})|^2 = N\hat{S}(\vec{q})|v_{ei}(\vec{q})|^2,$$

$$\hat{S}(\vec{q}) = \frac{1}{N}\sum_{ij}\exp[i\vec{q}(\vec{R}_i - \vec{R}_j)].$$

Averaging $\hat{S}(\vec{q})$ over the ion positions $\vec{R}_i$ and $\vec{R}_j$, one obtains the structure factor $S_{ii}(q)$ which is related to the pair distribution function of the ions $f_{ii}(r)$ (r is the ion distance, q a wave number). In the thermodynamic limit of a classical plasma with an ion number $N \to \infty$, one has

$$S_{ii}(q) = 1 + n_i \int d\vec{r}\, f_{ii}(r)\exp(i\vec{q}\vec{r}).$$

n_i designates the ion particle density.

A two-particle distribution function $f_{ab}(r)$ of particles of kind a and b may be found from the Ornstein-Zernicke equation [5]

$$f_{ab}(r) - 1 = c_{ab}(r) + n_c \int_0^\infty c_{ac}(|\vec{r} - \vec{r}_1|)h_{cb}(\vec{r}_1)\, d\vec{r}_1.$$

Here the total correlation function $h_{ab}(r) = f_{ab}(r) - 1$ is the sum of the direct correlation function c_{ab} describing the interaction between the two particles a and b, and an indirect contribution caused by the interaction with all other particles of kind c.

In MSA

$$f_{ab} = 0 \quad \text{at} \quad r < |\vec{r}_a - \vec{r}_b|,$$

$$c_{ab}(r) = -v_{ab}(r)/(k_B T),$$

(k_B - Boltzmann constant), while in HNCA

$$c_{ab}(r) = f_{ab}(r) - 1 - \ln f_{ab}(r) - v_{ab}(r)/(k_B T).$$

Calculating the ion structure factor $S_{ii}(q)$ in MSA, in this work expressions by Palmer and Weeks [4] given using complex numbers were rewritten in the following form using real numbers [1, 2]

$$S(q) = 1 - \frac{2A + C}{A + B + C},$$

$$A = 144\eta^2(M^2u^4 + Pu^2 + \tau^2 + 2\tau M u^2),$$

$$B = u^8 + u^4(\frac{R^4}{4} - 24\eta\tau - 24\eta R(\tau - P))$$

* Work financially supported by contract No. 05P12RDFN6.

$$+u^2(12\eta\tau R^2 + 144\eta^2(\tau - P)^2) + 144\eta^2\tau^2,$$

$$C = 24\eta \cos u\Big[Pu(-Ru^3 + 12\eta(\tau - P)u)$$

$$+(Mu^2 + \tau)(u^4 - \frac{R^2u^2}{2} - 12\eta\tau)\Big]$$

$$+24\eta \sin u\Big[Pu(u^4 - \frac{R^2u^2}{2} - 12\eta\tau)$$

$$-(Mu^2 + \tau)(-R^2u^3 + 12\eta(\tau - P)u)\Big],$$

$$R = \frac{6\eta}{1-\eta} - Q,$$

$$P = \frac{1+2\eta}{(1-\eta)^2} - \frac{Q}{2(1-\eta)} + \frac{\tau}{2},$$

$$M = \frac{Q^2}{24\eta} - \frac{1+\eta/2}{(1-\eta)^2},$$

$$Q = \frac{1+2\eta}{1-\eta}\left[1 - \left(1 + \frac{2(1-\eta)^3\tau}{(1+2\eta)^2}\right)^{1/2}\right],$$

$$u = 2R_iq, \;\; \tau = 2R_i\kappa_i,$$

$$\eta = \frac{4}{3}\pi n_i R_i^3, \;\; \kappa_i^2 = \frac{q_i^2 n_i}{\varepsilon_o k_B T}.$$

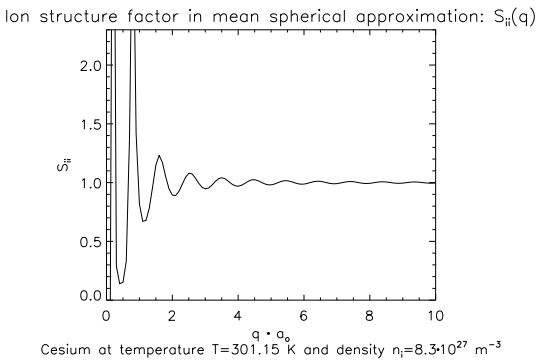

Figure 1: Structure factor of onefold ionized cesium at the melting point with $T = 303.15$ K, $n = 8.292 \cdot 10^{27}$ m^{-3}

To compare the numerical results for the static ion structure factor $S_{ii}(q)$ with former theoretical estimats [1, 2], first studies were performed for cesium at the melting point (Fig. 1). Further, the ion structure factor of other dense plasmas was studied, for instance of aluminum with threefold charged ions at the melting point (Fig. 2). In case of small plasma densities the results in MSA coincide with the results of a linearized Debye approximation. Besides, it is found that the agreement between theoretical results and experimental data may be improved by adjusting the hard core radius R_{ii}. This adjustment may even amount to a modification of R_{ij} by almost 100 percent.

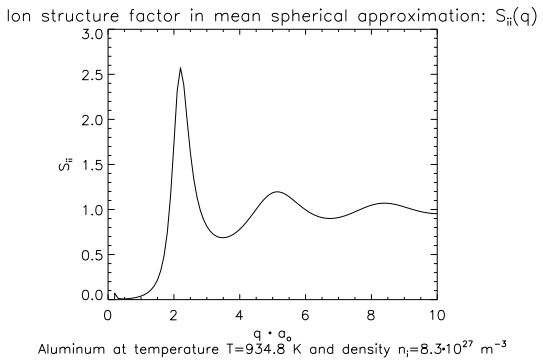

Figure 2: Structure factor of threefold ionized aluminum at melting temperature $T = 934,8$ K and $n = 8.292 \cdot 10^{27}$ m^{-3}

Conclusions

The present study of ion structure factors in Debye approximation and MSA shows that at solid body densities ion-structure effects in plasmas are essential. They cannot be described with sufficient accuracy using a Debye approximation. MSA and HNCA methods should be applied. Up to now, only ion structure effects at melting points are investigated in the present work, focusing on alkali metals like cesium and on aluminum. In future, also the structure factors of yet other elements at various degrees of ionisation will be studied. Moreover, it will be analysed how structure effects modify electrical and thermal conductivities of warm dense matter. First estimates show that transport coefficients may change by 100 percent at solid body densities because of ion structure effects [1, 2, 6].

References

[1] C.-V. Meister, "Zur Theorie der Leitfähigkeit und Thermodynamik nichtidealer Plasmen", PhD, University Rostock, June 1981.

[2] C.-V. Meister, G. Röpke, Electrical conductivity of non-ideal plasmas and the ion distribution function, Annalen der Physik, 39 (2) (1982) 133.

[3] V.S. Karakhtanov, R. Redmer, H. Reinholz, R. Röpke, Transport coefficients in dense plasmas including ion-ion structure factor, Contr. Plasma Phys. 51 (4) (2011) 355.

[4] R.G. Palmer, J.D. Weeks, Exact solution of the mean spherical model for charged hard spheres in a uniform neutralizing background, J. Chem. Phys., 58 (1973) 4171.

[5] R. Balescu, Equilibrium and nonequilibrium statistical mechanics, John Wiley and Sons, Chichester, New York, Sydney, Toronto (1975).

[6] C.-V. Meister, D.H.H. Hoffmann, Thermal parameters and transport coefficients of super-fragment separator targets, Workshop "Non-Ideal Plasma Physics 2014", Presidium of the Russian Academy of Sciences, Moscow, 02.12.14, oral pesentation.

Transport coefficients of FAIR S-FRS targets in Born approximation *

C.-V. Meister and D.H.H. Hoffmann
Technische Universität Darmstadt, Germany

Introduction

In the Super-FRS target and in the beam catchers at GSI stress waves are generated by intense, fast-extracted ion beams which deposit a high amount of energy within a very short time into the target material. This may cause material damage. In this connection, measurements of thermal parameters and eddy-current resistivity are planned as monitoring techniques. At the same time, to understand the physics of the destruction processes in more detail, also a comprehensive theoretical study of thermal parameters such as heat capacity, coefficient of thermal expansion as well as thermal conductivity in warm dense target matter is necessary [1].

Inelastic thermal spike model

The model used at GSI to calculate the heat transport in the material is the inelastic thermal spike one [2]. In the model, the electrons and the lattice (i.e. ions) are considered as two coupled subsystems. The kinetic energy of the projectiles is deposited into the electron system of the target, where thermalization occurs within about 10^{-15} s. The heated electrons transfer then their energy by electron-phonon coupling to the lattice, in which thermal equilibrium is reached after about 10^{-13} s. The heat distribution in the electron and lattice subsystems is described by classical heat transport equations. The energy exchange between electrons and lattice is taken into account by a coupling parameter g. Describing the penetration of the projectiles into the target by a cylindrical system, the heat transport equations read

$$C_e(T_e)\frac{\partial T_e}{\partial t} = \frac{1}{r}\frac{\partial}{\partial r}\left[rK_e(T_e)\frac{\partial T_e}{\partial r}\right] - g(T_e - T_a) + A(r,t),$$

$$C_a(T_a)\frac{\partial T_a}{\partial t} = \frac{1}{r}\frac{\partial}{\partial r}\left[rK_a(T_a)\frac{\partial T_a}{\partial r}\right] + g(T_e - T_a).$$

T_j, C_j, and K_j are temperature, specific heat coefficient, and thermal conductivity of the electrons ($j = e$) and the lattice ($j = a$), respectively. $A(r,t)$ describes the spacio-temporal deposition rate of the target energy to the electron subsystem, it is estimated by the Katz model [2]. Usually, the parameters of the lattice C_a and K_a have to be taken from experiments. In the present work, in case of not too large plasma parameters $\Gamma = V_{ei}/k_BT_e$, the heat capacity is estimated within the frame of a virial expansion in density order 5/2 [3].

* Work financially supported by contract No. 05P12RDFN6.

Transport coefficients in Born approximation

The thermal conductivity K is estimated using the Wiedemann-Franz law $L = e^2K/(k_B^2T\sigma)$ and calculating the electrical conductivity σ (e - elementary charge, k_B - Boltzmann constant, $T = T_e = T_i$). Here L is the Lorenz number. In the case of a non-degenerate plasma, the Lorenz number equals 4, if only electron-ion interaction is considered. If the electron-electron interaction is taken into account additionally, then L = 1.5966 [4]. For degenerate plasmas with free electrons, one has $L = \pi^2/3$.

The electrical conductivity σ is found using the method of Zubarev presented e.g. in [5,6]. The method corresponds to a linear response theory expressing σ by force-force correlation functions,

$$\sigma = \frac{e^2}{\Omega}\frac{N^*(N[G;G]\text{–}W[F;G]) - W^*(N[G;F]\text{–}W[F;F])}{[F;F][G;G] - [F;G][G;F]}.$$

F is the force related to the plasma particle momenta, and G is a force related to the heat current. The Hamiltonian of the plasma is described by the adiabatic one, i.e. the ion motion is neglected.

$$H = H_s - e\vec{E}\vec{R},$$

$$N^* = N + \frac{1}{m_e}[P_x;F], \quad W^* = W + \frac{1}{m_e}[P_x;G],$$

$$F = M_{ei}^{(0)} = \frac{i}{\hbar}[H_s,P_x], \quad G = M_{ei}^{(2)} + M_{ee}^{(2)} = \frac{i}{\hbar}[H_s,Q_x],$$

$$N = \frac{i}{\hbar}\mathrm{Sp}\{\rho_o[P_x,R_x]\}], \quad W = \frac{i}{\hbar}\mathrm{Sp}\{\rho_o[Q_x,R_x]\}],$$

$$\rho_o = \frac{1}{Z_0}e^{-\beta(H_s-\mu N)}, \quad A(t) = e^{iH_st/\hbar}Ae^{-iH_st/\hbar},$$

$$[A,B] = \int_{-\infty}^{0} dt\, e^{\eta t}\int_o^\beta d\tau \mathrm{Sp}\{\rho_o A(t - i\hbar\tau)B\}.$$

$\vec{E}$ describes the external electrical field, Ω is the plasma volume, N - its number density, m_e and κ_e designate mass and inverse screening length of the electron. μ is a chemical potential and $\beta = 1/(k_BT)$.

In Born approximation, i.e. in second order with respect to the interaction potential of the charged particles, one finds for the electron-ion correlation functions [5,6]

$$[M_{ei}^{(m)};M_{ei}^{(n)}] = \frac{Nm_e^2\Omega^2}{12\pi^3\hbar^3}I(q),$$

$$I(q) = \int_o^\infty dq\, q^3S(q)|V_{ei}(q)|^2Y^{mn}(q^2),$$

where $S(\vec{q})$ is the ion structure factor and $V_{ei}(q)$ - the Fourier transform of the screened electron-ion interaction potential assumed to be of the Hellmann-type,

$$V(q)^s_{ei} = -\frac{e^2}{\varepsilon_o \Omega}\left[\frac{1}{q^2+\kappa_e^2} - \frac{A}{(q^2+\alpha^2)(1+\kappa_e^2/q^2)}\right].$$

A and α are parameters depending on the considered target material. The function $Y^{mn}(q^2)$ may be written in the form [5] ($z = \beta\hbar^2 q^2/[8m_e] - \beta\mu_e$)

$$Y^{mn}(q^2) = \begin{cases} (e^z+1)^{-1} & \text{if } n=m=0, \\ 2(z+\beta\mu_e)/(e^z+1) + 2\ln(1+e^z) & \\ \quad \text{if } n=0, m=2 \text{ or } n=2, m=0, & \\ 4(z+\beta\mu_e)/(e^z+1) + 8(z+\beta\mu_e)\cdot & \\ \ln(1+e^{-z}) - 8\sum\limits_{\nu=1}^{\infty}(-1)^\nu e^{-\nu z}/\nu^2 & \\ \quad \text{if } n=m=2, z\geq 0, & \\ 4\frac{z+\beta\mu_e}{e^z+1} + 8(z+\beta\mu_e)\ln(1+e^{-z}) + 4z^2 & \\ +\frac{4\pi^2}{3} + 8\sum\limits_{\nu=1}^{\infty}(-1)^\nu e^{\nu z}/\nu^2 & \\ \quad \text{if } n=m=2, z\leq 0. \end{cases}$$

Γ	$\beta\mu_e$	n_e [m^{-3}]	κ_e [a_o^{-1}]
0.58	-10	$1.157\cdot 10^{21}$	$1.498\cdot 10^{-3}$
4.26	-4	$4.639\cdot 10^{23}$	$2.990\cdot 10^{-3}$
14.8	0	$1.951\cdot 10^{25}$	$1.730\cdot 10^{-1}$
36.5	6	$2.918\cdot 10^{26}$	$3.672\cdot 10^{-1}$
51.2	12	$8.040\cdot 10^{26}$	$4.390\cdot 10^{-1}$

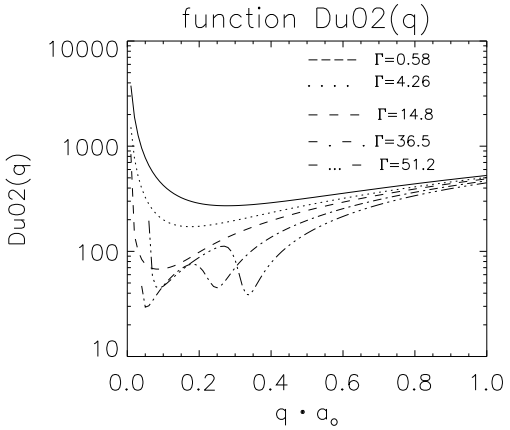

Figure 1: Integrand $I(q)$ of the correlation function $[M^{(0)}_{ei}; M^{(2)}_{ei}]$ for cesium at the melting temperature of 303.15 K and different plasma parameters Γ. $A = 1.371$, $\alpha = 1.037\ \mathring{A}^{-1}$. a_o describes the Bohr radius.

The integrand of the correlation functions (see Fig. 1) has to be calculated very carefully, special attention has to be paid to the structure factor at small wave numbers q having strong oscillations. The analysis showed, that the form of the integrand gets more and more complicated with higher order of the correlation (i.e. increasing m or n) and with growing plasma parameter. First results for the electrical conductivity of the cesium plasma at the melting point taking the ion structure factor into account, and neglecting it, are presented in tables (n_e - electron density, μ_e - chemical potential of the electrons). Further, using the Wiedemann-Franz law with a Lorenz number $L = \pi^2/3$, some estimates for the heat conductivity of a cesium plasma at melting temperature are obtained. There the influence of the ion structure factor is taken into account. In the literature, for cesium solids, a heat conductivity of 35.9 Wm^{-1}K^{-1} is given.

$$K \approx \frac{(4\pi\varepsilon_o)^2 k_B L \sigma^*}{e^4(\beta)^2\sqrt{m_e\beta}} \approx 10^{-3}\sigma^*\ \frac{\mathrm{W}}{\mathrm{Km}},\quad \sigma^* = \frac{e^2\sqrt{m_e\beta^3}}{(4\pi\varepsilon_o)^2}\sigma.$$

Γ	$\sigma^*(S(q)=1)$	$\sigma^*(S(q)\neq 1)$	K [Wm^{-1}K^{-1}]
0.58	0.1629	0.1716	$1.75\cdot 10^{-4}$
4.26	0.7767	0.9826	$1.00\cdot 10^{-3}$
14.8	20.15	80.91	0.08
36.5	222.4	3168	3.39
51.2	453.1	8094	8.23

Conclusions

Models for the thermal parameters of warm dense matter are presented. Based on former works by Röpke and Meister [5,6], the electrical conductivity is recalculated in Born approximation taking the ion-structure factor into account in mean spherical approximation. First results for thermal conductivities are found using the Wiedemann-Franz law with a Lorenz number given by Reinholz et al. [4].

In future, the presented models for thermal and transport parameters have to be further developed for non-fully ionized plasmas of yet higher densities and lower temperatures. Moreover, new models for the coupling coefficient g of the inelastic spike model have to be proposed.

References

[1] D.H.H. Hoffmann, C. Trautmann, Experimentelle Untersuchungen und Simulationen von Materialeigenschaften und kritischen Parametern für das Super-FRS-Target und Strahlfänger der FAIR-Anlage, BMBF-Projekt, Technische Universität Darmstadt, 2012.

[2] M. Toulemonde, W. Assmann, C. Dufour, A. Meftah, F. Studer, C. Trautmann, Experimental phenomena and thermal spike model description of ion tracks in amorphisable inorganic insulators, in: Ion beam science: Solved and unsolved problems, The Royal Danish Academy of Science and Letters (ed. Sigmund P 263392, 2006).

[3] W.-D. Kraeft, D. Kremp, W. Ebeling, G. Röpke, Quantum statistics of charged particle systems, Akademie-Verlag, Berlin 1986.

[4] H. Reinholz, R. Redmer, S. Nagel, Thermodynamic and transport properties of dense hydrogen plasmas, Physical Review E52, 5368-5386 (1995).

[5] C.-V. Meister, "Zur Theorie der Leitfähigkeit und Thermodynamik nichtidealer Plasmen", PhD, University Rostock, 1981.

[6] C.-V. Meister, G. Röpke, Electrical conductivity of non-ideal plasmas and the ion distribution function, Annalen der Physik 39 (2), 133-148 (1982).

[7] C.-V. Meister, B. Jiang, D.H.H. Hoffmann, Calculation of ion structre factors in warm dense matter, ibid.

Simple model for permittivity of a collisional plasma with account for contribution of electron-electron collisions*

H. B. Nersisyan[1,2], *M. E. Veysman*[3], *N. E. Andreev*[†3,4], *H. H. Matevosyan*[1], *and K. A. Sargsyan*[1]

[1]Theoretical Physics Division, Institute of Radiophysics and Electronics, 0203 Ashtarak, Armenia; [2]Center of Strong Fields Physics, Yerevan State University, 0025 Yerevan, Armenia; [3]Joint Institute for High Temperatures RAS, Moscow, 125412, Russia; [4]Moscow Institute of Physics and Technology (State University), Moscow, 113303, Russia

Simple model for the dielectric function of a completely ionized plasma with an arbitrary ionic charge, that is valid for the long-wavelength perturbations is derived using approximate solution of a linearized Fokker-Planck kinetic equation for electrons with a Landau collision integral.

The model accounts for both the electron-ion collisions and the collisions of the subthermal (cold) electrons with thermal ones. The relative contribution of the latter collisions into permittivity is treated phenomenologically introducing some parameter $\varkappa$ which is chosen in such a way to get well-known expression for stationary electric conductivity in low-frequency region and fulfill requirement of vanishing contribution of electron-electron collisions at high frequency region. This procedure ensures the applicability of the model in the wide ranges of plasma parameters and frequencies of electromagnetic radiation.

Unlike interpolation formula proposed earlier by Brantov [1], our model fulfills the Kramers-Kronning relations and gives generalization of the well-known Lee-More model for stationary conductivity [2] and similar models for dynamical conductivity [3, 4] for the cases of degenerate and strongly-coupled plasmas, but with account for electron-electron collisions for the case of plasmas with arbitrary ionic charge and for finite frequencies of laser radiation.

The permittivity of plasmas stipulated by *intraband* transitions is expressed as $\varepsilon = 1 - (\omega_p/\omega_0)^2 K_0(\omega)$, where ω_0 and $\omega_p = \sqrt{4\pi n_e e^2/m}$ are laser and plasma frequencies, respectively, $n_e = Zn_i$ is electrons concentration, n_i is ions concentration, Z is average ions charge, e and m are charge and mass of electrons, respectively; function

$$K_0 = \frac{-2i\chi_{Z_2}}{\xi_\omega \varepsilon_{\rm F}^{3/2}} \int_0^\infty F\left(1; \alpha_{_Z}; i\beta_{_Z}\xi^3\right) f_{\mathcal{F}}(\xi)[1 - f_{\mathcal{F}}(\xi)]\xi^7 d\xi$$

is expressed in terms of confluent hypergeometric function $F(a;b;z)$; the following designations are adopted here and futher: $\xi = \frac{v}{\sqrt{2}v_{\rm th}}, \xi_\omega = \frac{3\sqrt{\pi}}{4}\frac{\nu_e}{\omega}, \alpha_{_Z} = \frac{Z_*+8}{3}, \beta_{_Z} = \frac{Z_*}{3\xi_\omega}$, where v is electrons velocity, $v_{th} = \sqrt{T/m}$, T is electrons temperature, $E_{\rm F} = \frac{\hbar^2}{2m}(3\pi^2 n_e)^{2/3}$ is the Fermi energy, $E_F = E_F/T$, $\varepsilon_\mu = \mu/T$, μ is the chemical potential expressed in terms of Fermy energy as $\varepsilon_\mu = X_{1/2}\left(\frac{2}{3}\varepsilon_{\rm F}^{3/2}\right)$, where $X_{1/2}$ is the function inverse to the Fermi integral $F_{1/2}(x)$; $f_{\mathcal{F}}(\xi) = \left[1 + \exp(\xi^2 - \varepsilon_\mu)\right]^{-1}$; $\nu_e = \frac{4\sqrt{2\pi}n_e Z e^4}{3(mT^3)^{1/2}}\Lambda$ is the effective electron-ion collision frequency, expressed in terms of Coulomb logarithm Λ, which can be determined in wide range of plasma parameters by respective interpolation formulas [5–8]; $\chi_{_{Z_2}} = [1+5/Z_*]^{-1}$, $Z_* = Z/\varkappa$ is effective charge, determined in terms of function $\varkappa$, which is constructed in such a way [8] to ensure proper limits at high and lower laser frequencies and for non-degenerate [1] as well as for degenerate [7] matter:

$$\varkappa(\omega) = \varkappa_0/\left[1 + (C/\xi_\omega)^s\right], \quad \varkappa_0 = Z\left[\widetilde{\gamma}_\sigma^{-1}(Z) - 1\right]/5,$$
$$\widetilde{\gamma}_\sigma = \gamma_\sigma(Z) + \frac{1 - \gamma_\sigma(Z)}{1 + 0.6\ln\left(1 + (20\varepsilon_{\rm F})^{-1}\right)}, \ \gamma_\sigma = \frac{a+Z}{b+Z},$$

where constants $a = 0.87$, $b = 2.2$, $C = s = 1$.

Above formulas ensure proper well known high- and low-frequency skin effect asymptotics for nondegenerate [1, 9] and for degenerate Lorentz plasmas [2–4, 10] (when $Z \gg 1$ and one can disregard electron-electron collisions) and permits one to calculate optical properties of matter in wide range of parameters of laser and plasmas with arbitrary ions charge.

References

[1] A. V. BRANTOV, V. Y. BYCHENKOV, and W. ROZMUS, *JETP* **106**, 983 (2008).

[2] Y. T. LEE and R. M. MORE, *Phys. Fluids* **27**, 1273 (1984).

[3] S. E. KIRKWOOD, Y. Y. TSUI, R. FEDOSEJEVS, A. V. BRANTOV, and V. Y. BYCHENKOV, *Phys. Rev. B* **79**, 144120 (2009).

[4] M. BASKO, T. LÖWER, V. N. KONDRASHOV, A. KENDL, R. SIGEL, and J. MEYER-TER VEHN, *Phys. Rev. E* **56**, 1019 (1997).

[5] A. ESSER, R. REDMER, and G. RÖPKE, *Contributions to Plasma Physics* **43**, 33 (2003).

[6] S. SKUPSKY, *Phys. Rev. A* **36**, 5701 (1987).

[7] W. A. STYGAR, G. A. GERDIN, and D. L. FEHL, *Phys. Rev. E* **66** (2002).

[8] H. B. NERSISYAN, M. E. VEYSMAN, N. E. ANDREEV, and H. H. MATEVOSYAN, *Phys. Rev. E* **89**, 033102 (2014).

[9] M. E. VEYSMAN, B. CROS, N. E. ANDREEV, and G. MAYNARD, *Phys. Plasmas* **13** (2006).

[10] A. SELCHOW, G. RÖPKE, and K. MORAWETZ, *Nucl. Instrum. Methods Phys. Res., Sect. A* **441**, 40 (2000).

* The work is in line with RFBR project 15-52-05057

† andreev@ras.ru

On Quantum Bound of the Shear Viscosity of a Strongly Coupled Plasma

V.Mintsev, V.Fortov

Institute of Problems of Chemical Physics, 142432, Chernogolovka, Russia

String theory methods led to the hypothesis that the ratio of shear viscosity coefficient to volume density of entropy of any physical system has a lower bound [1].

$$\frac{\eta}{s} \geq \frac{\hbar}{4\pi k_B} = Q_L = 6.08 \cdot 10^{-13}\, K \cdot s$$

This paper is devoted to analysis of the behavior of the shear viscosity of strongly coupled electromagnetic plasma. Systems with strong coupling have a small viscosity compared to weakly coupled plasmas in which the viscosity is proportional to the mean free path. Today a huge array of experimental data on the thermodynamic, transport and optical properties of strongly coupled plasma was received, but there are no direct measurements of viscosity. For our purposes experimental data on measurements of electrical conductivity of hydrogen, deuterium and rare gases under intense shock compression and under quasiisentropic compression in multistep loading up to megabar pressures are the most interesting.

Here we have done estimations of the shear viscosity of strongly coupled plasma on its data on electrical conductivity. Let us first consider the classical fully ionized ideal plasma, composed of electrons with mass m_e with concentration n_e and mass ions m_j=M with concentration n_i and average charge Z. While observing the kinetic coefficients we follow the approach stated in monograph [2]. One can find the expression for shear viscosity coefficient η defined through electrical conductivity σ_{sp} [3]:

$$\eta = k_\gamma \frac{1}{Z^3}\sqrt{\frac{Mm_e}{e^2}}kT_i\left(\frac{T_i}{T_F}\right)^{3/2}\frac{\Lambda_{ei}(T_F)}{\Lambda_{ii}(T_i)}\sigma_{sp}$$

Where T_i and T_F – ion and electron component temperatures, Λ_{ii} and Λ_{ei} - Coulomb logarithms

To determine the thermodynamic parameters of the shock-compressed plasma with strong interparticle interaction "quasichemical" model SAHA was used, in which the Coulomb interaction is described within the Debye approximation in the grand canonical ensemble. Also it takes into account the degeneracy of the electronic component and the short-range repulsion of the atoms and ions in the approximation of soft spheres. This model has the correct asymptotic behavior of the ideal plasma model at low densities and good description of the experimental data in the region of strong coupling. Necessary for further evaluation the entropy density s was also estimated in the framework of the SAHA model, adjusted for the interparticle interaction and degeneracy.

The results of our calculations of the ratio of shear viscosity coefficient to the entropy density in the units of $\hbar/4\pi k_B$ in dependence on coupling parameter Γ are presented on the figure 1. Quantum lower bound in these variables is a unit Q_L =*1*. Here theoretical curves for strongly coupled plasma [24] for T=10^3 K и T=10^5 K are presented. The lower possible limit for one component plasma (OCP) is represented by the curve 3. It is seen, that the values of η/s at Γ*~1*, which are calculated using experimental data on conductivity of strongly coupled argon and xenon plasma and corresponding to relatively low pressures of *P~1-10 GPa* and temperatures of *T~(2-3)·10⁴ K,* are correspond η/s *~10^3* Q_L and well agree with theoretical models. The data in megabar range for rare gases are in the range η/s ~10^2-10 Q_L at Γ*~1÷10* and also do not contradict to the theoretical models. As for the data on hydrogen, deuterium and helium-hydrogen mixture, received in the region of "metallization" at P~150 GPa in different experimental systems by the method of quasiisentropic compression, they reach the values η/s *~(0.3-10)* Q_L. Thereby, the hydrogen plasma in the region of "metallization" possesses the lowest values of the shear viscosity to the entropy ratio. Note that in this case we have an extremely high value of the coupling parameter - Γ*~20-80.*

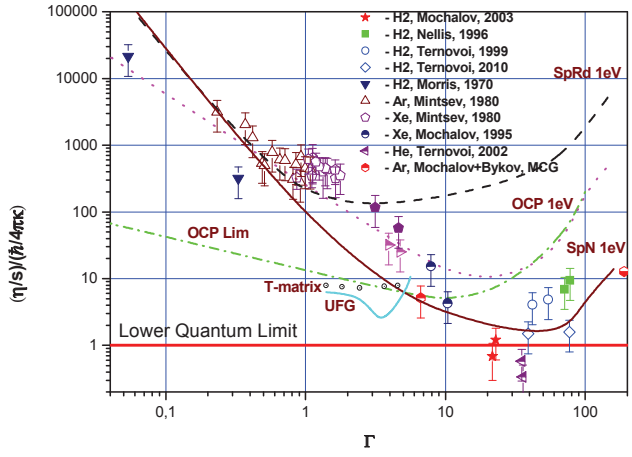

Figure 1. Dependence of the ratio of shear viscosity coefficient to entropy density on coupling parameter.

It is interesting to note, that the data on electrical conductivity of strongly coupled electromagnetic plasma, confirm the tendency of decreasing of the viscosity η/s with an increase in the correlation (Γ) and thus confirm trend of the transition of the physical system to the perfect frictionless fluid with the increasing of the interparticle interaction.

References

[1] P. Kovtun, D. T. Son and A. O. Starinets. Phys. Rev. Lett. **94** (2005) 111601.

[2] I.P.Shkarofsky, T.W.Jonston, M.P.Bachynski. *The particle kinetics of plasma*, Addison-Wesley Publ. Comp., 1966.

[3] V.E.Fortov, V.B.Mintsev, V.B. Phys. Rev Lett., **109** (2013) 055002,

Intense Coherent Gamma-Ray Source Based on the Collective Radiation of Positronium Atoms in a Bose-Einstein Condensate*

H.K. Avetissian†*, A.K. Avetissian, and G.F. Mkrtchian*
Centre of Strong Fields Physics, Yerevan State University, Yerevan 0025, Armenia

The creation of a γ-ray laser has been the subject of extreme interest since the realization of the first lasers. The annihilation of electron-positron pairs has been considered as one of the basic processes for the intense γ-ray sources. In our paper [1] it has been shown that effective γ-ray laser is feasible due to intrinsic instability of recoilless two-photon decay of positronium (Ps) atoms. The latter being a bound state of an electron and a positron plays a central role in achieving a fundamental understanding of diverse phenomena in many branches of contemporary physics. Apart from the laboratory-based experiments on the effective creation of Ps or even molecular Ps [2], Ps atoms are connected with the cosmic electron-positron annihilation radiation from the Galactic center with the rate $\sim 3\times10^{42}$ Ps atoms per second, resulting in a narrow 511 keV line [3].

Feasible experimental setup for γ-ray laser is shown in Fig. 1. Here we consider a cigar-shaped Bose-Einstein condensate (BEC) of width w and length L ($L >> w$). As far as ortho-positronium (o-Ps) has relatively long lifetime (142 ns) compared with para-positronium (p-Ps) - 125 ps, in laboratory based experiment it will be more suitable to obtain BEC for o-Ps. Hence, it is assumed that initially we have a BEC of spin polarized o-Ps ultra-cold atoms. Then, applied electromagnetic field initiates transition from o-Ps BEC to p-Ps one triggering collective annihilation of the condensate. A comprehensive investigation of a γ-ray laser at the collective annihilation of Ps atoms in a BEC state in the self-amplified spontaneous emission regime [1], shows that due to intrinsic instability of recoilless two-photon decay and shape of condensate, initial spontaneously emitted entangled photon pairs are amplified, leading to an exponential buildup of a macroscopic population into end-fire-modes. Thanks to BEC coherence, here we have an absolute instability; i.e., the number of photons grows in every point within a BEC with exponential growth rate

$$G=\sqrt{\frac{16\pi n_{eff}\alpha_0^5}{m}}=6\times\sqrt{n_{eff}[\mathrm{cm}^{-3}]}\mathrm{s}^{-1}. \quad (1)$$

Here n_{eff} is the effective density of BEC, m is the electron mass, and α_0 is the fine structure constant.

In Fig. 2 it is shown number of photons N_γ in the end-fire-modes versus effective density of p-Ps atoms in BEC for the given length $L=1.5$ cm and various widths: $w=L/\chi$. We assume that the photonic field begins in the vacuum state, while Ps field is in the Bose-Einstein condensate state. As is seen due to above mentioned instability and BEC shape, one can obtain intense, coherent and monochromatic γ radiation from a dense BEC of Ps atoms.

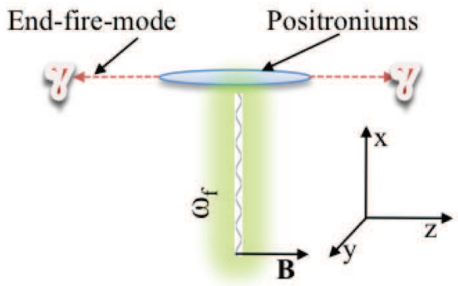

Figure 1: Feasible experimental setup for γ-ray laser.

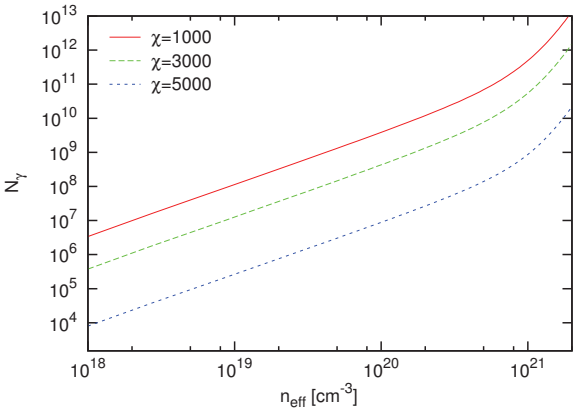

Figure 2: Number of photons in the end-fire-modes versus effective density of p-Ps atoms

While the parameters required for an efficient γ-ray laser are certainly very challenging, the ongoing and future progress in creation, trapping, and cooling of Ps atoms promises clear prospects to reach them.

References

[1] H.K. Avetissian, A.K. Avetissian, and G.F. Mkrtchian, Phys. Rev. Lett. 113, (2014) 023904.

[2] D. B. Cassidy and A. P. Mills, Jr., Nature (London) 449, (2007) 195.

[3] G. Weidenspointner et al., Astron. Astrophys. 450, (2006) 1013.

* Work supported by SCS of RA, Project No. 13-1C066.
† avetissian@ysu.am

Multiphoton Excitations and Harmonics Generation in Quantum Electrodynamic Vacuum*

H.K. Avetissian†*, A.K. Avetissian, B. R. Avchyan, and G.F. Mkrtchian*
Centre of Strong Fields Physics, Yerevan State University, Yerevan 0025, Armenia

Abrupt development of new technologies in laser physics led to the creation of powerful optical lasers of ultrarelativistic intensities [1] and further realization of x-ray free electron lasers [2], which allows one to implement coherent x-ray sources with the peak brightness - by ten orders of magnitude exceeding ones in conventional synchrotron sources. At the further advance of compression and focusing techniques for these lasers one can approach to the Schwinger field strengths. Interaction of such powerful lasers with quantum electrodynamic (QED) vacuum will have strictly multiphoton character allowing manifestation of nonlinear phenomena in a wide spectrum [3], and consequently, will open up a new research field with the high-energy transitions [4]. In particular, becomes real particle-antiparticle pairs creation/annihilation [5] and coherent generation of high harmonics from QED vacuum.

We have investigated the nonlinear electromagnetic properties of QED vacuum with the revealing of its coherent response to the multiphoton excitation by a hard x-ray radiation, at the conditions permitting a real pair creation/annihilation process (e.g., the recoil-free processes in counterpropagating laser fields or in a standing wave-field). The multiphoton effects become essential when the wave-particle interaction parameter $\xi = eE_0/(mc\omega) \sim 1$ (c is the light speed in vacuum, m and e are the electron mass and elementary charge, respectively, E_0 is the wave electric field amplitude, and ω is the wave carrier frequency), and the interaction behaviour depends on the quantum recoil parameter $q_r = mc^2/(\hbar\omega)$ as well.

In Fig. 1 it is shown electron/positron distribution function $\mathcal{N}(\mathbf{p}, t_f)$ (in arbitrary units) after the interaction of a standing wave-field formed by the two counterpropagating laser fields of relativistic intensities with the QED vacuum. The resulting wave-field is assumed to be linearly polarized with the frequency $\omega = mc^2/50\hbar \simeq 10\,\mathrm{keV}/\hbar$. The dimensionless field parameter is taken to be $\xi = 2.5$. It is also shown harmonics radiation at the induced electron-positron annihilation. In Fig. 2 it is shown the normalized coherent part of the vacuum harmonics emission rate as a function of the harmonic order. The interaction parameters are the same as for Fig. 1. For this setup one can achieve the large conversion efficiencies for the 3rd and 5th harmonics. In particular, for the interaction volume $(3\lambda)^3$, where $\lambda = 2\pi c/\omega$, the conversion efficiency for the 3rd harmonic is of the order of 10^{-3}.

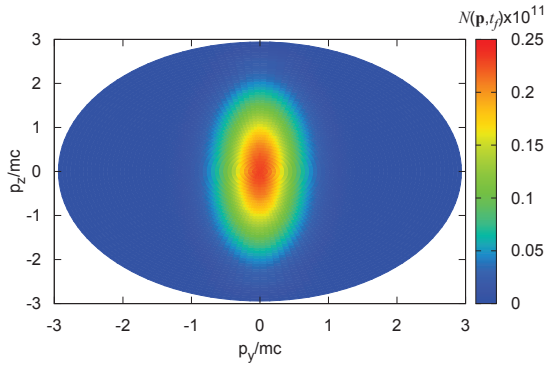

Figure 1: Creation of electron-positron pairs at the multiphoton excitation of QED vacuum.

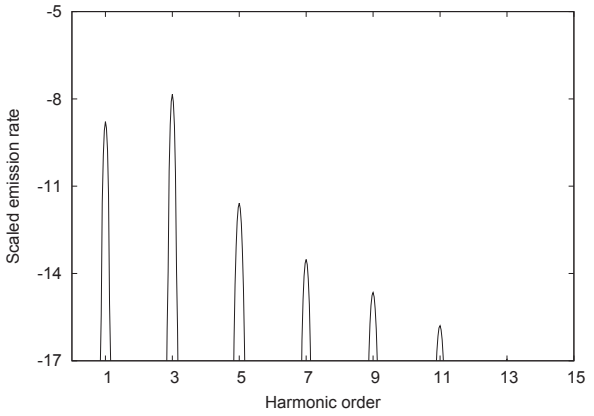

Figure 2: Coherent part of the vacuum harmonic emission rate as a function of the harmonic order.

References

[1] G.A. Mourou, T. Tajima, S.V. Bulanov, Rev. Mod. Phys. 78 (2006) 309.

[2] P. Emma, et al., Nature Photonics 4 (2010) 641.

[3] H.K. Avetissian, Relativistic Nonlinear Electrodynamics, Springer, New York, 2006.

[4] D.H.H. Hoffmann et al., Int. Jour. of Mod. Phys. E 18 (2009) 381.

[5] H.K. Avetissian et al., Phys. Rev. D 54, (1996) 5509; Phys. Rev. E 66 (2002) 016502; Nucl. Instr. and Meth. A 507 (2003) 582.

* Work supported by SCS of RA, Project No. 13-1C066.
† avetissian@ysu.am

List of Contributing Institutes

CEA/CESTA (Centre d'études scientifiques et techniques d'Aquitaine)
Le Barp, France

Commissariat à l'énergie atomique et aux énergies alternatives (CEA)
France

Czech Technical University
Prague, Czech Republic

Duke University
Durham, NC, USA

ExtreMe Matter Institute (EMMI)
Darmstadt, Germany

General Atomics Corporation
La Jolla, CA, USA

GSI Helmholtzzentrum für Schwerionenforschung GmbH
Darmstadt, Germany

Johann-Wolfang-Goethe-Universität
Institut für Angewandte Physik
Frankfurt, Germany

Handong Global University
Pohang, Republic of Korea

Helmholtz-Zentrum Dresden – Rossendorf
Dresden, Germany

Helmholtz-Institut Jena
Jena, Germany

Institute of Modern Physics (IMP)
Lanzhou, China

Institute of Problems of Chemical Physics (IPCP)
Chernogolovka, Russia

Institute of Space Science
Bucharest, Romania

Institute of Theoretical and Experimental Physics (ITEP)
Moscow, Russia

Jiaotong University, Joint Center of Xi'an
Xi'an, China

Joint Institute for High Temperatures, RAS
Moscow, Russia

Joint Institute of Nuclear Research
Dubna, Russia

Keldysh Institute of Applied Mathematics
Moscow, Russia

Korea Advanced Institute of Science and Technology (KAIST)
Daejeon, Republic of Korea

Lawrence Berkeley National Laboratory
Berkeley, CA, U.S.A.,

Lawrence Livermore National Laboratory
Livermore, CA, USA

Lebedev Physical Institute, RAS
Moscow, Russia

Los Alamos National Laboratory
Los Alamos, NM, USA

Massachusetts Institute of Technology
Cambridge, Massachusetts, USA

Max Planck Institute for Intelligent Systems
Stuttgart, Germany

Max-Planck-Institut für Physik komplexer Systeme (MPIPKS)
Dresden, Germany

Moscow State University
Moscow, Russia

Nagaoka University of Technology
Nagaoka, Japan

National Institute of Technology
Kagoshima College
Kirishima, Japan

National Laboratory for the Heavy Ion Research Facility in Lanzhou
Xi'an, China

National Security Technologies, LLC (NSTec)
Livermore, CA, USA

Nazarbayev University
Astana, Kazakhstan

Osaka University, Institute for Academic Initiatives
Suita, Osaka, 565-0871, Japan

Princeton Plasma Physics Laboratory
Princeton, NJ, U.S.A.

Sandia National Laboratories
Albuquerque, NM, USA

Stanford Linear Accelerator Center (SLAC)
Menlo Park, CA, USA

Technion
Haifa, Israel

Technische Universität Darmstadt
IKP, TQE
Darmstadt, Germany

Technische Universität Kaiserslautern, Fachbereich Physik und Landesforschungszentrum OPTIMAS
Kaiserslautern, Germany

Technische Universität München,
München, Germany

Universität Hamburg & CFEL, Department of Experimental Physics
Hamburg, Germany

Université Bordeaux
Bordeaux, France

University of California Berkeley
Berkeley, CA, USA

University of California Los Angeles (UCLA)
Los Angeles, CA, U.S.A

University of Chinese Academy of Sciences (UCAS)
Beijing, China

University of Rochester, Laboratory of Laser Energetics,
Rochester, NY, USA

University of Warwick, Centre for Fusion, Space- and Astrophysics
Physics Departement
Coventry, UK

VNIIEF
Sarov, Russia

Xianyang Normal University,
Ion Beam and Optical Physical Laboratory
Xianyang, China

Yerevan State University, Centre of Strong Fields Physics
Yerevan Armenia

Author Index